

Cover design: Squirrel On the Rock

Ghent University
Faculty of Pharmaceutical Sciences

**Injectable drug-loaded microbubbles: a magic
bullet for image-guided cancer therapy?**

**Injecteerbare geneesmiddel-beladen microbellen, een magische kogel
voor beeldvorming-gestuurde kankertherapie**

Bart Geers
Pharmacist

Thesis submitted to obtain the degree of
Doctor in Pharmaceutical Sciences

Proefschrift voorgedragen tot het bekomen van de graad van
Doctor in de Farmaceutische Wetenschappen

2013

Dean:

Prof. dr. apr. Stefaan C. De Smedt

Promotors:

Prof. dr. apr. Stefaan C. De Smedt
Prof. dr. apr. Jo Demeester

Co-promotor:

Dr. apr. Ine Lentacker

*Laboratory of General Biochemistry
and Physical Pharmacy*

Ik zal mezelf zijn tot aan de meet
(Raymond v/h Groenewoud)

De grootte van de bel definieert hoeveel ze kan dragen
(deze thesis)

Alles van Waarde is Weerloos
(lucebert)

The author and the (co-)promoters give the authorization to consult and to copy parts of this thesis for personal use only. Any other use is limited by the Laws of Copyright, especially the obligation to refer to the source whenever results from this thesis are cited.

De auteur en de (co-)promotoren geven de toelating dit proefschrift voor consultering beschikbaar te stellen en delen ervan te kopiëren voor persoonlijk gebruik. Elk ander gebruik valt onder de beperkingen van het auteursrecht, in het bijzonder met betrekking tot de verplichting uitdrukkelijk de bron te vermelden bij het aanhalen van resultaten uit dit proefschrift.

Gent, 28 maart 2013

De promotoren:

Prof. dr. apr. Stefaan C. De Smedt

De auteur:

Bart Geers

Prof. dr. apr. Jo Demeester

De co-promotor:

Dr. apr. Ine Lentacker

"FINAL".doc



FINAL.doc!



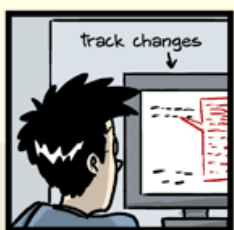
FINAL_rev.2.doc



FINAL_rev.6.COMMENTS.doc



FINAL_rev.8.comments5.
CORRECTIONS.doc



FINAL_rev.18.comments7.
corrections9.MORE.30.doc



FINAL_rev.22.comments49.
corrections.10.#@\$%WHYDID
ICOMETOGRADSCHOOL????.doc

JORGE CHAM © 2012

TABLE OF CONTENTS

Table of Contents	7
List of Abbreviations	15
Aim and Outline of this Thesis	19
Chapter 1: General Introduction	23
Chapter 2: Self-assembled liposome-loaded microbubbles	75
Chapter 3: Cell specific ultrasound-triggered drug delivery	105
Chapter 4: The influence of microbubble shell and the type of liposome loaded	135
Chapter 5: Delivery of small molecules with liposome-loaded microbubbles to tumors <i>in vivo</i> : a pilot study	167
Chapter 6: On the mechanisms behind sonoporation	183
General Conclusions and Future Outlook	211
Algemene Besluiten en Toekomstperspectieven	217
Curriculum Vitae	223

DANKWOORD

Een doctoraat is een wetenschappelijke verhandeling die op een zakelijke, opsommende manier een overzicht geeft van de belangrijkste observaties en inzichten die een student gedurende een periode van een viertal jaar heeft verzameld. Dit is dus geen plaats voor proza beste lezer, zoek dus niet naar spitsvondigheden en literaire hoogstandjes je zal enkel droge kost op uw boterham krijgen. Alhoewel, er is toch nog één plaats waar een iets vrijere interpretatie van de werkelijkheid is toegestaan, namelijk het dankwoord.

Vooreerst (dat schrijft het protocol ons voor) dien ik een eerste uitgebreid woord van dank te richten aan mijn (co-)promotoren.

Stefaan (Prof. Dr. De Smedt, decaan), ik herinner me nog zeer goed mijn eerste les fysicochemie van het geneesmiddel. Je startte de les toen met de gevleugelde woorden, “imagination is more important than knowledge” en meteen was de toon gezet (althans voor mij, de meeste medestudenten haakten hier al af). Het is een gave om mensen op een inspirerende manier les te geven en dat mag toch eens in de verf gezet worden, vooral omdat dit te weinig het geval is op hogeschoolniveau (waar knowledge toch meestal voorgaat op imagination). Het enthousiasme en de manier waarop je je zaken uitlegde deden me beslissen om me verder te verdiepen in hetgeen waarover je ons instrueerde. Nu staan we een halve generatie verder en kunnen we zeggen dat een klein stukje van de grote puzzel weer is ingevuld (hoewel eerder een kleine schilfer van een puzzelstuk). Dus Stefaan, bedankt om mij de kansen te geven om me op een academische manier te ontplooiën het is zeker de mooiste periode uit m’n leven geweest (tot nu toe) en ik blijf zeker nog (zij het van iets verdere afstand) mijn oren en ogen open houden naar wat er gebeurt op de faculteit.

Een aparte plaats in het bedankingsproces verdient **Ine**. Toen ik begon aan m'n project zat jij in dezelfde situatie als ik nu, je thesis moest af en je had een druk bezet leven als moeder van (bijna) twee kinderen. Door onze complementariteit hebben we denk ik toch maar mooi een traject afgewerkt en ons mannetje gestaan in het Sonodrugs project. Je liet me altijd de vrijheid om mijn eigen ding te doen, maar met je ervaring en kalmte bracht je me steeds terug op het juiste spoor. Vooral het feit dat je je gezin (van ondertussen drie prachtige kinderen) blijft combineren met wetenschap van een zéér (retorische klemtoon gevolgd door een korte pauze) hoog niveau is buitengewoon bewonderenswaardig. Ik gun je dan ook alle succes in je verdere academische carrière.

Jo (Prof. Demeester), als nestor van het labo en practicumgoeroe stond je ons steeds bij in ons creatieve denkproces, vooral als het op de iets wiskundigere problematiek aankwam. Je bent eveneens een bevlogen lesgever (zij het iets minder uitbundig als stefaan, maar iedere vogel zingt zoals hij gebekt is uiteraard) die me opzadelde met een voorliefde voor biochemische en biofysische processen en dat verdient op zich al een heuse bedanking. Ik zou je ook nog veel werkplezier mogen wensen in je laatste jaren op de faculteit en geniet na je carrière vooral van een portie welverdiende rust (eventueel opgeluisterd met wat barokmuziek).

Kevin, Ik heb je nog gekend als postdoc, maar al snel werd je verheven tot de adelstand. Ik heb je leren kennen als een geïnteresseerd iemand met de nodige ambitie. Ik wens je alle succes toe en ik hoop dat je de toekomstige apothekers op darwiniaanse wijze uitselecteert.

Niek, ook jij bedankt voor je input en uitgebreide discussies. Ik hoop dat je groep in Merelbeke gestaag zal groeien, zodanig dat ook het in vivo gedeelte van het drug/gene-delivery onderzoek een extra boost krijgt.

Ondertussen zijn we protocolair aanbeland aan het bedanken van m'n collegae, ik zal proberen bondig te zijn, doch iedereen een plaatsje te geven.

Eerst en vooral een dikke merci aan de mensen die dag in dag uit de gaten dichtfietsen in het administratieve werk, de mensen die alle moeite doen om ons in ideale omstandigheden aan de start van een congres of meeting te brengen.

Katharine je verwelkomde me op 1 augustus 2008 met de woorden "zijde gij Bart Geers?", maar sindsdien ben je altijd je charmante zelve net zoals **Ilse**. Het labo zonder jullie valt te vergelijken met de stuurcabine van de Costa Concordia, een schip zonder stuurman. **Bruno VdB**, Ik hoop dat je het niet naar je zin hebt in de kelders aan de Korte Meer en dat je beslist om nog eens terug te keren naar het FFW. Dan kan je nog eens mijmeren over de tijd van Roger (toen een demarrage op 50 km van de meet voor mietjes was, demarreren deed je principieel op 100 km van de meet) of gekscheren over de lotgevallen van Fweddy Maewtens, om nog maar te zwijgen over "Dieu" god hebbe zijn ziel "Spitteals" of levende legende burgemeester van Seraing "Guy Mathot".

Een belangrijk woord van dank gaat naar mijn practicumcollega's **Koen Rombouts, Koen Raemdonck, Broes, Katrien Forier, Marie-Luce** en niet te vergeten **Bart Lucas**. Het was altijd een zware periode, maar desalniettemin een hele mooie. Ik heb het nooit met tegenzin gedaan en ik hoop dat mijn geest nog een tijdje zal blijven rondwaaien rond het practicum. **Katrien en Koen**, ik ben er zeker van dat jullie dit werk in schoonheid zullen overnemen en op jullie beurt zullen doorgeven aan een volgende generatie.

Broes, ik heb je een klein beetje doen afzien op de kasseien van Wannegem-Lede, maar je wraak was zoet op de hellingen van de Franstalige en Kortrijkse Vlaamse Ardennen. Veel succes bij Ablynx maar voor iemand met jou onuitputtelijke bron aan talent (inclusief ultrasound-responsive gehoorbeentjes) is dat uiteraard niet nodig.

Koen Raemdonck, op wetenschappelijk vlak ken je geen gelijke, je literatuurkennis is outstanding en ik stond altijd versteld van je “ad rem” zijn. Gelukkig is er af en toe nog een quiz (al dan niet bevolkt met het plaatstelijke Vlaams nationalistisch genootschap) om de rollen om te keren. Niet twijfelen en doorgaan op je elan!

Buyens, altijd de lachende derde op het bureau maar o zo spitsvondig. Het ga je goed in het Brakelse (pas wel op met de “vissen” op het Ronde Van Vlaanderen diner).

Bubble collega’s **Heleen** en **Ine** veel succes met de afwerkingen van jullie lijvige doctoraten. Onder Ine’s vleugels zal dit zeker gesmeerd lopen. Ik ben er dan ook van overtuigd dat de genderproblematiek eigenhandig door jullie de wereld zal uitgeholpen worden.

Hendrik, je bent een vat vol wetenschappelijke weetjes dat helaas wordt overgebracht naar de Zwitserse alpen. Mocht je ooit terugkomen, breng dan wat Zwitserse francs voor ons mee.

Geertrui veel succes met je verdere acties in het leven, geniet van alles wat nog op je afkomt.

Oliwia, I would like to wish you lots of success finishing your PhD thesis and lots of fun with your little daughter.

Dries, jammer dat we je niet meer zoveel horen, maar je was toch een van de meest gerespecteerde collega's zowel op als naast het werk. Je zal je ambities waarmaken, daar ben ik van overtuigd.

Thomas, gooi alle handballen erin en vergeet niet af en toe een PC te rebooten. Het ga je goed in je verdere carrière en alle kalmte gewenst bij het in het gareel houden van de studenten.

Dan zijn er verder nog **Freya, Karen, Lynn, Laura, Stephan, Stefaan Soenen, Katrien R., Marie-luce, Nathalie, Stefaan Derveaux (Het ros beiaard doet zijn ronde), Elisa, George, Steven Cool** en vele anderen die ik rechtstreeks of onrechtstreeks in een professionele context ben tegengekomen. Aan allen Bedankt and to **Ranhua and Chaobo** Tzai Chen.

I would also like to thank all the colleagues working for the **Sonodrugs** consortium especially: Mariska, Pedro, Mareike, Marc, Marcel, Wafa, Simone, Chrit, Kostas, Charles, Ying, Ilya, Edwin, Ayache, Jean-Michel, Mike and Christophoros.

Last but not least zijn er mijn vrienden en familie...

FOB (Berre, Steng, Brecht, Seb, Gilbert, Beele en Steven) fantastisch dat we nu al een hele tijd nog steeds de moeite nemen om af en toe elkaar op te zoeken en een plezante tijd te beleven.

Vik, Wiezen, Joos, Bram (vooral bedankt voor het interview in de Ic Hou ;-)), Kerstekinderen, zeer bedankt voor jullie aanwezigheid bij mijn talloze "frein

gallekes" op de kasseien van de kwaremont of op de heuvels van Brabant, mijn(iets minder) glorieuze momenten in het uitgangseven of in de nabijheid van ons bijeengescharreld instrumentarium gehuld in zwarte schmink die ge der alleen maar afkrijgt door uwe kop te wassen me Drecht. Mannen Merci!

Pieter, Lieselot, Gaby, Eddy, Marc en Nico: Jullie zijn een bijzondere schoonfamilie en ik ben bijzonder gelukkig dat ik af en toe (al dan niet met jullie instemming) in jullie midden mag vertoeven.

An, fiere meter van onze zoon, en jongste zus. Je zat me bovenaan de trap op te wachten als ik niet op uur was na m'n eerste nachtelijke escapades, je leerde me hoe ik vergelijkingen moest oplossen in het 2^{de} middelbaar. Je hebt het blijkbaar goed gedaan.

Inge, Meter, bedankt om m'n klankbord te zijn als losgeslagen puber en vooral bedankt om me zoveel fruitpap te geven. Ik ben er groot van geworden nu!

Jean, Godfather, je hebt me zoveel geleerd als ik een jonge gast was en ik was zo trots op je als ik als kleine man naar je toonmomenten kwam kijken in het RITS met ons ma. Alleen die bakken bier en die sigaretten vond ik wel een beetje beangstigend. Merci broer!

Ma en Pa bedankt dat jullie ons allemaal zoveel kansen hebben gegeven, wat niet evident was in een gewoon gezin zoals het onze. Ik was misschien niet de gemakkelijkste maar ik ben zo fier op jullie dat jullie je opvoedingswerk zo goed hebben afgerond. Geniet nu van jullie tijd (soms wel goed gevuld met de kleinkinderen) en dikke merci.

Bol voor jou heb ik het laatste woord veil. Elke dag van mijn leven met jou is al een hele mooie geweest en er zullen er nog zovele mooie volgen. We zijn samen een enorm sterk team en vooral je bent de beste mama! Zonder je onvoorwaardelijke liefde en steun zou ik een totaal ander mens geworden zijn. Bedankt voor je geduld, compassie, irritatie en vooral ik zie je graag!

Stan dikke zoen vriendje!

Allemaal nog eens dik bedankt

Bart (Barry, Blues) Maart 2013

LIST OF ABBREVIATIONS

A	Amplitude
AAV	Adeno Associated Virus
BBB	Blood Brain Barrier
BSA	Bovine Serum Albumin
C₄F₁₀	Perfluorobutane
Cholesteryl-bodipy	Cholesteryl 4,4-difluoro-5,7-dimethyl-4-bora-3a,4a-diaza-s-indacene-3-dodecanoate
CLSM	Confocal Laser Scanning Microscopy
CSC	Cancer Stem Cell
CTC	Circulating Tumor Cell
DID	1,1'-dioctadecyl-3,3,3',3'-tetramethylindodicarbocyanine
DLS	Dynamic Light Scattering
DMEM	Dulbecco's Modified Eagles Medium
DNA	Desoxyribonucleic Acid
DOX	Doxorubicin
DPPC	Dipalmitoyl Phosphatidylcholine
DSPE	Distearyl Phosphatidyl Ethanolamine
DTT	Dithiotreitol
E-cadherin	Epidermal Cadherin
EGFP	Enhanced Green Fluorescent Protein
EMT	Epithelial Mesenchymal Transition
EPR	Enhanced Permeation and Retention

FBS	Fetal Bovine Serum
FDA	US Food and Drug Administration
HEPES	Hydroxyethyl Piperazineethenesulfonic Acid
HER2	Human Epidermal Growth Factor Receptor
HIFU	High Intensity Focused Ultrasound
HIV	Human Immunodeficiency Virus
HPV	Human Papillomavirus
Hz	Herz
ICG	Indocyanine Green
IR	Infrared
MMP	Matrix Metallo Proteinase
MPPC	Monopalmitoyl Phosphocholine
MRI	Magnetic Resonance Imaging
mRNA	Messenger RNA
MTT	Dimethylthiazol Diphenyltetrazolium Bromide
MWCO	Molecular Weight Cut Off
N-cadherin	Neuronal Cadherin
NHS	N-hydroxy Succinimide
P	Pressure
Pa	Pascal
PBS	Phosphate Buffered Saline
pDNA	Plasmid DNA
PDP	Pyridil Dithio Propioamide

PEG	Poly Ethylene Glycol
Pen	Penicillin
PET	Positron Emission Tomography
PFO	Pentafluoro-octanol
PLGA	Poly L Glycolic Acid
PLLA	Poly L Lactic Acid
RES	Reticulo Endothelial System
RNA	Ribonucleic Acid
SD	Standard Deviation
SF₆	Sulfur Hexafluoride
siRNA	Small Interfering RNA
Strep	Streptomycin
t	Time
T	Temperature
UCA	Ultrasound Contrast Agent
US	Ultrasound
UV	Ultraviolet
v	Velocity
VEGFR	Vascular Endothelial Growth Factor Receptor
W	Watt

Aim and Outline of this Thesis

Cancer has an enormous impact on modern society, on a yearly basis a significant number of patients dies as a consequence of this disease. Hence, a lot of effort is put in the elucidation of the molecular causes of cancer and in the development of new and better treatment options to cure cancer. Normally cancer is treated by surgical resection, radio- or chemotherapy. The latter is very frequently used, but unfortunately characterized by its devastating side-effects.

It would mean a huge breakthrough if one could develop a drug or a drug-delivery system that allows efficient treatment of the tumor site leaving other tissues unharmed. However, such time and space controlled drug-delivery remains a holy grail in medicine. It is the wish of every scientist or physician to design or have access to a device that only delivers therapeutic molecules at a certain target site (e.g. a tumor) but for the time being no such device has made it to the clinic. To design such a “magic bullet”, a concept that was first described by Ehrlich in the beginning of the 20th century, one needs to develop a drug carrier that responds to a stimulus applied by an external force or produced by the target tissue itself.

Pressure can be used as such an external trigger and an interesting source of pressure can be ultrasound. In this thesis we will focus on the development of small gas filled “microbubbles” that can be loaded with a drug-containing nanoparticle and that in response to a high intensity ultrasound field release their payload only there where ultrasound is applied. Additionally, this technique also benefits from the fact that ultrasound can be used diagnostically for imaging applications in combination with microbubbles. Hence it would become possible to image where the drug is located exactly while the imaging modality itself is able to trigger drug release from the microbubbles.

Drug-loaded microbubbles are promising drug-delivery vehicles, however specific issues that will help enabling the translation of these systems into the clinic need to be resolved. This thesis generally aims at developing an ideal carrier for ultrasound guided drug-delivery, which will help this technique to move on from bench to bedside.

In **chapter 1**, we highlight the most recent insights in (molecular) cancer development, to finally focus on strategies for site-directed cancer therapy and more particularly ultrasound assisted drug-delivery with microbubbles. Here, we emphasize on the basic aspects of ultrasound physics and its applications in drug-delivery and finally we describe the most recent advances in the use of microbubbles for this application.

In **chapter 2** we describe the development of a safe, stable and easy to produce formulation of liposome-loaded microbubbles by simple self-assembly of the involved components. We also show that this formulation is able to deliver very low doses of the anticancer drug doxorubicin (DOX) into cells efficiently. To allow targeting and hence drug-delivery with liposome-loaded microbubbles to specific cell types we've introduced a targeting moiety to our formulation (**chapter 3**). We show that anti N-cadherin targeted liposome-loaded microbubbles allow such cell type specific drug delivery to N-cadherin expressing cells in a mixture of 2 different cell types.

In **chapter 4** we compare drug-delivery from liposome-loaded microbubbles in function of the type of microbubble shell and in function of the type of liposome (thermosensitive or standard) loaded on the surface of the microbubble. We show that lipid-shelled microbubbles loaded with thermosensitive drug-filled liposomes are most efficient for drug-delivery applications *in vitro*. Finally, all

these newly developed and optimized materials were tested in xenograft tumor bearing mice (**chapter 5**)

In **chapter 6** we elucidate the mechanisms behind sonoporation which allows efficient uptake of drugs into cells. Here we investigate the intracellular fate of adeno associated virus (AAV) vectors loaded on the surface of the microbubbles with confocal scanning laser microscopy. We observe a direct cytoplasmic delivery of the loaded AAV vectors which explains a the effects observed in our material optimization studies *in vitro*.

Chapter 1

General introduction

Bart Geers¹, Heleen Dewitte¹, Stefaan C. De Smedt¹ and Ine Lentacker¹

Parts of this chapter have been published in the *journal of controlled release*, 164, 2012 p246-255 *Crucial factors and emerging concepts in ultrasound-triggered drug-delivery*

¹ laboratory of General Biochemistry and Physical Pharmacy, Harelbekestraat 72, 9000 Ghent, Belgium

THE IMPACT OF CANCER ON MODERN SOCIETY

Next to cardiovascular disorders cancer is the most important cause of death and its influence on mortality will inevitably become more and more important in the following years as population ages [1-3]. Taking a closer look at the frequency different types of cancers occur (table 1), one can observe that hormonal (or related) cancers like breast and prostate cancer are the most frequently occurring types of cancer. However, other cancers like lung cancer, colorectal cancers or pancreatic cancer have a significant impact on mortality as well.

Because of its devastating impact on mortality and morbidity of the population the disease causes a significant economic burden [4] as well. The total cost of cancer (in Europe) is estimated at 54 billion Euros per year.

Table 1: Total incidence and mortality of the different types of cancers in both sexes in Belgium. (Eurostat).

<u>Type of Cancer</u>	<u>Incidence</u>	<u>Mortality</u>
Prostate	9986	1571
Breast	9691	2421
Colon and rectum	8039	3109
Lung	7140	6532
Bladder	2202	880
Non-Hodgkin lymphoma	1912	653
Kidney	1676	603
Oral cavity and pharynx	1676	538
Melanoma of skin	1594	293
Stomach	1476	914
Leukemia	1447	940
Corpus uteri	1380	189
Pancreas	1093	1397
Esophagus	947	703
Ovary	929	712
Multiple myeloma	829	462
Brain/nervous system	790	614
Larynx	663	266
Cervix uteri	663	198
Thyroid	659	83
Liver	466	715
Hodgkin lymphoma	292	74
Testis	280	11

Consequently it is clear that a deepened understanding on the underlying pathofysiologic and molecular processes and the development of new and more effective therapies should be elaborated in the following years. In the next paragraphs we will shortly highlight a) recent insights in cancer development, b) the most important therapeutic interventions for cancer treatment c) we will have a look at some emerging concepts in cancer treatment with a clear focus on site-directed image guided drug-delivery) and finally we will look deeper into the concept of ultrasound and microbubble assisted drug delivery.

CANCER DEVELOPMENT AND ITS MOLECULAR MECHANISMS

Understanding the complex biomolecular nature of cancer isn't easy and requires insight in different scientific fields. Since life expectancy has changed dramatically in the past century the occurrence of this intriguing disease has grown. Cancer still remains somehow enigmatic because a lot of scientific questions about it remain unsolved. Here, we would like to give a short overview of the latest developments made in the understanding of this disease.

Cancer was essentially described as a malfunctioning of the genetic control mechanisms of cell growth and division [5,6]. But thanks to the increased technological development a deeper understanding in the basic molecular mechanisms has elucidated some of the more important aspects the disease especially during the last half of the 1990s.

Hanahan and Weinberg [7] described the six hallmarks of cancer (or the cancerous cell) in their 2002 review on cellular cancer development. According to their work a cancer cell or a "cancerous" tissue is characterized by the following hallmarks:

- Sustaining proliferative cell signaling
- Evading cell growth suppression
- Enabling replicative cellular immortality
- Activating invasion and metastasis
- Inducing angiogenesis
- Resisting apoptosis

These hallmarks not only emphasize that cancer basically is a cellular malfunctioning, the hallmarks point out the interaction with the surrounding

tissue as well. Inducing angiogenesis for example implies the integration and expression of pro-angiogenic factors at the tumor site that are not expressed by the tumor cells themselves. Indeed, the idea that a tumor is simply characterized by a group of “out of control” cells is slightly old-fashioned. The complex interactions of the cancer cell with its (micro) environment is probably more important than the deregulated cellular functions of the tumor cells themselves. Therefore *Hanahan and Weinberg* decided to add four extra hallmarks or hallmark characteristics in a follow-up review published in 2011 [8], namely:

- Evasion of immune destruction
- Deregulating cellular energetics
- Increased genome instability and mutational burden
- Inflammatory responses promoting the tumor

Figure 1 gives an interpretation of these modern insights and summarizes what might happen in tumor onset and progression. We hypothesize that normal tissue will acquire cancer-cell capacities upon accumulation of genetic instabilities inside the tissue. These can be due to aging but toxic stress (e.g.: tobacco smoke), environmental factors (e.g.: dioxins, UV-light) or viral infections (human papillomavirus (HPV) [9] or human immunodeficiency virus (HIV) [10]) can as well induce cells to acquire a cancerous phenotype. The onset and progression of cancer can be divided into 2 phases namely: primary tumor formation and metastatic disease respectively.

1st Phase: primary tumor formation

Typically most tumor cells will first acquire “cellular” hallmark characteristics. Tumor suppressor genes will be switched off and oncogenes will become

expressed enabling replicative immortality and evading tumor suppression. Interestingly the metabolism of the cells changes as well, because of the inadequate energy supplies to the cells [11].

Not only the tumor cell itself undergoes significant changes, the tumor micro-environment changes too and plays an active role in the occurrence of neoplasms [12-15]. New blood vessels will be formed to supply energy to the energy consuming cancer cells [16-19]. An inflammatory response is induced and immune cells are attracted to the tumor [20]. This immune response will not necessarily lead to the destruction of the tumor. It is observed that tumor cells evade this immune response [21] and that the molecular stress provided by this response even enhances tumor growth and its instability. The expression of matrix-metallo-proteases (MMPs) in tumors for example is significantly upregulated in some specific tumors [22]. This indicates indeed that immune response (MMP activity is related to the presence of immune cells like lymphocytes and neutrophils) has a modulatory effect on the tumor microenvironment.

We would also like to note that very recently, research on primary tumors focuses on abnormal cell phenotypes that arise as the tumor develops. Since a tumor is basically a hostile environment and tumor cells lack the necessary control mechanisms, we can envisage a tumor as a site where forced evolution can take place. Tumor cells can for example acquire resistance against anticancer drugs [15] [23]. Tumor cells can also adapt to the hostile tumor environment by transforming into a “dormant” phenotype. These dormant cancer cells are not characterized by expressing cancer cell hallmarks, however these cells can give rise to new tumors occurring multiple years after resection of the initial tumor.

These cells are often referred to as cancer stem cells (CSCs) [24] and their appearance is related to poor outcome and morbidities.

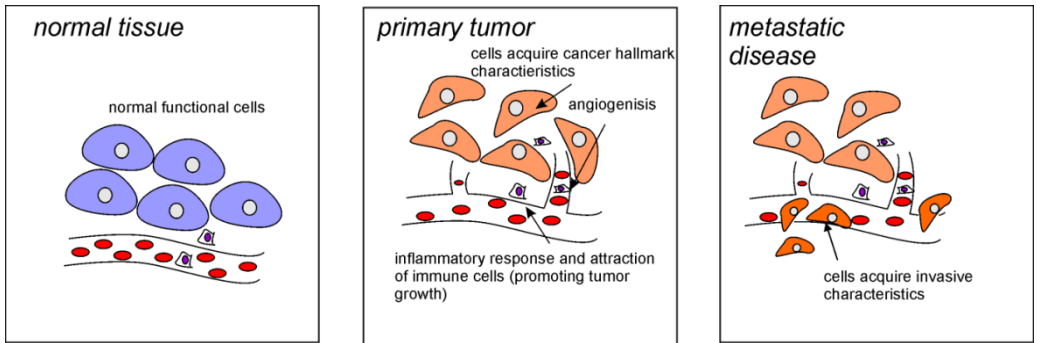


Figure 1: Schematic depiction of the process of tumor growth and cancer development.

2nd Phase: metastatic disease

The 2nd and last stage of cancer development is metastatic disease. Metastases are formed by tumor cells that try to escape the hostile tumor environment by acquiring an invasive phenotype [25,26]. This results in the appearance of tumor cells in the bloodstream (i.e.: circulating tumor cells CTCs). These CTCs can accumulate at certain areas where metastatic colonization can occur. Mostly, one can observe the appearance of liver, lung or peritoneal metastasis as shown by *Hess et al.* in a review of adenocarcinoma metastases [27]. Metastases can as well occur in environments that are “functionally” predetermined as metastatic niches like e.g. bone [28,29] and lymph node metastasis [30]. Bone marrow and lymph nodes indeed are tissues that are characterized by high concentrations of lymphatic cells or that have a lot of cellular activity. As said before these cells and their activity can sustain and remodel the cellular micro-environment and can hence construct an ideal environment for metastatic colonization. Metastasis is the last stage in cancer development and metastatic cancers are characterized by their poor outcome.

CLINICAL CANCER THERAPIES

Although its impact on mortality is significant, cancer can be cured if detected in an early stage of its development. In what follows we will give a short overview of the treatment options for cancer.

Surgical resection

Surgical resection normally is the first line treatment in tumors that are located in accessible tissues (e.g.: colorectal, breast, prostate or lung cancer). This is mostly

effective since the diseased tissue will be removed. In order to reduce the risk of relapse and metastases chemotherapy can be given as an adjuvant therapy [31].

Radiation therapy

Tumors that are not readily accessible for surgical resection can be treated with ionizing radiation. The ionizing radiation will destroy DNA in the radiated zones which leads to apoptosis of cancer cells. Despite its tumor killing efficiency there are cases reported of accidents with conventional radiotherapy which is a major drawback of this technique.

Chemotherapy

Chemotherapeutic drugs are used to eradicate remaining tumor cells upon surgical resection or as first line treatment in tumors that are not readily accessible. These small molecules can be classified according to their molecular structure or mode of action. The most frequently used (according to the Belgian drug repository/BCFI) are:

Alkylating agents

These are molecules containing highly reactive alkyl-groups (like N-mustard derivatives or platinum derivatives) that are able to alkylate cellular components like DNA. Hereby, cellular control mechanisms and DNA transcription and replication become deregulated resulting in apoptosis of the affected cell [35].

Chemotherapeutic antibiotics

Some antibiotics (produced by the *Streptomyces* fungus) do not specifically target bacterial biomolecular structures or processes, but interfere with human cellular

processes as well. These antibiotics (e.g.: doxorubicin [36]) can be used for the treatment of solid (breast, Kaposi's sarcoma) tumors.

Antimetabolites

Antimetabolites are molecules which are structurally similar to components involved in (nucleic acid) metabolism (e.g.: 5-fluorouracil) [37]. These molecules may become integrated into newly formed nucleotides and hence hamper nucleic acid synthesis in dividing cells [38].

Topoisomerase inhibitors

Topoisomerases are enzymes that maintain DNA-topology. Inhibition of these enzymes (by specific inhibitors like irinotecan [39]) by specific inhibitors hampers DNA supercoiling by these enzymes and hence DNA replication and transcription.

Microtubule inhibitors

Some molecules like taxanes [40] or vinca-alkaloids [41,42], inhibit microtubule formation upon cell division. Hereby, they are able to block mitosis and induce apoptosis in these dividing cells.

Personalized chemotherapy based on tumor profiling

An innovative new way of administering anti-cancer drugs is chemotherapy based on tumor profiling [43]. Due to recent technological advances it is nowadays possible to screen certain tumors for specific biomolecular markers. Screening for overexpression of the HER2 (Human Epidermal growth factor Receptor 2) protein in breast cancer is a textbook example of this kind of

personalized medicine [44]. HER2 is upregulated in some breast cancers and is treated by administration of the monoclonal antibody trastuzumab or Herceptin® [45-49]. Earlier HER2 overexpression was associated with poor outcome in breast cancer. Nowadays and thanks to Herceptin treatment HER2 positive tumors indeed show better therapeutic outcome.

Problems?

Despite their effectiveness chemotherapeutics still have their limitations and adverse effects [50,51]. Most patients suffer from nausea, hair loss or immune depression upon chemotherapy or radiation. This is caused by the high doses of drug needed to kill adequate amounts of tumor cells and the narrow therapeutic index of these drugs.

As envisioned in figure 2 it would mean a huge breakthrough if one could develop a drug or a drug-delivery system that allows efficient treatment of the tumor site leaving other tissues unharmed. However, such time and space controlled drug-delivery remains a holy grail in medicine. It is the wish of every scientist or physician to design or have access to a device that only delivers therapeutic molecules at a certain target site (e.g. a tumor) but for the time being no such device has made it to the clinic. To design such a “magic bullet”, a concept that was first described by Ehrlich in the beginning of the 20th century, one needs to develop a drug carrier that responds to a stimulus applied by an external force or produced by the target tissue itself. Cancer treatment as well is nowadays more focused on a more personalized approach. In this case, every tumor will be analyzed in detail before an ideal treatment scheme can be set up.

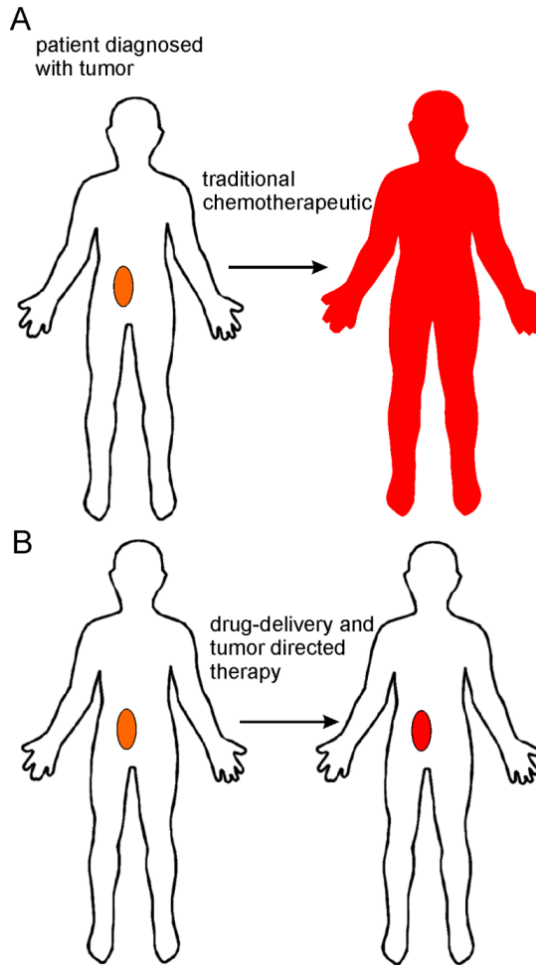


Figure 2: Schematic depiction of (A) the standard approach of chemotherapy and (B) tumor-directed drug-delivery.

TUMOR-DIRECTED DRUG-DELIVERY WITH NANOMEDICINES

As explained above, cancer therapy needs more subtle ways of treatment with anticancer drugs. Nano-sized drug-containing particles, or nanomedicines, are able to specifically accumulate in tumors [52,53]. In the next part of this chapter we will shortly highlight some examples of tumor-directed cancer therapy with nanomedicines that emerged in the past decades and may become or are being used in the clinic. As schematically depicted in figure 3, nanomedicines are (at least in one dimension) nanometer-sized particles (1-200 nm) that are filled with one or more therapeutic agents [54]. The latter can be a drug, but can as well be an imaging contrast agent. Usually nanoparticles are coated with polyethylenglycol (PEG) to avoid recognition by the immune system and compartments of the reticula endothelial system (RES) [55] and hence reach long circulation times (48 h) [56] allowing efficient accumulation of the nanomedicines in tumors.

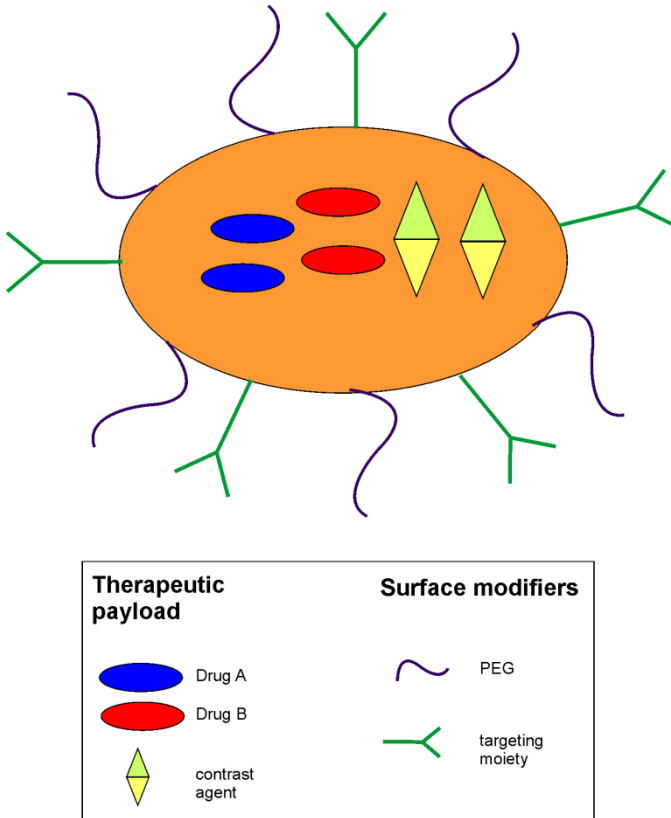


Figure 3: Schematic representation of a nanomedicine.

Macromolecular structures like nanomedicines are able to selectively penetrate into the tumor tissue via enhanced permeation and retention (EPR) as schematically depicted in figure 4. *Maeda et al.* [57-59] first described this concept more than 20 years ago and it remains up to now an important paradigm in tumor-directed drug-delivery. Basically, EPR is based upon the fact that tumor vascularization is leaky and disorganized. Not only the leaky nature of the neovascularization in the tumor can stimulate tumor accumulation of nanomedicines, but they can also have a targeting moiety incorporated [60].

Attaching such targeting moieties to a nanoparticle not only allows accumulation of nanomedicines in the blood vessel (due to upregulated expression of e.g. VEGFR, but may also allow tumor cell specific accumulation of these particles in the stroma of the tumor by targeting overexpressed folate receptors on tumor cells for example [61-63]. Nanoparticles can also be made sensitive to an external trigger (as explained below); such a trigger allows localized delivery of the therapeutic or diagnostic agent incorporated in the nanoparticle.

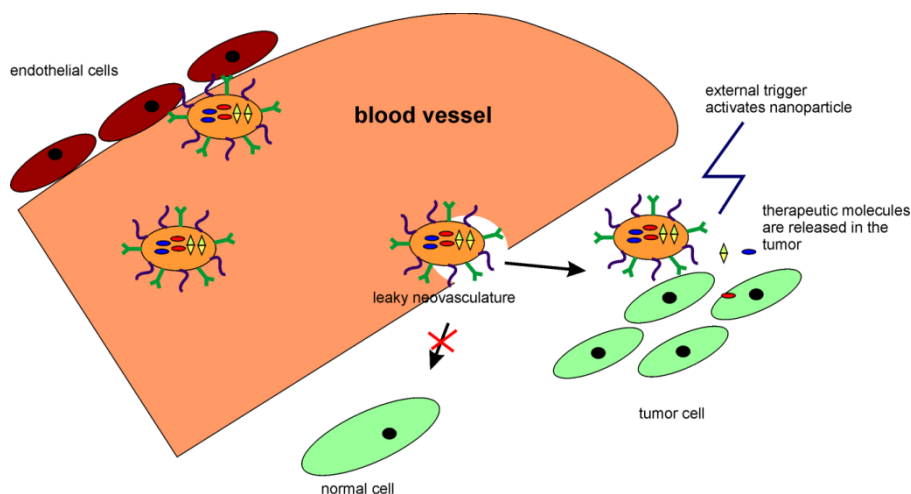


Figure 4: Schematic representation of the wide potential of delivery of therapeutic molecules with (targeted) nanomedicines.

Liposomes

The archetypal nanomedicine is a drug-filled liposome. Liposomes are nanoparticles that are confined by a phospholipid double membrane [64] as depicted in figure 5. Hence liposomes can be regarded as small containers with an intraliposomal space where a therapeutic moiety can be stored in without being

affected by blood components. The incorporation of cationic phospholipids may allow complexation of nucleic acids like pDNA, siRNA or mRNA, this type of complexes are called lipoplexes [65,66]. Liposomes can also be loaded with a drug by incorporation of a complexation buffer (e.g.: ammonium sulfate) in the intraliposomal space, amphiphilic drugs like doxorubicin can hence be loaded into liposomes with high efficiency [67].

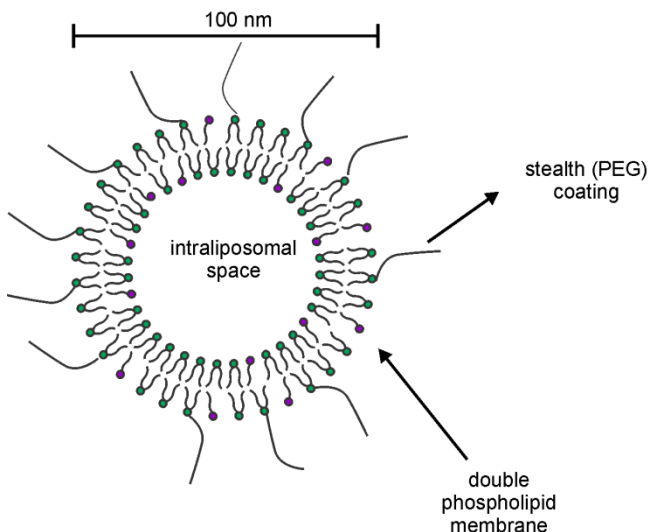


Figure 5: Schematic depiction of the structure of a liposome.

(Nano)theranostics

Every tumor is different; therefore it is important to evaluate tumor characteristics with a medical imaging modality. Magnetic Resonance imaging (MRI) [68,69] and functional positron emission tomography (PET) [70] are very useful tools for this purpose. MRI shows high spatial resolution and anatomic detail, where PET can provide sensitive molecular detection of small tumor volumes using contrast agents like F18-FDG (fluorodeoxyglucose) [71]. Imaging

hence provides essential information on tumor size, metabolic status and off course therapeutic evolution for a specific patient [72].

Coupling an imaging modality to a nano-sized drug-delivery vehicle would allow direct and personalized information on the process of drug-delivery (i.e.: theranostics). Theranostics is an emerging field that focuses on the combination of therapy with diagnostics via medical imaging techniques (e.g.: MRI, ultrasound) [73,74]. It involves the use of agents that are able a) to visualize a specific pathological process and b) simultaneously deliver a drug at this site. *Kiessling et al* [75] reported recently on the current status of different preclinical and clinical theranostic applications. It would be a breakthrough if one could design a drug-loaded (nano)particle which specifically detects pathophysiological processes like cancer and which delivers its drug at the site where a diagnostic signal is observed. *De Smet et al.* [76] described a thermosensitive nanoparticle (liposome) that contained both a drug and a MRI contrast agent. This contrast agent however will only give a significant MR relaxation signal upon release of the drug out of the liposome [77], due to thermally induced liposomal membrane destabilization. *De Smet et al.* show a correlation between drug release and contrast agent release. This kind of approach indeed can provide patient specific information during the administration of the drug thanks to an integrated approach that is “image guided”.

Drug-delivery triggered by an external stimulus

Different external stimuli such as electromagnetic waves (IR, UV of visible light) or magnetic and electrochemical forces can be used to trigger drug release from nanoparticles at the tumor site only, as reviewed by *Timko et al* [78]. As explained in the previous section one can locally increase the temperature inside a tumor,

hence temperature sensitive particles that are loaded with a chemotherapeutic will only release their content in areas where the temperature is increased. This temperature increase can be monitored by MR thermometry since hyperthermia is only allowed up to 42°C. Recently, shear stress has been described as an external trigger for drug-release from nanoparticles as well [79]. Such nanoparticles may be useful in tissues/tumors where blood vessels are obstructed.

Not only temperature can be used as an external trigger to induce drug release, pressure can be used as an external trigger as well and an interesting source of pressure can be ultrasound. This thesis will further explore the use of these systems as drug-delivery agents and more specifically their use for small molecule delivery.

ULTRASOUND-TRIGGERED DRUG-DELIVERY

Ultrasound

Sound is a longitudinal pressure wave, when the frequency of this wave exceeds 20 kHz, which is the typical human audible range, it is called ultrasound [80]. Ultrasound waves are generated by transducers which are piëzo-electric crystals producing elastic vibrations upon electrical stimulation. Basically, an ultrasound wave is characterized by alternating regions of high and low pressure, as shown in figure 6, and is usually transmitted in pulses (i.e. a defined number of cycles) with a certain frequency, amplitude and wavelength (defined in table 2).

Table 2: parameters characterizing the ultrasonic wave.

Frequency	f	Number of pressure cycles per sec (Hz)
Wavelength	λ	Time between two equivalent points in the waveform
Amplitude	A	Interval between both peak pressures (peak positive pressure (PPP) and peak negative pressure (PNP))

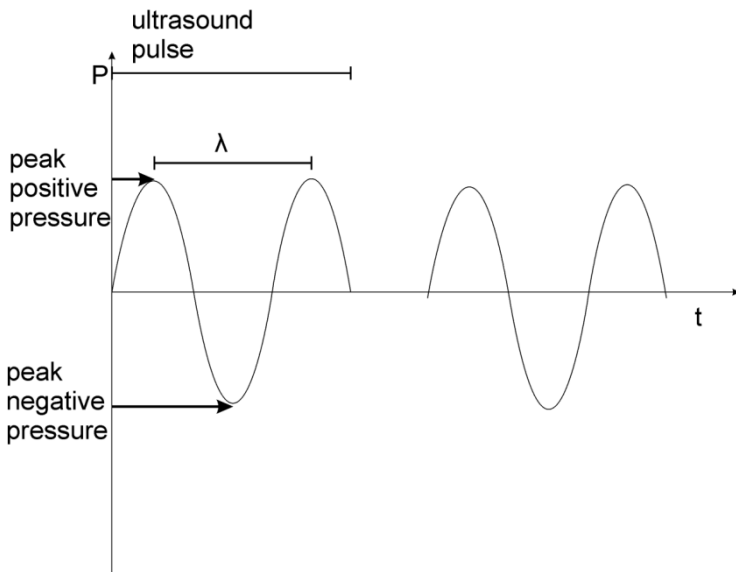


Figure 6: Schematic representation of an ultrasound wave.

Imaging

Ultrasounds most well-known application is medical imaging (e.g. echography). Ultrasound Imaging is based on the fact that an ultrasound wave becomes reflected by tissues with an acoustic impedance different from the surrounding medium [82]. This “scattered” ultrasound signal or “echo” can be received by the ultrasound transducer which can transform this received signal into an electrical signal. By measuring the time, amplitude and frequency interval between the outgoing pulse and the incoming scattered pulse one is able to build up an ultrasound image.

Ultrasound contrast imaging

Gramiak et al. [90] discovered in 1968 that the injection of agitated saline enhanced ultrasound echo contrast in the aortic root. The reason for this enhanced contrast was the presence of small gas bubbles due to agitation of the saline. This concept was further developed and resulted in the birth of imaging with ultrasound contrast agents (UCA's) or microbubbles. Ultrasound contrast imaging is based upon the fact that these compressible gas bubbles start to oscillate under influence of the ultrasonic pressure field (as explained below). Figure 7 gives an example of an ultrasound image of the same tumor obtained by “standard” ultrasound imaging and by ultrasound contrast imaging. This example indicates clearly, that standard imaging is more suitable for determining tissue delineation, there where contrast enhanced images show the internal blood flow in the tissue.

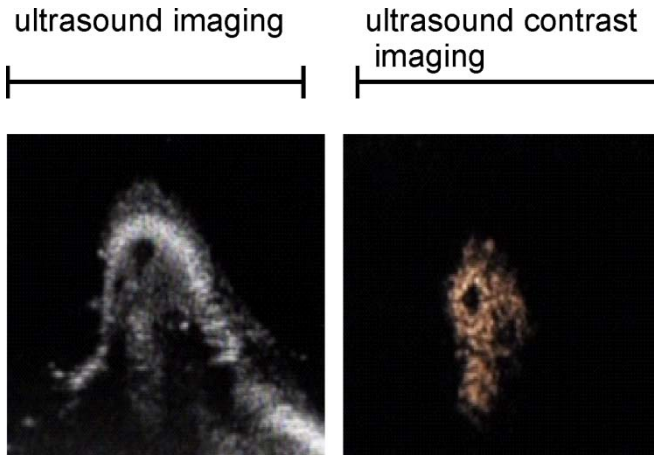


Figure 7: Example of an ultrasound image of a tumor with “standard” ultrasound imaging and contrast enhanced ultrasound imaging.

Biomedical and therapeutic applications of ultrasound

Ultrasound can be used in both diagnostic (ultrasound imaging) and therapeutic applications. The type of ultrasound used in these applications largely depends on the mechanical power of the ultrasound wave. This mechanical power is defined by the mechanical index (MI) and depends on frequency and pressure amplitude of the ultrasound pulse [81].

$$MI = \frac{\text{Peak Negative Pressure}}{\sqrt{\text{frequency}}}$$

As shown in figure 8 biomedical applications of ultrasound can be classified into 3 categories based upon the ultrasound frequency and hence MI used. A) high frequency (>3 MHz) ultrasound is usually used in diagnostic imaging (low MI) or therapeutic application using high acoustic pressures; b) In drug-delivery with ultrasound contrast agents and ultrasound contrast imaging usually frequencies

around 1 MHz are used and finally c) low frequency ultrasound is used in therapeutic applications using destructive shock waves.

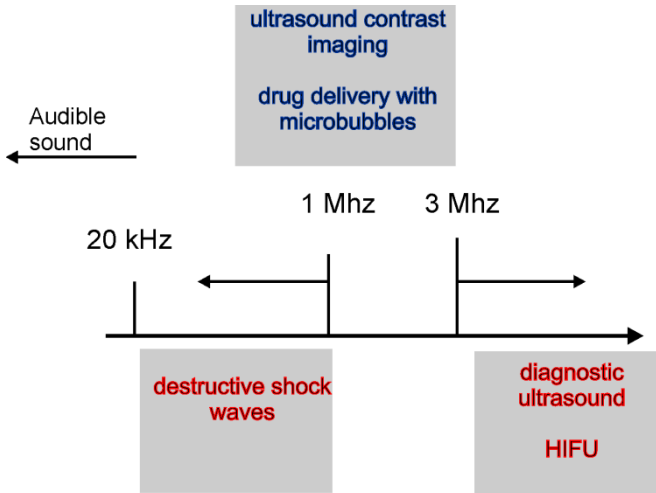


Figure 8: Ultrasound applications in function of frequency.

The higher the mechanical index, the more likely it becomes that ultrasound induces bio-effects in the affected tissue [83,84], which can be used therapeutically. Ultrasound energy can be absorbed by the tissue, which leads to heat formation [85]. For this purpose, high frequency ultrasound characterized by high acoustic pressures can be used to cause localized overheating and hence mechanical killing of cells without any surgery. Therefore, ultrasound needs to be focused into a small volume which causes strong mechanical (heating) effects in the focus of the ultrasound beam leaving other tissues unharmed. This technique is called high intensity focused ultrasound (HIFU) [86,87] and is used clinically for tumor ablation. As shown above low frequency ultrasound can be used for therapeutic application as well. Low frequency ultrasound produces high MI shock waves

that can dissolve bile or kidney stones [88] (e.g.: Lithotripsy). These high MI shock waves can be used to destroy drug-loaded liposomes as well [89].

Ultrasound contrast agents (microbubbles)

As shown in figure 9, microbubbles are micron sized (1-10 μm) gas bubbles (microbubbles) stabilized by a shell. An overview of commercially available products is given in table 3.

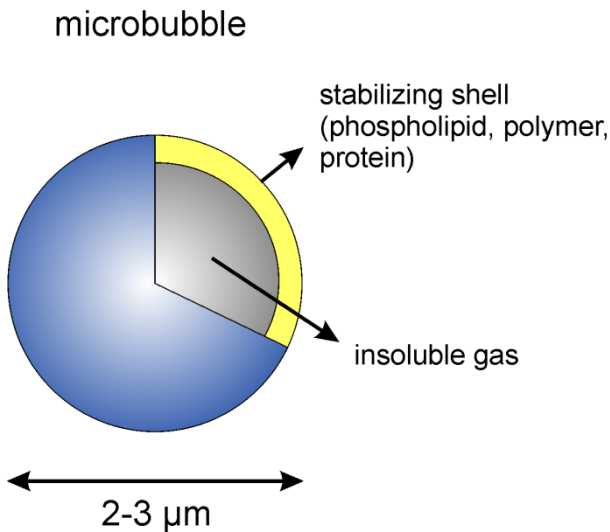


Figure 9: Schematic representation of an ultrasound contrast agent (UCA) or “microbubble”.

Gas bubbles are essentially unstable and without an appropriate coat they will immediately dissolve. The latter is a consequence of the surface tension between the gas-liquid interfaces. Surface tension (σ) results in an increased pressure at the concave sides of the microbubble and this ΔP (difference in hydrostatic pressure between the inside and the outside of the microbubble (with radius r)) is given by the Laplace equation.

$$\text{(Laplace equation)} \Delta P = \frac{2\sigma}{r}$$

This equation indeed tells us that in case of a relatively small microbubble (2 μm); an internal overpressure will exist unless one is able to decrease the surface tension. Indeed, as shown in table 3, most commercially available microbubbles do have a surfactant shell (albumin/phospholipid) and contain a hydrophobic gas that does not directly dissolve in the blood compartment. Both albumin and phospholipids have the advantage that these materials can spontaneously adsorb to newly formed hydrophobic gas bubbles, moreover these materials are elastic and withstand differences in pressure and hence are well suited for application as UCA's [91]. Polymeric shells (cross-linked albumin, poly-L-lactic acid (PLLA)) are stiffer and their response to ultrasound is more difficult to model [92].

Table 3: Overview of commercially available UCA's.

Name	Manufacturer	Year	Gas	Coating	Approved	Available
Optison	GE healthcare	1997	C ₃ F ₈	Human albumin	EU/USA	EU/USA
Sonovue	Bracco	2001	SF ₆	Phospholipids	EU, China, Korea, India, Hong Kong, Singapore	EU, China, Korea, India, Hong Kong, Singapore
Definity	Lantheus	2001	C ₃ F ₈	Phospholipids	Worldwide	Worldwide
Sonazoid	Amersham	2006	C ₄ F ₁₀	Phospholipids	Japan	Japan

Biophysical aspects of microbubbles

Microbubbles are suitable contrast agents because of their interaction with the ultrasound wave [93]. As schematically depicted in figure 10, the highly compressible microbubble will start to oscillate in response to the exerted cycles of positive and negative pressure. These oscillations itself produce ultrasonic signals that can be detected by the ultrasound transducer. Increased pressure will compress the microbubbles while negative pressure will induce rarefaction of the bubbles. This process, called cavitation, has been investigated in detail by *Bouakaz, Versluis and de Jong* [94] using high speed light microscopy. Driven at a pressure of at least tens of kilopascals it is observed that microbubble oscillations contain a wide range of frequency components [95,96]. Hence the echoes resulting from microbubble oscillation contain components that can be used for “microbubble-specific” imaging; hence it is indeed possible to observe single microbubbles in ultrasound contrast imaging. Cavitation at higher acoustical pressures will induce more violent microbubble oscillations, eventually resulting in microbubble destruction (so called ‘inertial cavitation’) [97]. Microbubble destruction can result in fragmentation of the microbubbles and/or in the dissolution of the encapsulated gas [98]. Inertial cavitation can be useful in imaging, this to evaluate blood flow abnormalities by means of destruction replenishment imaging [99].

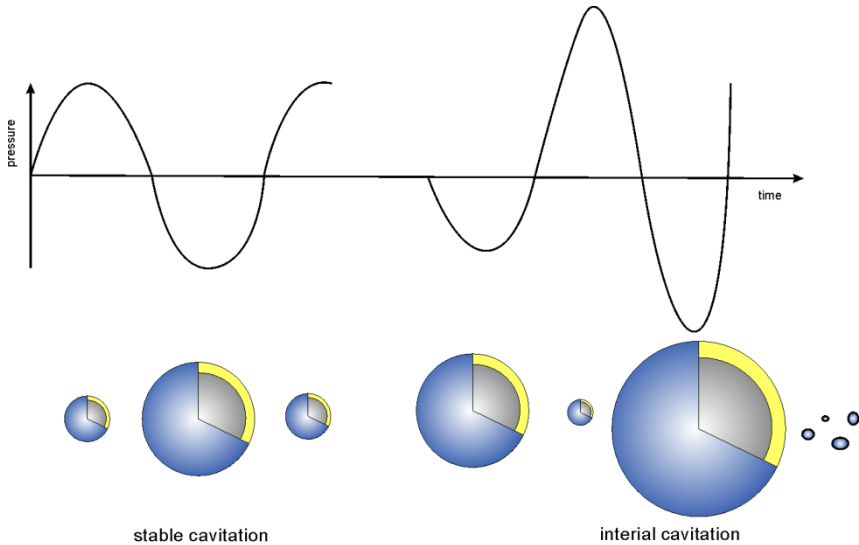


Figure 10: Schematic of the behavior of a microbubble during ultrasound application.

Microbubbles and ultrasonic drug-delivery

The use of microbubbles for drug-delivery has drawn attention to the scientific community when *Unger et al.* [100] reported on this type of drug-delivery in the late 1990s. Basically drug-delivery with microbubbles is based on inertial cavitation of the microbubble at high acoustic pressures which, as described earlier, results in the destruction or fragmentation of the microbubble. If a drug is located in the vicinity of a microbubble or is associated with it, a high pressure ultrasound wave can trigger a) release of drugs from the microbubbles and/or b) uptake of drugs into cells or tissues. Drug-associated microbubbles can be visualized with ultrasound imaging as well, hence enabling image-guided drug-delivery.

Having a closer look at the basic mechanisms behind ultrasonic drug-delivery with microbubbles one can easily envision that the ultrasound wave itself will

play a major role in this process. An ultrasound wave basically has 3 characteristics that may play a role in ultrasonic drug-delivery with microbubbles: a) the number of cycles per ultrasound pulse, b) the peak negative pressure and c) the frequency. In most ultrasonic drug-delivery related reports ultrasound waves with a frequency of around 1 MHz are used, the major reason being that the frequency which allows the microbubbles to respond upon ultrasound exposure indeed depends on the size of the bubbles which, in most studies, is between 1 and 3 μm . Peak negative pressure will define the type of microbubble cavitation (stable or inertial cavitation) as this pressure defines the mechanical index of the ultrasound wave.

If one compares ultrasound settings used in different studies where microbubbles are used for drug-delivery, the number of acoustic cycles (i.e. the number of acoustic oscillations per ultrasound pulse) applied to the samples differs significantly. As shown by *Mannaris et al.* [101], bubbles can oscillate at lower pressures when up to 100 cycles are used. However, when more cycles are applied combined with higher pressures, the bubbles become instantaneously destroyed. Subsequently, under such conditions one does no longer study microbubble related effects on drug-delivery but rather effects from ultrasound forces. These forces may play an important role in *in vivo* drug and gene delivery, although this still has not been investigated in detail. Studies on ultrasonic drug-delivery were indeed performed, reporting the use of 10000 cycles and high acoustic pressure [102]. This study clearly shows these settings do have an effect on drug-delivery and the effects generated will not be caused by imploding microbubbles.

Sonoporation

Cell membranes can become temporarily permeablized (so-called sonoporation) due to the localized mechanical effects related to microbubble implosion [103]. This process is believed to be an important driving force for drug-delivery with ultrasound and microbubbles. Different mechanisms of sonoporation are described in literature.

Membrane poration enabling direct cytoplasmic entry of molecules

At higher acoustic pressures (above a threshold of approximately 500 kPa [104]), the microbubbles will highly likely show inertial cavitation. This may result in the formation of shock waves and micro-jets directed towards the cell membranes [105-107]. Microjets are directed towards the cell surface because the hydrostatic pressure of the fluid surrounding the bubble will be stronger at the side of the microbubble opposite from the membrane (as shown in figure 11). These mechanical effects will induce shear stress on the cell membranes which may become locally and temporarily perforated. Different studies report that such effects may indeed porate cell membranes [104,108-110] and may facilitate the delivery of nanoparticles into the cytoplasm of cells [111,112].

Stimulation of endocytosis

In other studies lower acoustic pressures are used. Under these conditions, the bubble will “gently” oscillate and disturb its surroundings. If a microbubble is located near the cell membrane, these gentle oscillations may induce cell membrane instabilities which may stimulate endocytosis [104,113].

Temporal window upon sonoporation and two-step delivery protocols

Several research groups have demonstrated the existence of cell membrane pores upon applying ultrasound lasting in the order of seconds to minutes [110,114-116]. However, Yudina and colleagues recently claimed pore opening lasting up to 24h [117]. This was evidenced by evaluating the uptake of the small molecule Sytox Green as a function of time in sonoporated glioma cells. Although a further confirmation of the observations of *Yudina et al.* would be useful, these findings open up new perspectives for ultrasonic drug-delivery.

The same group also proposed a two-step delivery protocol combining the benefits of temperature sensitive liposomes (being liposomes that release their content at temperatures around 41°C) and sonoporation [118]. A proof of concept paper was published using TO-PRO-3 loaded thermosensitive liposomes and diagnostic microbubbles. Upon heating by high intensity focused ultrasound (HIFU), TO-PRO-3 became released from the temperature sensitive liposomes while the membrane permeabilization promoted the uptake of TO-PRO-3 in the cancer cells. Based upon their findings that drug uptake can last for several hours after sonoporation, the authors also suggested it could be even more advantageous first to sonoporate the tissue (taking advantage of the temporal window), followed by different applications of the nanoparticles.

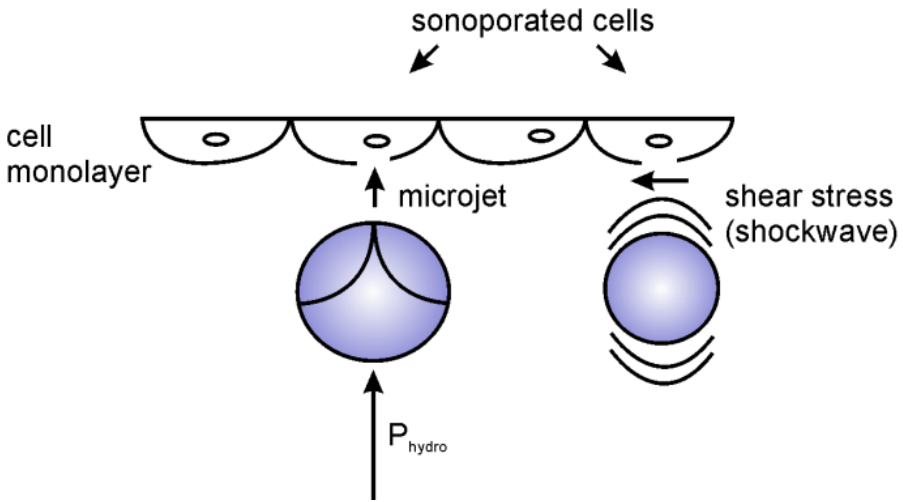


Figure 11: Bio-effects caused by microbubble implosion.

ADVANCES IN MICROBUBBLE DESIGN

As schematically represented in figure 12, four types of ‘microbubble modifications’ have been reported so far for ultrasonic drug-delivery: a) drug-loaded microbubbles; b) *in situ* formed microbubbles or nanodroplets; c) acoustically active liposomes (sometimes called ‘nanobubbles’) and d) targeted microbubbles.

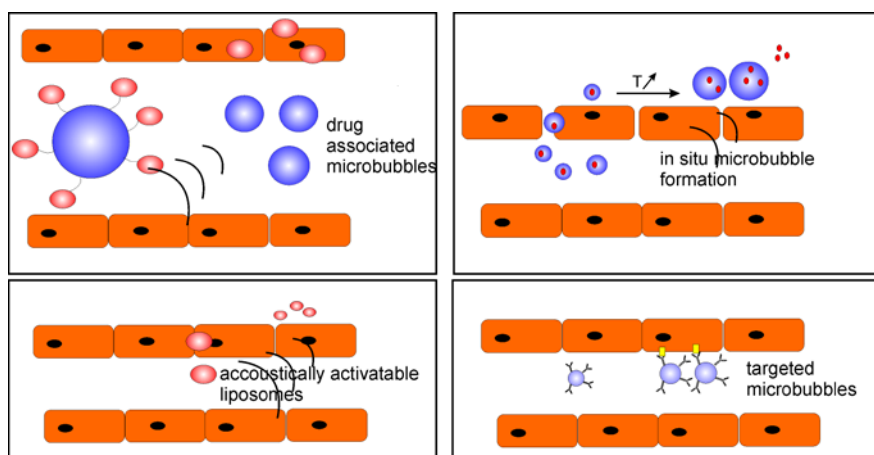


Figure 12: Schematic overview of microbubble modifications reported for ultrasonic drug-delivery. (A) envisions drug-loaded microbubbles releasing their associated payload upon insonation, (B) shows nanodroplets that are able to extravasate due to Enhanced Permeation and Retention (EPR) and form microbubbles after phase transition *in situ*, (C) depicts nano-sized acoustically active liposomes in tumor tissue and finally (D) shows microbubbles associated with a targeting moiety that adhere to target molecules in tissue expressing pathophysiologic epitopes.

Drug-loaded microbubbles

Since the 90s a number of research groups have attempted to design microbubbles which can carry a therapeutic payload. As shown in figure 13 drug-delivery from microbubbles by ultrasound is an attractive concept for various reasons; a) using low acoustic pressures the drug-loaded microbubbles can be visualized, being attractive for 'image guided drug-delivery'; b) many drugs, especially biological drugs like nucleic acids and proteins need to be protected from degradation upon administration, which can be accomplished by formulating them associated with microbubbles; c) the loading of the drugs into microbubbles can also prevent their uptake in untreated tissue (i.e. tissue that is not exposed to ultrasound) and thus reduce side-effects; d) upon applying ultrasound, both local drug release and cell membrane permeabilization (sonoporation) can occur.

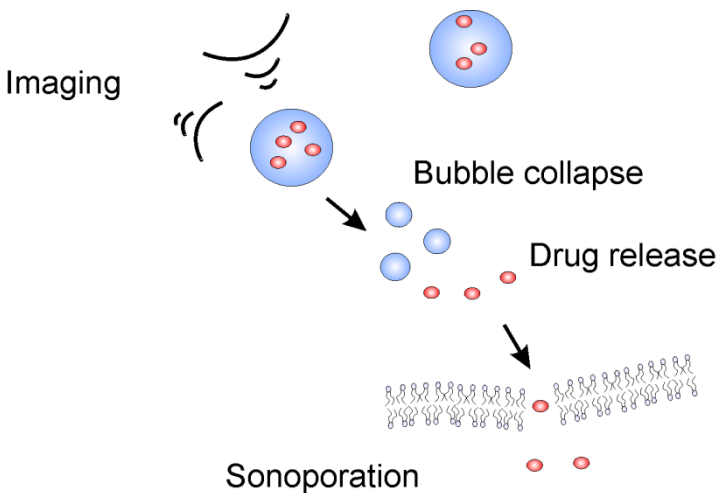


Figure 13: Schematic overview of the wide potential of drug-loaded microbubbles.

Figure 14 shows the most important strategies of drug loading in microbubbles. A straightforward strategy to load the microbubbles with drugs is associating them with the shell or more particularly with its building blocks. Another way of loading is by encapsulating the drug into an oil reservoir present in the core of the microbubble. Finally, drugs can also be packed into nanoparticles that are subsequently attached to the microbubble's surface. The following section gives an update on the recent progress in the design of drug-loaded microbubbles. For a complete overview on drug-loaded microbubbles we refer to *Lentacker et al.* and *Tinkov et al.* [119,120].

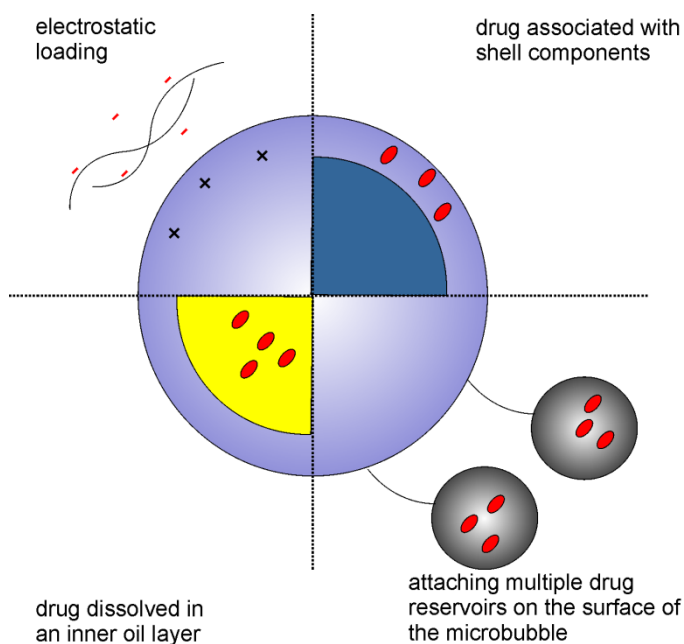


Figure 14: Schematic overview of the most important ways of drug loading into a microbubble.

Loading through electrostatic binding

A first strategy to attach therapeutics to the microbubble shell is through electrostatic interactions, initially explored to load microbubbles with pDNA. As an example, *Frenkel et al.* [121] used albumin-shelled microbubbles as a template for pDNA attachment. A layer-by-layer approach can be used to alternately deposit cationic polymers and anionic nucleic acids on the microbubble shell, which clearly improves the electrostatic loading of the microbubbles with nucleic acids [122]. *Sirsi et al.* [123] recently reported on lipid-shelled microbubbles that were covalently coated with PolyEthyleneGlycol-PolyEthyleneImine (PEG-PEI) copolymers, followed by the electrostatic deposition of pDNA onto such cationically charged microbubbles. Ultrasound induced gene expression in tumor tissue was clearly observed, being significantly higher than the gene expression in control samples being untreated tumors. Similar results were obtained with plasmid conjugated microbubbles, that showed a significant increase in gene transfection in smooth muscle cells as well [124].

Tinkov et al. [125] described an attractive method to complex Doxorubicin (DOX) onto microbubbles using electrostatic interactions. They prepared an anionic microbubble by incorporating an anionic phospholipid 1,2-dipalmitoyl-sn-glycero-3-phospho-1'-rac-glycerol (DPPG) in the shell which can form a complex with the cationic glycane-group in the DOX molecule. This method showed efficient incorporation of DOX into the microbubbles' shell (up to 40 µg DOX per ml microbubble dispersion); tumor cell destruction was obtained after injection of these bubbles in rats bearing pancreatic tumors and exposure of the tumor to ultrasound. The same strategy was recently used by *Ting et al.* [126] to prepare 1,3-bis(chloroethyl)-1-nitrosourea (BCNU) loaded microbubbles. Focused

ultrasound was used to locally implode BCNU carrying microbubbles at the blood brain barrier (BBB) of rats. This resulted in a significantly higher uptake of BCNU in glioma tumors implanted in the rats and a slower tumor progression when compared to BBB disruption with microbubbles and ultrasound co-administered with BCNU.

A serious drawback of electrostatic drug loading of microbubbles could be premature release of the drug in the body. Indeed, once injected in the bloodstream charged blood components like serum albumin can compete or interact with the charged microbubble shell. This can result in a release of the attached drug or in the formation of large aggregates which can block the vasculature [127]. Sirsi and colleagues also showed that charged microbubbles can influence circulation times by adhering nonspecifically to the vasculature close to the injection place. This can have a significant impact on the amount of microbubbles reaching the target tissue.

Drug reservoirs

As an alternative, some research groups have tried to create a drug reservoir inside the microbubble. One example is the use of double emulsion techniques to obtain polymer coated oil-filled microcapsules [128]. Another technique, as described by *Tartis et al.* [129], involves the incorporation of a drug-containing oil-phase within lipid-coated microbubbles. These oil filled microbubbles retain their responsiveness to ultrasound and can be destructed at higher ultrasound intensities thereby releasing their content. The fact that only lipid-soluble drugs can be incorporated however, limits the use of such systems.

Another, more versatile method to prepare drug-loaded microbubbles, is the attachment of multiple drug reservoirs (i.e. drug-loaded nanoparticles) to the microbubbles' surface. The major benefit of this concept is that it creates a higher drug loading capacity, as plenty of small drug-filled pods are attached to the surface. Another advantage is that different types of therapeutics can become stored in microbubbles. Liposomes, for example, can be loaded with both hydrophilic and hydrophobic drugs and can carry larger molecules like pDNA, siRNA or mRNA [130]. Biotinylated lipid coated bubbles can be easily prepared by introducing a phospholipid containing a PEG-biotin group into the microbubble shell. Such biotin containing bubbles can be incubated with avidin, enabling the subsequent attachment of biotinylated (drug containing) nanoparticles. Our group showed that this concept can be used to enhance the uptake and therapeutic efficiency of both small (DOX) [131] and high molecular weight drugs (pDNA, siRNA, mRNA) [112,132,133].

Ultrasound responsive liposomes (nanobubbles)

A major disadvantage of microbubbles as drug carriers is their relatively large size (1-6 μm). Due to this feature, microbubbles have a rather short half-life, i.e. in the order of minutes [130,134]. Upon injection such microbubbles will circulate a few times, but will inevitably get stuck in the lungs where gas exchange occurs. Consequently, microbubble-ultrasound triggered drug-delivery will be mainly restricted to cardiovascular targets and to tumor endothelia.

To solve this problem, several papers report on so-called nanobubbles [135,136], also called 'bubble liposomes' [137], which are smaller than 1 μm , combining the benefits of a liposome (small size, long circulation time) with ultrasound responsiveness. These small bubbles are generally prepared by sonicating

liposomes in the presence of fluorinated gases. With these nanobubbles successful delivery of pDNA, siRNA and coumarin [138] has been demonstrated both in *in vitro* and *in vivo* models.

In situ generation of microbubbles from nanodroplets

A very intelligent suggestion for circumventing the short half-life of drug-loaded microbubbles is the design of nanoscopic droplets based on perfluorocarbons with a relatively low boiling point (e.g. perfluoropentane or perfluorohexane). These so-called 'nanodroplets' can convert into their gaseous form upon ultrasound exposure. The advantage of the use of liquid perfluorocarbons is that they can be emulsified in water when stabilized by an appropriate surfactant (e.g. pluronic, lipids) [139-141]. Such nanodroplets are typically smaller than 200nm, which allows them to extravasate from the leaky tumor vasculature. [142]. When the tumor tissue is subsequently treated with ultrasound, a liquid to gas phase transition occurs due to a local temperature increase in combination with the low pressure phase generated by the ultrasound [143]. As a consequence, ultrasound responsive microbubbles are formed *in situ*.

Alternatively, perfluorocarbons with a low boiling point can be encapsulated in inorganic mesoporous silica-nanoparticles which can incorporate various types of drugs as well [144][145]. Perfluorocarbon-drug-loaded silica-nanoparticles may well provide a solution for the different challenges we are facing with regard to drug-loaded ultrasound contrast agents, namely sufficient extravasation in tissues and high loading of (multiple) compounds.

Targeted microbubbles for drug-delivery

Recently there is growing interest in the use of ‘targeted microbubbles’ for diagnostic molecular imaging. Such microbubbles should be able to interact with molecules that become expressed in specific pathologies. In this case antibodies [146] or even nanobodies [147] are coupled to the surface of the bubbles, typically through avidin-biotin coupling [148]. Aptamers, nucleic acids that show affinity for specific molecules, can be used as targeting moieties as well [149]. Aptamer-loaded nanobubbles [150] have been described and show potential for targeting specific cell types. Clearly, targeted microbubbles can be of interest for drug-delivery as well as the amount of drug closely located near the target tissue may become enhanced [151].

Therapeutic moieties benefiting from ultrasound-triggered delivery

The therapeutic moieties reported in the context of ultrasonic delivery can be divided in three different groups (Figure 15): a) low molecular weight drugs like some anticancer drugs, b) large biomolecules like genetic drugs and proteins and, finally, c) drugs encapsulated in nanoparticles.

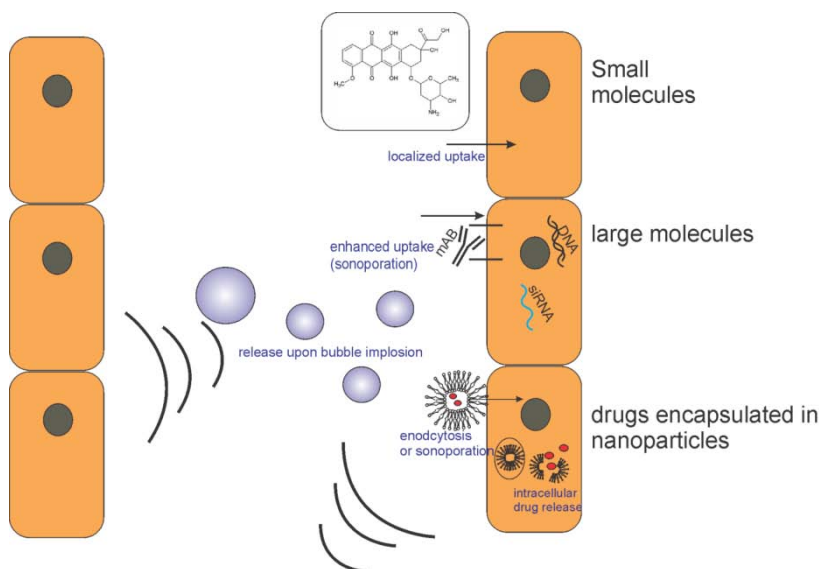


Figure 15: Schematic representation of different therapeutic moieties which can be delivered using microbubbles and ultrasound.

Depending on its characteristics a drug can benefit from ultrasound triggered drug-delivery differently, as ultrasound and microbubbles will either enhance the uptake of a molecule or particle that shows limited uptake or it will localize their bioavailability.

Small therapeutic molecules

The “small therapeutics” used in ultrasonic drug-delivery studies are mostly antineoplastic drugs like DOX or Paclitaxel. Upon injection such low molecular weight drugs will distribute throughout the body and easily accumulate in different cell types, causing cytotoxic (side) effects. The most important reason why these drugs would benefit from ultrasonic drug-delivery is the fact that drug uptake would become limited to the ultrasound treated tissue. A more efficient

localized delivery to the tumor can substantially reduce the required dose and lower side effects.

Large therapeutic molecules

Large molecules like nucleic acids (pDNA, siRNA, mRNA) and proteins are under investigation for ultrasonic delivery as well. Unlike small molecules these macromolecules show inefficient uptake in target tissues. As Figure 15 envisions, ultrasound mediated microbubble destruction can be used to locally permeabilize cell membranes which should enhance the uptake of large molecules.

The most important studies report on the delivery of genes into cells, *in vitro* and/or *in vivo*. Most studies involve pDNA, associated with a microbubble [152] or co-administered [153,154] with them. Due to its negative electrostatic loading pDNA will not penetrate into cells, but if it is located near a microbubble imploding in the vicinity of a cell it may profit from the temporal permeabilization of the cell membrane (sonoporation) [116].

Drugs encapsulated in nanoparticles

Not only single molecules can benefit from ultrasonic delivery. Several publications have shown that microbubbles and ultrasound can be used to improve the extravasation of a variety of nanoparticles that can be loaded with a drug or have a therapeutic effect themselves. PLGA nanoparticles [155], magnetic nanoparticles [156], liposomes and lipoplexes [157], gold nanoparticles and silica nanoparticles [158] were used in combination with microbubbles and ultrasound. Through encapsulating the drug molecules in nanoscopic particles they become well protected against degradation, which is a major challenge, especially for biological drugs.

Preclinical evidence

Searching for *in vivo* evidence for ultrasonic drug-delivery with microbubbles, a difference is observed between the number of studies reporting the co-administration approach (i.e. the co-administration of drugs and microbubbles), and the number of reports in which drug-loaded microbubbles are studied.

There is clear preclinical evidence available in literature with regard to the co-administration approach. Many studies, as e.g. performed by *Hynynen, McDannold* and co-workers, show enhanced drug-delivery after injection of diagnostic microbubbles (Sonovue® or Definity®) and applying ultrasound allowing bubbles to implode at the target site. For example, enhanced drug [159] or Magnetic Resonance (MR) contrast-agent [160] delivery into the brain of rats has been shown. In these brain delivery studies, a transient disruption of the Blood Brain Barrier (BBB), induced by microbubble implosion has been reported. An enhanced delivery of Evans blue in muscles [161] has been shown as well following the co-administration approach. The progress in this particular field has been reviewed by *Vykhodtseva et al.*[162].

The number of *in vivo* studies with drug-loaded microbubbles is rather limited, is probably due to the fact that 'loading microbubbles with drugs' is a recent strategy in ultrasonic drug-delivery. Indeed, while in co-administration approved commercial (clinically used) microbubbles can be used, custom-made (still often poorly characterized) drug-loaded microbubbles need to be designed. *Rapoport et al.* showed reduced tumor growth with Paclitaxel-loaded nanodroplets [163]. *Tinkov* [164] showed enhanced DOX-uptake in tumors with DOX-loaded microbubbles. Acoustically active pDNA bubble liposomes resulted in enhanced gene transfection in the mouse abdomen [165]. Finally, *Müller et al.* [166] reported

an improved gene transduction in the heart of rats using microbubbles with adeno-associated viral vectors electrostatically attached to the surface of the bubbles.

REFERENCES

- [1] C. Leaf, Why we're losing the war on cancer and how to win it, *Fortune*, 149 (2004) 76
- [2] G.L.G. Miklos, The Human Cancer Genome Project - one more misstep in the war on cancer, *Nature Biotechnology*, 23 (2005) 535-537.
- [3] J. Ferlay, P. Autier, M. Boniol, M. Heanue, M. Colombet, and P. Boyle, Estimates of the cancer incidence and mortality in Europe in 2006, *Annals of Oncology*, 18 (2007) 581-592.
- [4] N.J. Meropol and K.A. Schulman, Cost of cancer care: Issues and implications, *Journal of Clinical Oncology*, 25 (2007) 180-186.
- [5] D.P. Cahill, K.W. Kinzler, B. Vogelstein, and C. Lengauer, Genetic instability and darwinian selection in tumours, *Trends Cell Biol.*, 9 (1999) M57-M60.
- [6] D. Radisky, C. Hagios, and M.J. Bissell, Tumors are unique organs defined by abnormal signaling and context, *Semin. Cancer Biol.*, 11 (2001) 87-95.
- [7] D. Hanahan and R.A. Weinberg, The hallmarks of cancer, *Cell*, 100 (2000) 57-70.
- [8] D. Hanahan and R.A. Weinberg, Hallmarks of cancer: the next generation, *Cell*, 144 (2011) 646-674.
- [9] M. Arbyn, S. de Sanjose, M. Saraiya, M. Sideri, J. Palefsky, C. Lacey, M. Gillison, L. Bruni, G. Ronco, N. Wentzensen, J. Brotherton, Y.L. Qiao, L. Denny, J. Bornstein, L. Abramowitz, A. Giuliano, M. Tommasino, and J. Monsonogo, EUROGIN 2011 roadmap on prevention and treatment of HPV-related disease, *International Journal of Cancer*, 131 (2012) 1969-1982.
- [10] A.E. Grulich, M.T. van Leeuwen, M. Falster, and C.M. Vajdic, Incidence of cancers in people with HIV/AIDS compared with immunosuppressed transplant recipients: a meta-analysis, *Lancet*, 370 (2007) 59-67.
- [11] G.L. Semenza, Tumor metabolism: cancer cells give and take lactate, *J. Clin. Invest*, 118 (2008) 3835-3837.
- [12] T. Bogenrieder and M. Herlyn, Cell-surface proteolysis, growth factor activation and intercellular communication in the progression of melanoma, *Crit Rev. Oncol. Hematol.*, 44 (2002) 1-15.
- [13] T. Bogenrieder and M. Herlyn, Axis of evil: molecular mechanisms of cancer metastasis, *Oncogene*, 22 (2003) 6524-6536.
- [14] T. Bogenrieder and M. Herlyn, The molecular pathology of cutaneous melanoma, *Cancer Biomark.*, 9 (2010) 267-286.
- [15] R. O'Connor, M. Clynes, P. Dowling, N. O'Donovan, and L. O'Driscoll, Drug resistance in cancer - searching for mechanisms, markers and therapeutic agents, *Expert Opinion on Drug Metabolism & Toxicology*, 3 (2007) 805-817.
- [16] P. Carmeliet and R.K. Jain, Angiogenesis in cancer and other diseases, *Nature*, 407 (2000) 249-257.

- [17] P. Carmeliet and R.K. Jain, Molecular mechanisms and clinical applications of angiogenesis, *Nature*, 473 (2011) 298-307.
- [18] R.K. Jain and P.F. Carmeliet, Vessels of death or life, *Sci. Am.*, 285 (2001) 38-45.
- [19] M. Potente, H. Gerhardt, and P. Carmeliet, Basic and therapeutic aspects of angiogenesis, *Cell*, 146 (2011) 873-887.
- [20] M. Schaefer and S. Werner, Cancer as an overhealing wound: an old hypothesis revisited, *Nature Reviews Molecular Cell Biology*, 9 (2008) 628-638.
- [21] L. Yang, Y. Pang, and H.L. Moses, TGF-beta and immune cells: an important regulatory axis in the tumor microenvironment and progression, *Trends in Immunology*, 31 (2010) 220-227.
- [22] B.Z. Qian and J.W. Pollard, Macrophage Diversity Enhances Tumor Progression and Metastasis, *Cell*, 141 (2010) 39-51.
- [23] N. Kartner, J.R. Riordan, and V. Ling, Cell-Surface P-Glycoprotein Associated with Multidrug Resistance in Mammalian-Cell Lines, *Science*, 221 (1983) 1285-1288.
- [24] T. Brabletz, A. Jung, S. Spaderna, F. Hlubek, and T. Kirchner, Opinion - Migrating cancer stem cells - an integrated concept of malignant tumour progression, *Nature Reviews Cancer*, 5 (2005) 744-749.
- [25] C.L. Chaffer and R.A. Weinberg, A Perspective on Cancer Cell Metastasis, *Science*, 331 (2011) 1559-1564.
- [26] C. Coghlin and G.I. Murray, Current and emerging concepts in tumour metastasis, *J. Pathol.*, 222 (2010) 1-15.
- [27] K.R. Hess, G.R. Varadhachary, S.H. Taylor, W. Wei, M.N. Raber, R. Lenzi, and J.L. Abbruzzese, Metastatic patterns in adenocarcinoma, *Cancer*, 106 (2006) 1624-1633.
- [28] G.D. Roodman, Mechanisms of disease: Mechanisms of bone metastasis, *New England Journal of Medicine*, 350 (2004) 1655-1664.
- [29] L.R. Patel, D.F. Camacho, Y. Shiozawa, K.J. Pienta, and R.S. Taichman, Mechanisms of cancer cell metastasis to the bone: a multistep process, *Future Oncology*, 7 (2011) 1285-1297.
- [30] K. Kawada and M.M. Taketo, Significance and Mechanism of Lymph Node Metastasis in Cancer Progression, *Cancer Research*, 71 (2011) 1214-1218.
- [31] T. Liu, Y. Wang, S. Chen, and Y. Sun, An updated meta-analysis of adjuvant chemotherapy after curative resection for gastric cancer, *Ejso*, 34 (2008) 1208-1216.
- [32] O. Holmberg, H. Huiizenga, M.H. Idzes, J.V. Lebesque, R.E. Vijlbrief, and B.J. Mijnheer, In vivo determination of the accuracy of field matching in breast cancer irradiation using an electronic portal imaging device, *Radiother. Oncol.*, 33 (1994) 157-166.
- [33] O. Holmberg, Accident prevention in radiotherapy, *Biomed. Imaging Interv. J.*, 3 (2007) e27.
- [34] O. Holmberg, J. Malone, M. Rehani, D. McLean, and R. Czarwinski, Current issues and actions in radiation protection of patients, *Eur. J. Radiol.*, 76 (2010) 15-19.
- [35] D. Wang and S.J. Lippard, Cellular processing of platinum anticancer drugs, *Nat. Rev. Drug Discov.*, 4 (2005) 307-320.
- [36] R.H. Blum and S.K. Carter, Adriamycin. A new anticancer drug with significant clinical activity, *Ann. Intern. Med.*, 80 (1974) 249-259.
- [37] S.S. COHEN, J.G. FLAKS, H.D. BARNER, M.R. Loeb, and J. LICHTENSTEIN, THE MODE OF ACTION OF 5-FLUOROURACIL AND ITS DERIVATIVES, *Proc. Natl. Acad. Sci. U. S. A.*, 44 (1958) 1004-1012.

- [38] S. Hatse, C.E. De, and J. Balzarini, Role of antimetabolites of purine and pyrimidine nucleotide metabolism in tumor cell differentiation, *Biochem. Pharmacol.*, 58 (1999) 539-555.
- [39] E. Idelevich, S. Man, K. Lavrenkov, A. Gluzman, D.B. Geffen, and A. Shani, Irinotecan combined with bolus 5-fluorouracil and folinic acid for metastatic colorectal cancer: is this really a dangerous treatment?, *J. Chemother.*, 16 (2004) 487-490.
- [40] W.J. Gradishar, S. Tjulandin, N. Davidson, H. Shaw, N. Desai, P. Bhar, M. Hawkins, and J. O'Shaughnessy, Phase III trial of nanoparticle albumin-bound paclitaxel compared with polyethylated castor oil-based paclitaxel in women with breast cancer, *J. Clin. Oncol.*, 23 (2005) 7794-7803.
- [41] M.A. Jordan, R.H. Himes, and L. Wilson, Comparison of the effects of vinblastine, vincristine, vindesine, and vinepidine on microtubule dynamics and cell proliferation in vitro, *Cancer Res.*, 45 (1985) 2741-2747.
- [42] M.A. Jordan, D. Thrower, and L. Wilson, Mechanism of inhibition of cell proliferation by Vinca alkaloids, *Cancer Res.*, 51 (1991) 2212-2222.
- [43] E.C. Hayden, Personalized cancer therapy gets closer, *Nature*, 458 (2009) 131-132.
- [44] S.L. Moulder, F.M. Yakes, S.K. Muthuswamy, R. Bianco, J.F. Simpson, and C.L. Arteaga, Epidermal growth factor receptor (HER1) tyrosine kinase inhibitor ZD1839 (Iressa) inhibits HER2/neu (erbB2)-overexpressing breast cancer cells in vitro and in vivo, *Cancer Research*, 61 (2001) 8887-8895.
- [45] D.J. Slamon, B. Leyland-Jones, S. Shak, H. Fuchs, V. Paton, A. Bajamonde, T. Fleming, W. Eiermann, J. Wolter, M. Pegram, J. Baselga, and L. Norton, Use of chemotherapy plus a monoclonal antibody against HER2 for metastatic breast cancer that overexpresses HER2, *New England Journal of Medicine*, 344 (2001) 783-792.
- [46] E.H. Romond, E.A. Perez, J. Bryant, V.J. Suman, C.E. Geyer, N.E. Davidson, E. Tan-Chiu, S. Martino, S. Paik, P.A. Kaufman, S.M. Swain, T.M. Pisansky, L. Fehrenbacher, L.A. Kutteh, V.G. Vogel, D.W. Visscher, G. Yothers, R.B. Jenkins, A.M. Brown, S.R. Dakhil, E.P. Mamounas, W.L. Lingle, P.M. Klein, J.N. Ingle, and N. Wolmark, Trastuzumab plus adjuvant chemotherapy for operable HER2-positive breast cancer, *New England Journal of Medicine*, 353 (2005) 1673-1684.
- [47] M.J. Piccart-Gebhart, M. Procter, B. Leyland-Jones, A. Goldhirsch, M. Untch, I. Smith, L. Gianni, J. Baselga, R. Bell, C. Jackisch, D. Cameron, M. Dowsett, C.H. Barrios, G. Steger, C.S. Huang, M. Andersson, M. Inbar, M. Lichinitser, I. Lang, U. Nitz, H. Iwata, C. Thomssen, C. Lohrich, T.M. Suter, J. Ruschoff, T. Suto, V. Greatorex, C. Ward, C. Strahle, E. McFadden, M.S. Dolci, and R.D. Gelber, Trastuzumab after adjuvant chemotherapy in HER2-positive breast cancer, *New England Journal of Medicine*, 353 (2005) 1659-1672.
- [48] M.A. Cobleigh, C.L. Vogel, D. Tripathy, N.J. Robert, S. Scholl, L. Fehrenbacher, J.M. Wolter, V. Paton, S. Shak, G. Lieberman, and D.J. Slamon, Multinational study of the efficacy and safety of humanized anti-HER2 monoclonal antibody in women who have HER2-overexpressing metastatic breast cancer that has progressed after chemotherapy for metastatic disease, *Journal of Clinical Oncology*, 17 (1999) 2639-2648.
- [49] M.D. Pegram, A. Lipton, D.F. Hayes, B.L. Weber, J.M. Baselga, D. Tripathy, D. Baly, S.A. Baughman, T. Twaddell, J.A. Glaspy, and D.J. Slamon, Phase II study of receptor-enhanced chemosensitivity using recombinant humanized anti-p185(HER2/neu) monoclonal antibody plus cisplatin in patients with HER2/neu-overexpressing metastatic breast cancer refractory to chemotherapy treatment, *Journal of Clinical Oncology*, 16 (1998) 2659-2671.
- [50] H. Idani, J. Matsuoka, T. Yasuda, K. Kobayashi, and N. Tanaka, Intra-tumoral injection of doxorubicin (adriamycin) encapsulated in liposome inhibits tumor growth, prolongs

survival time and is not associated with local or systemic side effects, *International Journal of Cancer*, 88 (2000) 645-651.

[51] C. Collins and P.L. Weiden, Cardiotoxicity of 5-Fluorouracil, *Cancer Treatment Reports*, 71 (1987) 733-736.

[52] B. Sumer and J. Gao, Theranostic nanomedicine for cancer, *Nanomedicine. (Lond)*, 3 (2008) 137-140.

[53] M. Ferrari, Cancer nanotechnology: opportunities and challenges, *Nat. Rev. Cancer*, 5 (2005) 161-171.

[54] V.P. Torchilin, Multifunctional nanocarriers, *Adv. Drug Deliv. Rev.*, 58 (2006) 1532-1555.

[55] J.M. Harris and R.B. Chess, Effect of pegylation on pharmaceuticals, *Nat. Rev. Drug Discov.*, 2 (2003) 214-221.

[56] A. Gabizon, M. Chemla, D. Tzemach, A.T. Horowitz, and D. Goren, Liposome longevity and stability in circulation: effects on the in vivo delivery to tumors and therapeutic efficacy of encapsulated anthracyclines, *J. Drug Target*, 3 (1996) 391-398.

[57] H. Maeda, L.W. Seymour, and Y. Miyamoto, Conjugates of Anticancer Agents and Polymers - Advantages of Macromolecular Therapeutics In vivo, *Bioconjugate Chemistry*, 3 (1992) 351-362.

[58] H. Maeda, J. Wu, T. Sawa, Y. Matsumura, and K. Hori, Tumor vascular permeability and the EPR effect in macromolecular therapeutics: a review, *Journal of Controlled Release*, 65 (2000) 271-284.

[59] Y. Matsumura and H. Maeda, A New Concept for Macromolecular Therapeutics in Cancer-Chemotherapy - Mechanism of Tumoritropic Accumulation of Proteins and the Antitumor Agent Smancs, *Cancer Research*, 46 (1986) 6387-6392.

[60] T. Lammers, W.E. Hennink, and G. Storm, Tumour-targeted nanomedicines: principles and practice, *Br. J. Cancer*, 99 (2008) 392-397.

[61] J.F. Kukowska-Latallo, K.A. Candido, Z. Cao, S.S. Nigavekar, I.J. Majoros, T.P. Thomas, L.P. Balogh, M.K. Khan, and J.R. Baker, Jr., Nanoparticle targeting of anticancer drug improves therapeutic response in animal model of human epithelial cancer, *Cancer Res.*, 65 (2005) 5317-5324.

[62] A. Gabizon, A.T. Horowitz, D. Goren, D. Tzemach, H. Shmeeda, and S. Zalipsky, In vivo fate of folate-targeted polyethylene-glycol liposomes in tumor-bearing mice, *Clin. Cancer Res.*, 9 (2003) 6551-6559.

[63] A. Gabizon, A.T. Horowitz, D. Goren, D. Tzemach, F. Mandelbaum-Shavit, M.M. Qazen, and S. Zalipsky, Targeting folate receptor with folate linked to extremities of poly(ethylene glycol)-grafted liposomes: in vitro studies, *Bioconjug. Chem.*, 10 (1999) 289-298.

[64] V.P. Torchilin, Recent advances with liposomes as pharmaceutical carriers, *Nat. Rev. Drug Discov.*, 4 (2005) 145-160.

[65] D. Hoekstra, J. Rejman, L. Wasungu, F. Shi, and I. Zuhorn, Gene delivery by cationic lipids: in and out of an endosome, *Biochem. Soc. Trans.*, 35 (2007) 68-71.

[66] L. Wasungu and D. Hoekstra, Cationic lipids, lipoplexes and intracellular delivery of genes, *J. Control Release*, 116 (2006) 255-264.

[67] A. Gabizon, D. Tzemach, L. Mak, M. Bronstein, and A.T. Horowitz, Dose dependency of pharmacokinetics and therapeutic efficacy of pegylated liposomal doxorubicin (DOXIL) in murine models, *J. Drug Target*, 10 (2002) 539-548.

[68] O. Diou, N. Tsapis, and E. Fattal, Targeted nanotheranostics for personalized cancer therapy, *Expert. Opin. Drug Deliv.*, (2012).

- [69] O. Diou, N. Tsapis, C. Giraudeau, J. Valette, C. Gueutin, F. Bourasset, S. Zanna, C. Vauthier, and E. Fattal, Long-circulating perfluorooctyl bromide nanocapsules for tumor imaging by 19FMRI, *Biomaterials*, 33 (2012) 5593-5602.
- [70] C.C. Wagner and O. Langer, Approaches using molecular imaging technology - use of PET in clinical microdose studies, *Advanced Drug Delivery Reviews*, 63 (2011) 539-546.
- [71] P. Lee, P. Kupelian, J. Czernin, and P. Ghosh, Current concepts in F18 FDG PET/CT-based radiation therapy planning for lung cancer, *Front Oncol.*, 2 (2012) 71.
- [72] E. Terreno, F. Uggeri, and S. Aime, Image guided therapy: The advent of theranostic agents, *Journal of Controlled Release*, 161 (2012) 328-337.
- [73] T. Lammers, S. Aime, W.E. Hennink, G. Storm, and F. Kiessling, Theranostic nanomedicine, *Acc. Chem. Res.*, 44 (2011) 1029-1038.
- [74] T. Lammers, F. Kiessling, W.E. Hennink, and G. Storm, Nanotheranostics and image-guided drug delivery: current concepts and future directions, *Mol. Pharm.*, 7 (2010) 1899-1912.
- [75] F. Kiessling, S. Fokong, P. Koczera, W. Lederle, and T. Lammers, Ultrasound microbubbles for molecular diagnosis, therapy, and theranostics, *J. Nucl. Med.*, 53 (2012) 345-348.
- [76] M. De Smet, S. Langereis, S. van den Bosch, and H. Grull, Temperature-sensitive liposomes for doxorubicin delivery under MRI guidance, *J. Control Release*, 143 (2010) 120-127.
- [77] S. Langereis, J. Keupp, J.L. van Velthoven, I.H. de Roos, D. Burdinski, J.A. Pikkemaat, and H. Grull, A temperature-sensitive liposomal 1H CEST and 19F contrast agent for MR image-guided drug delivery, *J. Am. Chem. Soc.*, 131 (2009) 1380-1381.
- [78] B.P. Timko, T. Dvir, and D.S. Kohane, Remotely triggerable drug delivery systems, *Adv. Mater.*, 22 (2010) 4925-4943.
- [79] N. Korin, M. Kanapathipillai, B.D. Matthews, M. Crescente, A. Brill, T. Mammoto, K. Ghosh, S. Jurek, S.A. Bencherif, D. Bhatta, A.U. Coskun, C.L. Feldman, D.D. Wagner, and D.E. Ingber, Shear-Activated Nanotherapeutics for Drug Targeting to Obstructed Blood Vessels, *Science*, 337 (2012) 738-742.
- [80] P. Hauff, M. Reinhardt, and S. Foster, Ultrasound basics, *Handb. Exp. Pharmacol.*, (2008) 91-107.
- [81] J. Wu and W.L. Nyborg, Ultrasound, cavitation bubbles and their interaction with cells, *Adv. Drug Deliv. Rev.*, 60 (2008) 1103-1116.
- [82] S.L. Mulvagh, A.N. DeMaria, S.B. Feinstein, P.N. Burns, S. Kaul, J.G. Miller, M. Monaghan, T.R. Porter, L.J. Shaw, and F.S. Villanueva, Contrast echocardiography: current and future applications, *J. Am. Soc. Echocardiogr.*, 13 (2000) 331-342.
- [83] S.B. Barnett, G.R. Ter Haar, M.C. Ziskin, W.L. Nyborg, K. Maeda, and J. Bang, Current status of research on biophysical effects of ultrasound, *Ultrasound Med. Biol.*, 20 (1994) 205-218.
- [84] S.B. Barnett, H.D. Rott, G.R. Ter Haar, M.C. Ziskin, and K. Maeda, The sensitivity of biological tissue to ultrasound, *Ultrasound Med. Biol.*, 23 (1997) 805-812.
- [85] M.J. Voogt, S.M. van, M.E. Ikin, R. Deckers, K.L. Vincken, L.W. Bartels, W.P. Mali, and M.A. van den Bosch, Targeted vessel ablation for more efficient magnetic resonance-guided high-intensity focused ultrasound ablation of uterine fibroids, *Cardiovasc. Intervent. Radiol.*, 35 (2012) 1205-1210.
- [86] D.R. Daum, N.B. Smith, R. King, and K. Hynynen, In vivo demonstration of noninvasive thermal surgery of the liver and kidney using an ultrasonic phased array, *Ultrasound Med. Biol.*, 25 (1999) 1087-1098.
- [87] J.E. Kennedy, G.R. Ter Haar, and D. Cranston, High intensity focused ultrasound: surgery of the future?, *Br. J. Radiol.*, 76 (2003) 590-599.

- [88] A.R. Shukla, D.L. Hoover, Y.L. Homsy, S. Perlman, S. Schurman, and E.M. Reisman, Urolithiasis in the low birth weight infant: the role and efficacy of extracorporeal shock wave lithotripsy, *J. Urol.*, 165 (2001) 2320-2323.
- [89] S.L. Huang and R.C. MacDonald, Acoustically active liposomes for drug encapsulation and ultrasound-triggered release, *Biochim. Biophys. Acta*, 1665 (2004) 134-141.
- [90] R. Gramiak, P.M. Shah, and D.H. Kramer, Ultrasound cardiography: contrast studies in anatomy and function, *Radiology*, 92 (1969) 939-948.
- [91] M.A. Borden, D.E. Kruse, C.F. Caskey, S. Zhao, P.A. Dayton, and K.W. Ferrara, Influence of lipid shell physicochemical properties on ultrasound-induced microbubble destruction, *IEEE Trans. Ultrason. Ferroelectr. Freq. Control*, 52 (2005) 1992-2002.
- [92] S. Hernet and A.L. Klibanov, Microbubbles in ultrasound-triggered drug and gene delivery, *Adv. Drug Deliv. Rev.*, 60 (2008) 1153-1166.
- [93] S. Qin, C.F. Caskey, and K.W. Ferrara, Ultrasound contrast microbubbles in imaging and therapy: physical principles and engineering, *Phys. Med. Biol.*, 54 (2009) R27-R57.
- [94] A. Bouakaz, M. Versluis, and J.N. de, High-speed optical observations of contrast agent destruction, *Ultrasound Med. Biol.*, 31 (2005) 391-399.
- [95] K.E. Morgan, J.S. Allen, P.A. Dayton, J.E. Chomas, A.L. Klibanov, and K.W. Ferrara, Experimental and theoretical evaluation of microbubble behavior: effect of transmitted phase and bubble size, *IEEE Trans. Ultrason. Ferroelectr. Freq. Control*, 47 (2000) 1494-1509.
- [96] P.A. Dayton, K.E. Morgan, A.L. Klibanov, G.H. Brandenburger, and K.W. Ferrara, Optical and acoustical observations of the effects of ultrasound on contrast agents, *IEEE Trans. Ultrason. Ferroelectr. Freq. Control*, 46 (1999) 220-232.
- [97] J. Wu and W.L. Nyborg, Ultrasound, cavitation bubbles and their interaction with cells, *Adv. Drug Deliv. Rev.*, 60 (2008) 1103-1116.
- [98] D.J. May, J.S. Allen, and K.W. Ferrara, Dynamics and fragmentation of thick-shelled microbubbles, *IEEE Trans. Ultrason. Ferroelectr. Freq. Control*, 49 (2002) 1400-1410.
- [99] E. Quaia, Assessment of tissue perfusion by contrast-enhanced ultrasound, *Eur. Radiol.*, 21 (2011) 604-615.
- [100] E.C. Unger, T. Porter, W. Culp, R. Labell, T. Matsunaga, and R. Zutshi, Therapeutic applications of lipid-coated microbubbles, *Adv. Drug Deliv. Rev.*, 56 (2004) 1291-1314.
- [101] C. Mannaris and M.A. Averkiou, Investigation of microbubble response to long pulses used in ultrasound-enhanced drug delivery, *Ultrasound Med. Biol.*, 38 (2012) 681-691.
- [102] R. Seip, C.T. Chin, C.S. Hall, B.I. Raju, A. Ghanem, and K. Tiemann, Targeted ultrasound-mediated delivery of nanoparticles: on the development of a new HIFU-based therapy and imaging device, *IEEE Trans. Biomed. Eng.*, 57 (2010) 61-70.
- [103] Y. Qiu, Y. Luo, Y. Zhang, W. Cui, D. Zhang, J. Wu, J. Zhang, and J. Tu, The correlation between acoustic cavitation and sonoporation involved in ultrasound-mediated DNA transfection with polyethylenimine (PEI) in vitro, *J. Control Release*, 145 (2010) 40-48.
- [104] M. Afadzi, C.d. Davies, Y.H. Hansen, T. Johansen, O.K. Standal, R. Hansen, S.E. Masoy, E.A. Nilssen, and B. Angelsen, Effect of Ultrasound Parameters on the Release of Liposomal Calcein, *Ultrasound in Medicine and Biology*, 38 (2012) 476-486.
- [105] S. Mitragotri, Healing sound: the use of ultrasound in drug delivery and other therapeutic applications, *Nat. Rev. Drug Discov.*, 4 (2005) 255-260.
- [106] C.D. Ohl and R. Ikink, Shock-wave-induced jetting of micron-size bubbles, *Phys. Rev. Lett.*, 90 (2003) 214502.
- [107] C.D. Ohl, M. Arora, R. Ikink, N. de Jong, M. Versluis, M. Delius, and D. Lohse, Sonoporation from jetting cavitation bubbles, *Biophys. J.*, 91 (2006) 4285-4295.

- [108] R. Karshafian, P.D. Bevan, R. Williams, S. Samac, and P.N. Burns, Sonoporation by ultrasound-activated microbubble contrast agents: effect of acoustic exposure parameters on cell membrane permeability and cell viability, *Ultrasound Med. Biol.*, 35 (2009) 847-860.
- [109] R. Karshafian, S. Samac, P.D. Bevan, and P.N. Burns, Microbubble mediated sonoporation of cells in suspension: clonogenic viability and influence of molecular size on uptake, *Ultrasonics*, 50 (2010) 691-697.
- [110] S. Mehier-Humbert, T. Bettinger, F. Yan, and R.H. Guy, Plasma membrane poration induced by ultrasound exposure: implication for drug delivery, *J. Control Release*, 104 (2005) 213-222.
- [111] B. Geers, I. Lentacker, A. Alonso, N.N. Sanders, J. Demeester, S. Meairs, and S.C. De Smedt, Elucidating the mechanisms behind sonoporation with adeno-associated virus-loaded microbubbles, *Mol. Pharm.*, 8 (2011) 2244-2251.
- [112] I. Lentacker, N. Wang, R.E. Vandembroucke, J. Demeester, S.C. De Smedt, and N.N. Sanders, Ultrasound exposure of lipoplex loaded microbubbles facilitates direct cytoplasmic entry of the lipoplexes, *Mol. Pharm.*, 6 (2009) 457-467.
- [113] B.D. Meijering, L.J. Juffermans, A. van Wamel, R.H. Henning, I.S. Zuhorn, M. Emmer, A.M. Versteilen, W.J. Paulus, W.H. van Gilst, K. Kooiman, N. de Jong, R.J. Musters, L.E. Deelman, and O. Kamp, Ultrasound and microbubble-targeted delivery of macromolecules is regulated by induction of endocytosis and pore formation, *Circ. Res.*, 104 (2009) 679-687.
- [114] R.K. Schlicher, J.D. Hutcheson, H. Radhakrishna, R.P. Apkarian, and M.R. Prausnitz, Changes in cell morphology due to plasma membrane wounding by acoustic cavitation, *Ultrasound Med. Biol.*, 36 (2010) 677-692.
- [115] A. van Wamel, K. Kooiman, M. Emmer, F.J. ten Cate, M. Versluis, and N. de Jong, Ultrasound microbubble induced endothelial cell permeability, *J. Control Release*, 116 (2006) e100-e102.
- [116] A. van Wamel, K. Kooiman, M. Hartevelde, M. Emmer, F.J. ten Cate, M. Versluis, and N. de Jong, Vibrating microbubbles poking individual cells: drug transfer into cells via sonoporation, *J. Control Release*, 112 (2006) 149-155.
- [117] A. Yudina, M. Lepetit-Coiffe, and C.T. Moonen, Evaluation of the temporal window for drug delivery following ultrasound-mediated membrane permeability enhancement, *Mol. Imaging Biol.*, 13 (2011) 239-249.
- [118] A. Yudina, S.M. de, M. Lepetit-Coiffe, S. Langereis, R.L. Van, P. Smirnov, V. Bouchaud, P. Voisin, H. Grull, and C.T. Moonen, Ultrasound-mediated intracellular drug delivery using microbubbles and temperature-sensitive liposomes, *J. Control Release*, 155 (2011) 442-448.
- [119] I. Lentacker, S.C. De Smedt, and N.N. Sanders, Drug-loaded microbubble design for ultrasound triggered delivery, *Soft Matter*, 5 (2009) 2161-2170.
- [120] S. Tinkov, R. Bekeredjian, G. Winter, and C. Coester, Microbubbles as ultrasound triggered drug carriers, *J. Pharm. Sci.*, 98 (2009) 1935-1961.
- [121] P.A. Frenkel, S. Chen, T. Thai, R.V. Shohet, and P.A. Grayburn, DNA-loaded albumin microbubbles enhance ultrasound-mediated transfection in vitro, *Ultrasound Med. Biol.*, 28 (2002) 817-822.
- [122] M.A. Borden, C.F. Caskey, E. Little, R.J. Gillies, and K.W. Ferrara, DNA and polylysine adsorption and multilayer construction onto cationic lipid-coated microbubbles, *Langmuir*, 23 (2007) 9401-9408.
- [123] S.R. Sirsi, S.L. Hernandez, L. Zielinski, H. Blomback, A. Koubaa, M. Synder, S. Homma, J.J. Kandel, D.J. Yamashiro, and M.A. Borden, Polyplex-microbubble hybrids for ultrasound-guided plasmid DNA delivery to solid tumors, *J. Control Release*, 157 (2012) 224-234.

- [124] L.C. Phillips, A.L. Klibanov, B.R. Wamhoff, and J.A. Hossack, Targeted gene transfection from microbubbles into vascular smooth muscle cells using focused, ultrasound-mediated delivery, *Ultrasound Med. Biol.*, 36 (2010) 1470-1480.
- [125] S. Tinkov, G. Winter, C. Coester, and R. Bekerredjian, New doxorubicin-loaded phospholipid microbubbles for targeted tumor therapy: Part I--Formulation development and in-vitro characterization, *J. Control Release*, 143 (2010) 143-150.
- [126] C.Y. Ting, C.H. Fan, H.L. Liu, C.Y. Huang, H.Y. Hsieh, T.C. Yen, K.C. Wei, and C.K. Yeh, Concurrent blood-brain barrier opening and local drug delivery using drug-carrying microbubbles and focused ultrasound for brain glioma treatment, *Biomaterials*, 33 (2012) 704-712.
- [127] A.C. Camarozano, Garcia de Almeida Cyrino FZ, D.A. Bottino, and E. Bouskela, Effects of microbubbles and ultrasound on the microcirculation: observation on the hamster cheek pouch, *J. Am. Soc. Echocardiogr.*, 23 (2010) 1323-1330.
- [128] K. Kooiman, M.R. Bohmer, M. Emmer, H.J. Vos, C. Chlon, W.T. Shi, C.S. Hall, S.H. de Winter, K. Schroen, M. Versluis, N. de Jong, and A. van Wamel, Oil-filled polymer microcapsules for ultrasound-mediated delivery of lipophilic drugs, *J. Control Release*, 133 (2009) 109-118.
- [129] M.S. Tartis, J. McCallan, A.F. Lum, R. LaBell, S.M. Stieger, T.O. Matsunaga, and K.W. Ferrara, Therapeutic effects of paclitaxel-containing ultrasound contrast agents, *Ultrasound Med. Biol.*, 32 (2006) 1771-1780.
- [130] S. Hernot and A.L. Klibanov, Microbubbles in ultrasound-triggered drug and gene delivery, *Adv. Drug Deliv. Rev.*, 60 (2008) 1153-1166.
- [131] I. Lentacker, B. Geers, J. Demeester, S.C. De Smedt, and N.N. Sanders, Design and evaluation of doxorubicin-containing microbubbles for ultrasound-triggered doxorubicin delivery: cytotoxicity and mechanisms involved, *Mol. Ther.*, 18 (2010) 101-108.
- [132] M.L. De Temmerman, H. Dewitte, R.E. Vandenbroucke, B. Lucas, C. Libert, J. Demeester, S.C. De Smedt, I. Lentacker, and J. Rejman, mRNA-Lipoplex loaded microbubble contrast agents for ultrasound-assisted transfection of dendritic cells, *Biomaterials*, 32 (2011) 9128-9135.
- [133] R.E. Vandenbroucke, I. Lentacker, J. Demeester, S.C. De Smedt, and N.N. Sanders, Ultrasound assisted siRNA delivery using PEG-siPlex loaded microbubbles, *J. Control Release*, 126 (2008) 265-273.
- [134] M.S. Tartis, D.E. Kruse, H. Zheng, H. Zhang, A. Kheirloom, J. Marik, and K.W. Ferrara, Dynamic microPET imaging of ultrasound contrast agents and lipid delivery, *J. Control Release*, 131 (2008) 160-166.
- [135] R. Suzuki, E. Namai, Y. Oda, N. Nishiie, S. Otake, R. Koshima, K. Hirata, Y. Taira, N. Utoguchi, Y. Negishi, S. Nakagawa, and K. Maruyama, Cancer gene therapy by IL-12 gene delivery using liposomal bubbles and tumoral ultrasound exposure, *Journal of Controlled Release*, 142 (2010) 245-250.
- [136] Y. Wang, X. Li, Y. Zhou, P. Huang, and Y. Xu, Preparation of nanobubbles for ultrasound imaging and intracellular drug delivery, *International Journal of Pharmaceutics*, 384 (2010) 148-153.
- [137] F.Y. Yang, T.T. Wong, M.C. Teng, R.S. Liu, M. Lu, H.F. Liang, and M.C. Wei, Focused ultrasound and interleukin-4 receptor-targeted liposomal doxorubicin for enhanced targeted drug delivery and antitumor effect in glioblastoma multiforme, *J. Control Release*, (2012).
- [138] Y. Wang, X. Li, Y. Zhou, P. Huang, and Y. Xu, Preparation of nanobubbles for ultrasound imaging and intracellular drug delivery, *International Journal of Pharmaceutics*, 384 (2010) 148-153.
- [139] Z. Gao, A.M. Kennedy, D.A. Christensen, and N.Y. Rapoport, Drug-loaded nano/microbubbles for combining ultrasonography and targeted chemotherapy, *Ultrasonics*, 48 (2008) 260-270.

- [140] N. Rapoport, K.H. Nam, R. Gupta, Z. Gao, P. Mohan, A. Payne, N. Todd, X. Liu, T. Kim, J. Shea, C. Scaife, D.L. Parker, E.K. Jeong, and A.M. Kennedy, Ultrasound-mediated tumor imaging and nanotherapy using drug-loaded, block copolymer stabilized perfluorocarbon nanoemulsions, *J. Control Release*, 153 (2011) 4-15.
- [141] P.S. Sheeran, S. Luois, P.A. Dayton, and T.O. Matsunaga, Formulation and acoustic studies of a new phase-shift agent for diagnostic and therapeutic ultrasound, *Langmuir*, 27 (2011) 10412-10420.
- [142] J. Fang, H. Nakamura, and H. Maeda, The EPR effect: Unique features of tumor blood vessels for drug delivery, factors involved, and limitations and augmentation of the effect, *Advanced Drug Delivery Reviews*, 63 (2011) 136-151.
- [143] P.S. Sheeran, V.P. Wong, S. Luois, R.J. McFarland, W.D. Ross, S. Feingold, T.O. Matsunaga, and P.A. Dayton, Decafluorobutane as a phase-change contrast agent for low-energy extravascular ultrasonic imaging, *Ultrasound Med. Biol.*, 37 (2011) 1518-1530.
- [144] X. Wang, H. Chen, Y. Chen, M. Ma, K. Zhang, F. Li, Y. Zheng, D. Zeng, Q. Wang, and J. Shi, Perfluorohexane-encapsulated mesoporous silica nanocapsules as enhancement agents for highly efficient high intensity focused ultrasound (HIFU), *Adv. Mater.*, 24 (2012) 785-791.
- [145] C.E. Ashley, E.C. Carnes, G.K. Phillips, D. Padilla, P.N. Durfee, P.A. Brown, T.N. Hanna, J. Liu, B. Phillips, M.B. Carter, N.J. Carroll, X. Jiang, D.R. Dunphy, C.L. Willman, D.N. Petsev, D.G. Evans, A.N. Parikh, B. Chackerian, W. Wharton, D.S. Peabody, and C.J. Brinker, The targeted delivery of multicomponent cargos to cancer cells by nanoporous particle-supported lipid bilayers, *Nat. Mater.*, 10 (2011) 389-397.
- [146] B.A. Kaufmann, J.M. Sanders, C. Davis, A. Xie, P. Aldred, I.J. Sarembock, and J.R. Lindner, Molecular imaging of inflammation in atherosclerosis with targeted ultrasound detection of vascular cell adhesion molecule-1, *Circulation*, 116 (2007) 276-284.
- [147] S. Hernot, S. Unnikrishnan, Z. Du, T. Shevchenko, B. Cosyns, A. Broisat, J. Toczek, V. Cavelliers, S. Muyldermans, T. Lahoutte, A.L. Klibanov, and N. Devoogdt, Nanobody-coupled microbubbles as novel molecular tracer, *J. Control Release*, 158 (2012) 346-353.
- [148] E.A. Ferrante, J.E. Pickard, J. Rychak, A. Klibanov, and K. Ley, Dual targeting improves microbubble contrast agent adhesion to VCAM-1 and P-selectin under flow, *J. Control Release*, 140 (2009) 100-107.
- [149] L. Yang, X. Zhang, M. Ye, J. Jiang, R. Yang, T. Fu, Y. Chen, K. Wang, C. Liu, and W. Tan, Aptamer-conjugated nanomaterials and their applications, *Adv. Drug Deliv. Rev.*, 63 (2011) 1361-1370.
- [150] C.H. Wang, S.T. Kang, Y.H. Lee, Y.L. Luo, Y.F. Huang, and C.K. Yeh, Aptamer-conjugated and drug-loaded acoustic droplets for ultrasound theranosis, *Biomaterials*, 33 (2012) 1939-1947.
- [151] K. Kooiman, M. Foppen-Harteveld, A.F. van der Steen, and J.N. de, Sonoporation of endothelial cells by vibrating targeted microbubbles, *J. Control Release*, 154 (2011) 35-41.
- [152] I. Lentacker, B.G. De Geest, R.E. Vandenbroucke, L. Peeters, J. Demeester, S.C. De Smedt, and N.N. Sanders, Ultrasound-responsive polymer-coated microbubbles that bind and protect DNA, *Langmuir*, 22 (2006) 7273-7278.
- [153] A. Ghanem, C. Steingen, F. Brenig, F. Funcke, Z.Y. Bai, C. Hall, C.T. Chin, G. Nickenig, W. Bloch, and K. Tiemann, Focused ultrasound-induced stimulation of microbubbles augments site-targeted engraftment of mesenchymal stem cells after acute myocardial infarction, *Journal of Molecular and Cellular Cardiology*, 47 (2009) 411-418.
- [154] H. Leong-Poi, M.A. Kuliszewski, M. Lekas, M. Sibbald, K. Teichert-Kuliszewska, A.L. Klibanov, D.J. Stewart, and J.R. Lindner, Therapeutic arteriogenesis by ultrasound-mediated

VEGF(165) plasmid gene delivery to chronically ischemic skeletal muscle, *Circulation Research*, 101 (2007) 295-303.

[155] M. Figueiredo and R. Esenaliev, PLGA Nanoparticles for Ultrasound-Mediated Gene Delivery to Solid Tumors, *J. Drug Deliv.*, 2012 (2012) 767839.

[156] T.B. Brismar, D. Grishenkov, B. Gustafsson, J. Harmark, A. Barrefelt, S.V. Kothapalli, S. Margheritelli, L. Oddo, K. Caidahl, H. Hebert, and G. Paradossi, Magnetite Nanoparticles Can Be Coupled to Microbubbles to Support Multimodal Imaging, *Biomacromolecules.*, (2012).

[157] I. Lentacker, R.E. Vandenbroucke, B. Lucas, J. Demeester, S.C. De Smedt, and N.N. Sanders, New strategies for nucleic acid delivery to conquer cellular and nuclear membranes, *J. Control Release*, 132 (2008) 279-288.

[158] M. Seo, I. Gorelikov, R. Williams, and N. Matsuura, Microfluidic assembly of monodisperse, nanoparticle-incorporated perfluorocarbon microbubbles for medical imaging and therapy, *Langmuir*, 26 (2010) 13855-13860.

[159] L.H. Treat, N. McDannold, N. Vykhodtseva, Y. Zhang, K. Tam, and K. Hynynen, Targeted delivery of doxorubicin to the rat brain at therapeutic levels using MRI-guided focused ultrasound, *Int. J. Cancer*, 121 (2007) 901-907.

[160] F. Marquet, Y.S. Tung, T. Teichert, V.P. Ferrera, and E.E. Konofagou, Noninvasive, transient and selective blood-brain barrier opening in non-human primates in vivo, *PLoS. One.*, 6 (2011) e22598.

[161] M.R. Bohmer, C.H. Chlon, B.I. Raju, C.T. Chin, T. Shevchenko, and A.L. Klibanov, Focused ultrasound and microbubbles for enhanced extravasation, *J. Control Release*, 148 (2010) 18-24.

[162] N. Vykhodtseva, N. McDannold, and K. Hynynen, Progress and problems in the application of focused ultrasound for blood-brain barrier disruption, *Ultrasonics*, 48 (2008) 279-296.

[163] N. Rapoport, Z. Gao, and A. Kennedy, Multifunctional nanoparticles for combining ultrasonic tumor imaging and targeted chemotherapy, *J. Natl. Cancer Inst.*, 99 (2007) 1095-1106.

[164] S. Tinkov, C. Coester, S. Serba, N.A. Geis, H.A. Katus, G. Winter, and R. Bekeredjian, New doxorubicin-loaded phospholipid microbubbles for targeted tumor therapy: in-vivo characterization, *J. Control Release*, 148 (2010) 368-372.

[165] K. Un, S. Kawakami, M. Yoshida, Y. Higuchi, R. Suzuki, K. Maruyama, F. Yamashita, and M. Hashida, The elucidation of gene transferring mechanism by ultrasound-responsive unmodified and mannose-modified lipoplexes, *Biomaterials*, 32 (2011) 4659-4669.

[166] O. Mueller, S. Schinkel, J. Kleinschmidt, H. Katus, and R. Bekeredjian, Augmentation of AAV-mediated cardiac gene transfer after systemic administration in adult rats, *Gene Therapy*, 15 (2008) 1558-1565.

Chapter 2

Self-assembled liposome-loaded microbubbles

Bart Geers¹, Ine Lentacker¹, Niek N. Sanders², Joseph Demeester¹, Stephen Meairs³, Stefaan C. De Smedt^{1*}

This chapter has been published: self-assembled liposome-loaded microbubbles: The missing link for safe and efficient ultrasound triggered drug-delivery. *Journal of Controlled Release*; 2011; 152; pp 249-56

¹ Ghent Research Group on Nanomedicines, Lab of General Biochemistry and Physical Pharmacy, Faculty of Pharmaceutical Sciences, Ghent University, Harelbekestraat 72, 9000 Gent, Belgium

² Laboratory of Gene Therapy, Faculty of Veterinary Medicine, Ghent University, Heidestraat 19, 9820 Merelbeke, Belgium

³Department of Neurology, Universitätsklinikum Mannheim, Heidelberg University, Theodor-Kutzer-Ufer 1-3, 66167 Mannheim, Germany

Liposome-loaded microbubbles have been recently introduced as a promising drug delivery platform for ultrasound guided drug delivery. In this paper we design liposome-loaded (lipid-shelled) microbubbles through the simple self-assembly of the involved compounds in a single step process. We thoroughly characterized the liposome-loading of the microbubbles and evaluated the cell killing efficiency of this material using doxorubicin (DOX) as a model drug. Importantly, we observed that the DOX liposome-loaded microbubbles allowed killing of melanoma cells even at very low doses of DOX. These findings clearly prove the potential of liposome-loaded microbubbles for ultrasound targeted drug delivery to cancer tissues.

INTRODUCTION

Microbubbles are gas filled microspheres that are a few microns in size, are usually filled with an hydrophobic gas and are stabilized by a surfactant (lipid, protein or polymer) shell, to enhance their shelf life and circulation time in blood after injection. Because of the difference in density between the gas core of the microbubble and the surrounding fluid, microbubbles start to oscillate when subjected to high frequency (1-10 MHz) ultrasound. This “cavitation” of microbubbles has been intensively studied by means of high speed optical imaging [1-3] and can be divided into respectively stable and inertial cavitation. In an ultrasound field with a low acoustical pressure microbubbles are stably cavitating and will oscillate around a given diameter. Inertial cavitation on the other hand occurs at higher acoustical pressures, the movement of the microbubbles becomes more violent which leads to destruction of the microbubbles [4]. This microbubble destruction produces distinct nonlinear acoustic echoes which are very useful in contrast enhanced ultrasound imaging [5]. Cavitation of microbubbles may also induce biological and mechanical effects on the surrounding space which may be particularly useful for drug delivery [6].

When microbubble collapse occurs in the vicinity of cells it has been shown that plasma membranes are temporarily permeabilized through the formation of transient pores in the cellular membrane, induced by micro-jets and shockwaves produced after microbubble collapse [3,7]. This phenomenon is called sonoporation [6]. It is believed that sonoporation is strongly dependent on the acoustical properties of the applied ultrasound field [8,9]. Such transient pores also enhance the uptake of macromolecules in cells [10]. Recent studies show that sonoporation effects may last up to 24 hours after ultrasound treatment [11]. The

use of microbubbles in combination with ultrasound may even induce openings in the blood-brain barrier which could be of interest to tackle drug delivery into the brain which currently remains a huge challenge [12,13].

Only if the drug molecules are physically located in the vicinity of microbubbles subjected to ultrasound, it is expected that sonoporation will enhance drug uptake by cells. Moreover, as these effects will only occur where and when ultrasound is applied, drug delivery is expected only to happen in the insonated tissue. Hence, for ultrasound targeted drug delivery it is crucial to design microbubbles which can be loaded with drug molecules. Meanwhile a number of concepts for drug loaded microbubbles are under investigation [14-16]. Basically, microbubbles can be loaded with drugs in three ways: (a) the drug can be incorporated in the microbubble shell [17], (b) (lipophilic) drugs can be incorporated in an inner oil phase present in the microbubbles [18] or (c) “colloidally drug loaded microbubbles” can be obtained through the attachment of drug containing nanoparticles (like e.g. liposomes) on the microbubbles’ surface as reviewed by *Bohmer et al.* and *Lentacker et al.* [19,20]. Independent on the way the microbubbles become loaded with drugs, they should fulfill at least the following requirements: (a) the microbubbles should be loaded with a sufficient amount of drug; (b) the shelf-life of the drug-loaded microbubbles should be long enough and (c) the drug-loaded microbubbles should be designed without the incorporation of toxic or immunogenic substances. We believe that loading the surface of microbubbles with drug containing liposomes is a promising concept for ultrasound guided drug delivery as: (a) more drugs can be loaded on microbubbles compared with other loading strategies, (b) a plethora of knowledge is available on liposomes for drug delivery which can be perfectly

used to develop the colloiddally loaded microbubble concept and (c) importantly, certain liposomes are safe and even already used in clinical practice.

Recently doxorubicin (DOX)-liposome loaded microbubbles [21] and lipoplex-loaded microbubbles (containing pDNA or siRNA) could be designed and it was found that in combination with ultrasound, such microbubbles strongly improved both doxorubicin (DOX) cytotoxicity and pDNA [16,22] and siRNA [23] delivery to cells *in vitro*. However, the complex microbubble preparation method, the immunogenic nature of avidin-biotin chemistry used to link the liposomes/lipoplexes to the microbubbles and the successive washing steps, made these materials not ideal for easy clinical use. It is clear that the concept of liposome-/lipoplex-loaded microbubbles needs further development and improvement. In this work we faced the challenge to design DOX-liposome loaded lipid shelled microbubbles through the self-assembly of the involved compounds. Importantly, the method we propose involves just a single step and allows to make a sterile material. As illustrated in Figure 1 and further explained in the results section, to a mixture of phospholipids, so named “functionalized DOX-liposomes” (i.e. DOX-liposomes containing maleimide functionalized PEG-lipids) and a hydrophobic gas were added. We show that under appropriate conditions these compounds self-assemble into DOX-liposome loaded microbubbles which are responsive to ultrasound and efficiently kill cells.

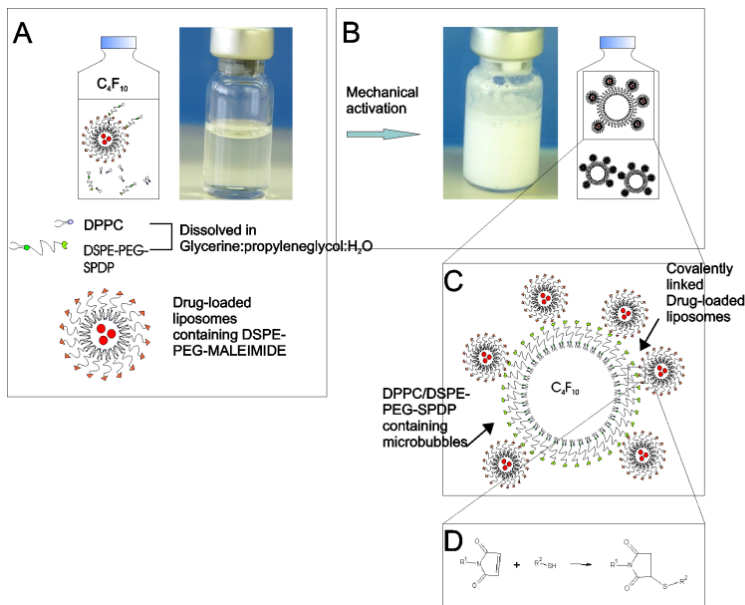


Figure 1: Schematic depiction of the preparation of liposome-loaded through self-assembly of the different constituents: Drug loaded liposomes containing DSPE-PEG-maleimide and perfluorobutane (C_4F_{10}) gas were added to vials containing: DPPC and DSPE-PEG-SPDP dissolved in a glycerin:propyleneglycol:H₂O mixture (A) and were mechanically activated using a Capmix™ device. This mechanical activation gives rise to lipid-shelled microbubbles (B) loaded with liposomes. These microbubbles are filled with the hydrophobic C_4F_{10} gas (C). The liposomes become coupled to the microbubbles' surface through covalent thiol-maleimide linkages (D). Note that the microbubbles are a few microns in size while the liposomes are some hundreds of nanometers.

MATERIALS AND METHODS

Preparation and characterization of functionalized microbubbles

“Functionalized microbubbles” (i.e. microbubbles containing thiol-functionalized PEG-lipids) were prepared starting from a lipid solution being a mixture of 1,2-

dipalmitoyl-*sn*-glycero-3-phosphocholine (DPPC) and 1,2-distearoyl-*sn*-glycero-3-phosphoethanolamine-N-[PDP(polyethylene glycol)-2000] (DSPE-PEG-PDP) (Avanti polar lipids, Alabaster, AL) in a 1:2:7 glycerine-propyleneglycol-H₂O solvent (Sigma-aldrich, Bornem, Belgium), the molar ratio of the lipids in the lipid solutions was respectively 97:3, 92:8 and 65:35. The lipid solution was prepared as follows. Aliquots of both lipids, dissolved in CHCl₃, were transferred into a round bottom flask. After CHCl₃ evaporation, the lipid film was dissolved in a 1:2:7 glycerine-propyleneglycol-H₂O mixture to obtain a clear solution with a final lipid concentration of 4×10^{-4} mmol/ml (or 2×10^{-4} mmol/ml for microbubbles used in the cell experiments). Aliquots of this lipid solution were transferred into 2.5 ml chromatography vials, which headspace was filled with C₄F₁₀ gas (F2 chemicals, Preston, UK). Finally, functionalized microbubbles (with an average size of 3 μ m) were obtained by high speed shaking of the lipid solution in a Capmix™ device (3M-ESPE, Diegem, Belgium) during 15 sec. The size and the concentration of the microbubbles in the dispersion (i.e. number of microbubbles per mL) were determined with a Beckman-coulter Multisizer 4 (Beckman-coulter, Brea, CA)

Preparation of non-functionalized microbubbles

Preparation of so named “non-functionalized microbubbles” occurred as described above for the functionalized bubbles, however 1,2-distearoyl-*sn*-glycero-3-phosphoethanolamine-N-[methoxy(polyethylene glycol)-2000 (DSPE-MPEG) (Avanti polar lipids, Alabaster, AL) was used as a PEG-lipid instead of DSPE-PEG-PDP.

Preparation and characterization of bodipy-labeled and DOX-liposomes

Bodipy-labeled liposomes were prepared by transferring DPPC, DSPE-PEG-maleimide) (Avanti polar lipids, Alabaster, AL), cholesterol (Sigma-alldrich, Bornem, Belgium) and cholesteryl-bodipy (Invitrogen, Merelbeke, Belgium), all dissolved in CHCl_3 , in a 49:15:35:1 molar ratio to a round bottom flask. After CHCl_3 evaporation, the remaining lipid film was rehydrated with HEPES buffer (50 mM, pH 7.4, Sigma-alldrich, Bornem, Belgium) to obtain a liposomal dispersion with a final lipid concentration of 16 mg/ml. The liposomal dispersion was hereafter extruded through a 200 nm filter using a mini-extruder at 60 °C (Avanti polar lipids, Alabaster, AL).

DOX-liposomes were prepared as described by *Lentacker et al.* [21]. Briefly, DPPC, DSPE-PEG-maleimide and cholesterol dissolved in CHCl_3 at a concentration of 20 mg/ml and 10 mg/ml respectively, were transferred in a round bottom flask in a 49:15:36 molar ratio. After evaporation the remaining lipid film was rehydrated with ammonium sulfate buffer (250 mM) to obtain a liposomal dispersion with a final lipid concentration of 16 mg/ml. The resulting liposome dispersion was extruded through a 200 nm filter using a mini-extruder at 60 °C. After extrusion the excess of ammonium sulfate was removed by overnight dialysis against distilled water (MWCO: 8000 Da, Spectra/Por Biotech, Compton, CA). Hereafter the liposomal dispersion was aliquoted into 450 μl aliquots and liposomes were loaded with DOX by adding 50 μl of a doxorubicin.HCl (Sigma-alldrich, Bornem, Belgium) 10 mg/ml solution. Non-encapsulated DOX was removed in a second overnight dialysis against distilled water. Final DOX concentration was evaluated using absorbance spectrometry using an Envision plate-reader and reached between 0.5 and 0.8 mg/ml (Perkin-elmer, Waltham, MA)

Preparation of liposome-loaded microbubbles

Liposome-loaded microbubbles were prepared by adding a certain volume of the liposome dispersion to the lipid solution used for the preparation of microbubbles (see above, under 1.1 and 1.2). Liposome-loaded microbubbles were obtained by high-speed shaking of this liposome/lipid mixture in a Capmix™ device. The loading of the microbubbles with (bodipy-containing) liposomes was visualized using a Nikon EZC1 confocal microscope equipped with a 60x lens imaging using the 490 nm excitation light, while fluorescence was detected at 551 nm.

Evaluation of the loading of the microbubbles with liposomes by flow cytometry

How different parameters influence the loading of microbubbles with bodipy-labeled liposomes was determined using a flow cytometer (BD FACScalibur, Erembodegem, Belgium). Therefore 300 μl of (bodipy-) liposome-loaded microbubbles were diluted in 300 μl of HEPES buffer. The 488 nm laser of the flow cytometer was used to excite the bubbles while the emitted fluorescence was detected in the 530 nm channel FL1. Results were expressed as mean fluorescence per microbubble using unloaded microbubbles as a blank. For measurements on microbubbles in plasma, platelet poor plasma was obtained by centrifuging whole blood samples first at 300 g for 10 min and subsequently at 3200 g for 10 min. 20 μl of (bodipy-) liposome-loaded microbubbles were suspended in 150 μl of plasma and diluted with 200 μl HEPES buffer. All the flow cytometry experiments were performed in triplicate and the presented data are the mean values.

Evaluation of the loading of the microbubbles with liposomes by Coulter Counter measurements

The loading of the microbubbles with liposomes was further studied by the electrical sensing zone method with a Beckman-Coulter Multisizer 4 Coulter Counter. For each Coulter Counter experiment 20 μl of (liposome-loaded) microbubbles were diluted in 10 ml of Phosphate Buffered Saline (PBS, GIBCO, Merelbeke, Belgium); 50 μl of this dilution was applied in the Multisizer 4 which was equipped with a 20 μm aperture tube. The liposome-loaded microbubbles used in the Coulter Counter experiments were obtained by transferring 1 ml of lipid solution (lipid concentration: 4×10^{-4} mmol/ml) and respectively 0, 35, 100 and 200 μl bodipy liposomes into a 2.5 ml chromatography vial, followed by high-speed shaking in the Capmix™ device.

We determined respectively the number of (unloaded and liposome-loaded) microbubbles per mL and the volume of all bubbles present in 1 ml of dispersion (i.e. “total volume per ml”). The volume of a single microbubble could then be determined by equation (1).

$$(1) \text{ volume per bubble} = \frac{\text{total volume per ml}}{\text{number of bubbles per ml}}$$

The volume increase of a microbubble upon loading with liposomes (i.e. “liposome volume per bubble”) could be calculated by equation (2) below.

$$(2) \text{ liposome volume per bubble} = \text{volume of a loaded bubble} - \text{volume of an unloaded bubble}$$

Dividing this liposome volume per microbubble by the volume of a single (spherical) liposome (with an average diameter of approximately 200 nm as was

determined by dynamic light scattering) gives an estimation of the amount of liposomes loaded on one microbubble (equation 3).

$$(3) \text{ number of liposomes per bubble} = \frac{\text{liposome volume per bubble (2)}}{\text{volume of one liposome}}$$

All measurements were performed at least in triplicate and results are presented as the mean of three different measurements.

Ultrasound induced DOX-release

The release of doxorubicin from the liposomes was determined by fluorescence measurements. The following samples were prepared for the release experiments. One ml of lipid solution was mixed with 10 or 20 μl of DOX-liposomes with a DOX-concentration of 0.1 mg/ml and C_4F_{10} gas. After shaking the lipid/liposome mixture in the CapmixTM device the mixture was diluted with PBS to a final volume of 10 ml and injected in an OpticellTM (Biocrystal, Westerville, OH) plate. This plate was submerged in a water bath (37°C) with an absorbing rubber and subjected to ultrasound during 15 s using the Sonitron device (Artison Corporation, Inola, OK, USA) equipped with a 2 cm ultrasound probe [22,24]. This probe was used with an ultrasound frequency of 1 MHz with 20 % duty cycle at an ultrasound intensity of 2 W/cm². Subsequently, the fluorescence of each sample was measured in a Wallac envision plate reader (λ_{exc} 500 nm, λ_{em} 550 nm). Each experiment was performed at least in triplicate.

Cell culture and cytotoxicity tests

BLM cells [24] (melanoma cells) were cultured in F12-supplemented Dulbecco's modified Eagles medium (DMEM-F12) which contained 1% Penicillin/Streptomycin, 2mmol/l glutamine, 10 % Fetal bovine serum (FBS) (all purchased from Gibco, Merelbeke, Belgium) and 100 mmol/l HEPES pH 7.2. Cells

were grown in a humidified incubator at 37°C in a 5 % CO₂ atmosphere. BLM cells were seeded in Opticell™ plates (1.3 × 10⁶ cells per Opticell™) and were grown to 90 % confluence, which was reached two days after seeding. Before experiments were performed, cells were washed with PBS. Subsequently, DOX-liposome loaded microbubbles were added to the cells. The following samples were prepared for the cytotoxicity experiments. To 500 µl of lipid solution (lipid concentration of 2 × 10⁻⁴ mmol/ml) respectively 10, 100, 250 or 500 µl of DOX liposomes (with a DOX concentration of 0.54 mg/ml) were added; HEPES-buffer (50 mM, pH 7.4) was added until a final volume of 1 ml was reached. Before shaking vials were filled with C₄F₁₀ gas. After shaking in the Capmix™ device, the 1 ml microbubble dispersion was added to 10 ml of optimem and this mixture was added to the cells in Opticell™ plates. Subsequently, these plates were submerged in a warm water bath (37°C) with a bottom of ultrasound absorbing rubber. Ultrasound was delivered by moving the Sonitron ultrasound probe over the whole plate during 10-15 sec. We used 1 MHz ultrasound with a 20 % duty cycle with an ultrasound intensity of 2 W/cm². During ultrasound application cells were located on the top membrane of the Opticell™, in this way microbubbles are directly contacting the cells during sonication. After ultrasound application cell displacement was evaluated by means of microscopy and was always minimal with the microbubble concentrations used for these experiments. After 4 hours of incubation, microbubbles were removed; cells were washed with PBS and incubated in fresh culture medium. After 24 hours cells were washed and the MTT reagent (Cell proliferation kit I, Roche diagnostics, Leuven, Belgium) was added for 4 hours. Subsequently, the solubilization reagent was added and cells were incubated overnight to allow cell lysis at 37°C. The next day, the absorbance of each plate was measured in an absorbance plate reader at

respectively 590 nm (OD_{590}) to determine the formed formazan and at 690 nm (OD_{690}) as a reference. The results of the cytotoxicity measurements are expressed as percentages; the viability of the cells which were only treated with optimem was considered to be 100 %, while the viability of cells exposed to phenol was considered to be 0 %. Experiments were performed at least in triplicate.

Statistical analysis

All data are presented as means +/- one standard deviation. A student's t-test was performed to determine whether datasets differed significantly. A p-value smaller than 0.05 was regarded as significant.

RESULTS

Preparation of liposome-loaded microbubbles by self-assembly

As schematically presented in Figure 1, to make liposome-loaded microbubbles, to a mixture of the (functionalized) lipids DPPC and DSPE-PEG-SPDP, dissolved in a glycerin-propylene glycol-water solvent at a concentration below their critical micellar concentration [25], liposomes containing DSPE-PEG-maleimide were added. We observed that liposomes dispersed in the lipid solution are stable and can be stored during at least several weeks (data not shown). Therefore we stored the liposome/lipid dispersion at 4°C in chromatography vials. To “activate” the mixture, which refers to formation of liposome loaded microbubbles (Figure 1C), the vials' headspaces were filled with perfluorobutane gas and subsequently mixed with a high speed shaking-device (Capmix™ or Vialmix™). The Capmix™ disperses the lipophilic perfluorobutane in the lipid solution. Hence, the hydrophobic tails of the dissolved lipids interact with the dispersed gas and stabilize the gas bubbles formed. Because functionalized (SPDP-) PEG-lipids were

used which can interact with the functionalized (maleimide-)PEG-lipids of the liposomes (Figure 1D), liposome-loaded microbubbles were spontaneously formed during this process as can be seen in the confocal image in Figure 2B and its corresponding transmission image (Figure 2A) clearly show bodipy-labeled liposomes at the surface of the microbubbles.

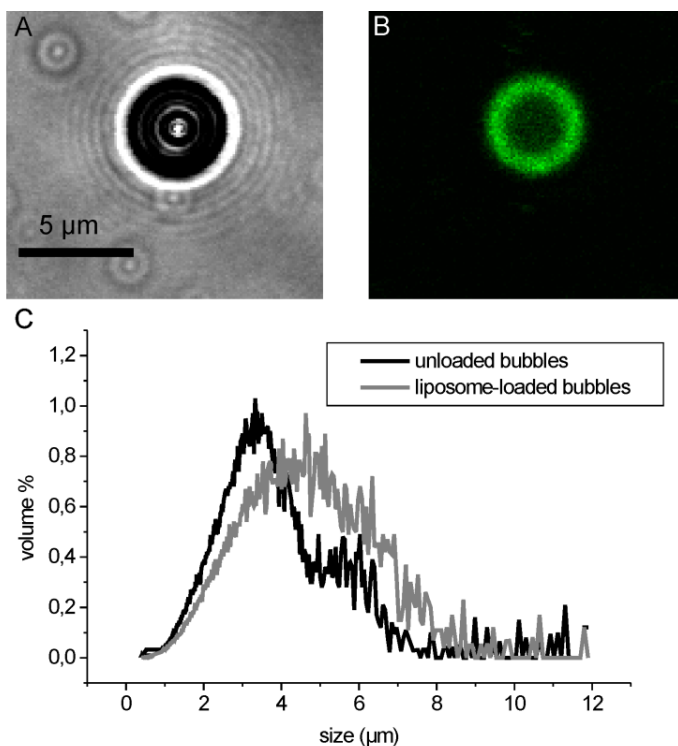


Figure 2: Microscopy and Coulter Counter studies of liposome-loaded microbubbles: Transmission image (A) and confocal image (B) of a (bodipy-labeled) liposome-loaded microbubble. Size distributions of unloaded and liposome loaded microbubbles as obtained by Coulter Counter measurements (C) show an increase in mean size when liposomes are bound to the microbubbles' surface.

Subsequently we measured the size distribution and microbubble concentration of respectively unloaded and loaded microbubbles by Coulter Counter (Figure 2C). The unloaded microbubbles showed an average volume diameter of 3.6 μm while the diameter of liposome-loaded microbubbles equaled 4.0 μm . The microbubble dispersions contained respectively 1.23×10^9 (unloaded) and 1.04×10^9 (loaded) microbubbles/ml. The 400 nm increase in average diameter of the bubbles upon loading with liposomes strongly indicates the formation of a single liposome layer at the microbubble surface as the hydrodynamic diameter of a single liposome is about 200 nm.

Improving the liposome-loading of the microbubbles

Clearly, the more liposomes could be loaded onto the microbubble shell, the more drug could be released when the microbubble collapses. In a next step we evaluated whether the microbubble loading could be increased by using higher amounts of DSPE-PEG-SPDP lipids in the microbubble shell. We evaluated the amount of liposomes loaded per bubble through the use of bodipy-labeled liposomes and quantifying the fluorescence of the bodipy-liposome-loaded microbubbles through flow cytometry. Figure 3 clearly shows that the mean fluorescence per bubble increases upon a) adding more liposomes to the mixture and b) using higher amounts of DSPE-PEG-SPDP in the lipid mixture. Coulter Counter measurements on the corresponding bubbles also clearly indicate that upon using 35% DSPE-PEG-SPDP the microbubbles become substantially larger which explains the increased loading capacity of these microbubbles as more surface space per bubble is available. We noticed that it is possible to incorporate even higher amounts of DSPE-PEG-SPDP-lipids in the bubbles; however, the resulting microbubbles were unstable. Hence, we concluded that the use of a 35% molar ratio of DSPE-PEG-SPDP-lipids is optimal for liposome loading.

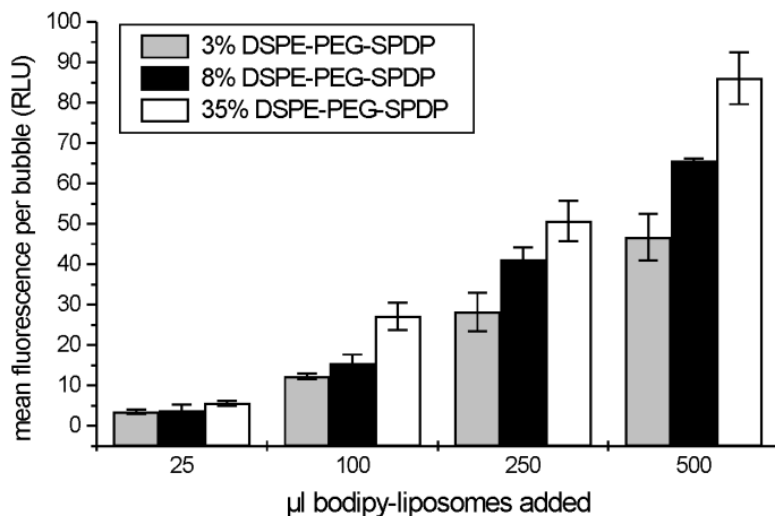


Figure 3: flow cytometry measurements of liposome-loading with increased PEGylation: Results of flow cytometry on bodipy-liposome loaded microbubbles: mean fluorescence per bubble in function of the amount of bodipy-liposomes added to the lipid mixture.

Behavior of liposome-loaded microbubbles in plasma

Clearly, successful ultrasound triggered drug release assumes that the microbubbles keep the drug as long as ultrasound energy is not applied. To judge whether liposome-loaded microbubbles remain stable once injected in plasma and do not release drug due to interactions with plasma components, we performed flow cytometry measurements on microbubbles loaded with bodipy-liposomes dispersed in human platelet poor plasma (Figure 4). We could not observe significant differences in the fluorescence of liposome-loaded microbubbles dispersed in respectively plasma and buffer indicating that liposome-loaded microbubbles remain stable in plasma. Hence we predict that

the liposomes will remain bound to the bubbles after injection in the bloodstream, at least as long as they are not exposed to ultrasound.

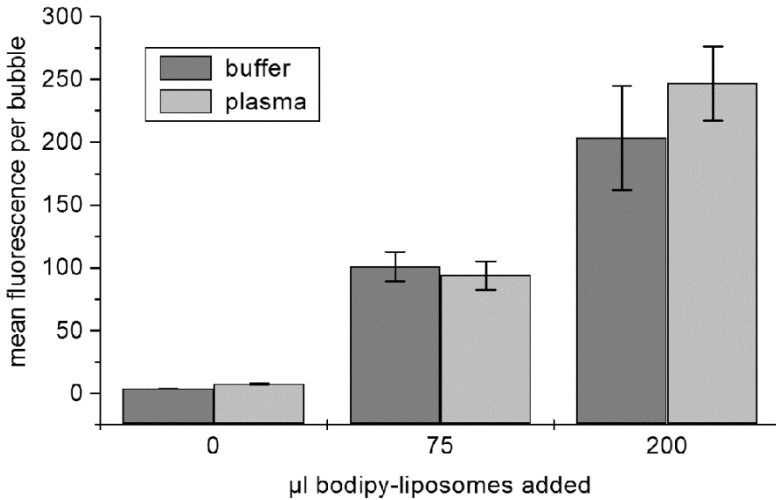


Figure 4: flow cytometry assessment of the stability of liposome-loading in plasma: Results of flow cytometry on bodipy-liposome-loaded microbubbles: mean fluorescence per bubble in function of the amount of bodipy-liposomes added to the lipid mixture.

Aspecific interactions between the liposomes and the microbubbles

Subsequently we evaluated whether liposomes can stick (i.e. become aspecifically bound) to the microbubbles. Therefore we prepared microbubbles with DSPE-MPEG lipids without functional end groups, thereby avoiding covalent binding. Figure 5A shows the fluorescence of non-functionalized microbubbles exposed to bodipy-liposomes, as measured through flow cytometry. Clearly, liposomes bind aspecifically to the microbubbles. However, as could be expected, liposome

loading of the microbubbles through covalent interactions enables significantly higher loading, which is of interest for use in drug delivery. One could speculate about the nature of the aspecific interactions between the liposomes and microbubbles. Entanglements between PEG-chains on the liposomes and microbubbles may contribute to this phenomenon.

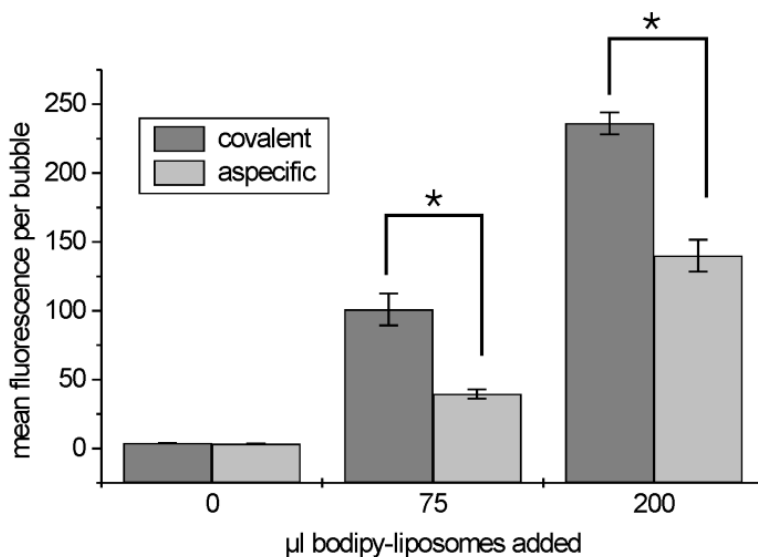


Figure 5: Flow cytometry assessment of aspecific liposome-loading: Results of flow cytometry on bodipy-liposome loaded microbubbles: mean fluorescence per bubble in function of the amount of bodipy-liposomes added to the lipid mixture. The microbubbles contained 35 mol% DSPE-PEG-SPDP, the liposomes contained respectively 35% DSPE-mPEG or DSPE-PEG-maleimide.

Coulter Counter measurements gain further insight in the amount of liposomes loaded

Although flow cytometry experiments revealed clear information on the loading of the microbubbles with liposomes, it remained impossible to estimate the number of liposomes loaded per microbubble. This information is of interest as it

defines the drug dose which can be loaded on the microbubbles' surface. We reasoned that measuring the increase in volume of a microbubble upon loading it with liposomes (defined as "liposome volume per bubble") in equation (2)) could give us valuable information. Dividing this "liposome volume per bubble" by the volume of one liposome allows us to estimate this number. Figure 6 shows the results of these experiments. For microbubbles with covalently attached liposomes we estimated that between 600 and 1300 liposomes can be loaded on the microbubbles' surface, which is significantly higher than the number which can be loaded through aspecific interactions. These data confirm the results obtained by Klibanov et al. [26] where it is claimed that approximately 2000 liposomes with a diameter of $0.1\mu\text{m}$ can be bound to one bubble with a diameter of $2.5\mu\text{m}$. interestingly, the results obtained through Coulter Counter measurements confirm the data observed in Figure 5A which were obtained through flow cytometry.

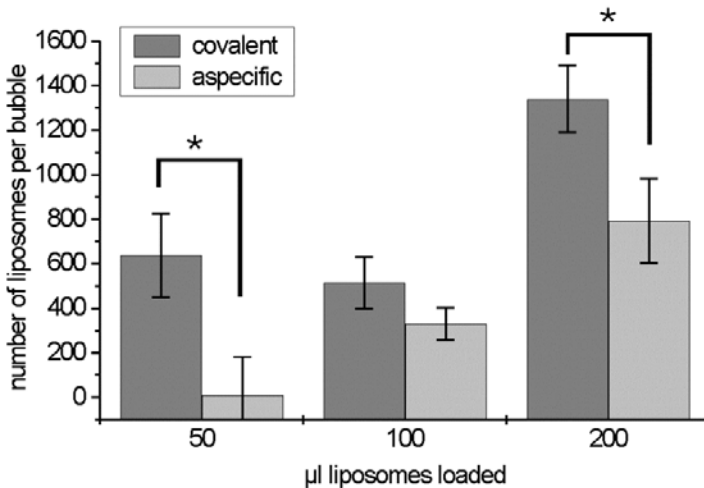


Figure 6: Estimation of the number of liposomes per bubble: Estimated number of liposomes per microbubble (containing 35 mol% DSPE-PEG-SPDP) as measured by Coulter Counter.

Ultrasound induced DOX release from DOX-liposome-loaded microbubbles

Next we evaluated whether applying ultrasound on the DOX-liposome microbubble results in the release of DOX from the liposomes. As DOX encapsulated in liposomes has lower fluorescence intensity than the corresponding amount of freely dissolved DOX, an increase in fluorescence could be expected upon applying ultrasound to the DOX-liposome loaded microbubbles. We measured a significant increase in fluorescence when liposome-loaded microbubbles are subjected to ultrasound, which indicates that free doxorubicin is released from the liposomes after insonation.

Biological efficacy of DOX-loaded liposome bubbles treated with ultrasound

In a next step we evaluated the tumor cell killing efficacy of DOX-liposome loaded microbubbles. Figure 7B shows the results of an *in vitro* cytotoxicity assay using different cell killing strategies. Clearly, ultrasound treatment of DOX-liposome loaded microbubbles (white bars) results in a significantly stronger killing of the cells. The x-axis in Figure 7B indicates the concentration of DOX in the Opticells™. Note that a higher DOX concentration was obtained through the use of microbubbles which were more loaded with DOX-liposomes (i.e. the number of DOX-liposome loaded microbubbles per Opticell™ was constant). Clearly, the 'heavier' the microbubbles are loaded with DOX-liposomes the more cytotoxic they are. Importantly, without ultrasound DOX-liposome loaded microbubbles do not kill cells (dark gray bars in Figure 7B). As the DOX-liposome loaded microbubbles are not cytotoxic as long as they are not subjected to ultrasound, we suggest that such bubbles in combination with ultrasound may allow targeted release of DOX. We would like to note that, as the cytotoxicity

experiments were done on a cell monolayer, cells were occasionally (physically) removed from this layer due to the ultrasound energy or the microbubbles treatment itself. This could induce false positive results in the cytotoxicity experiments, although microbubble concentrations are used that induced a minimal cell displacement as verified microscopy (data not shown). The bars in Figure 7A show that at microbubble concentrations used in the experiments there was no significant killing of the cells due to the microbubble destruction itself; the observed cytotoxicity was similar to that observed with the blank (optimem).

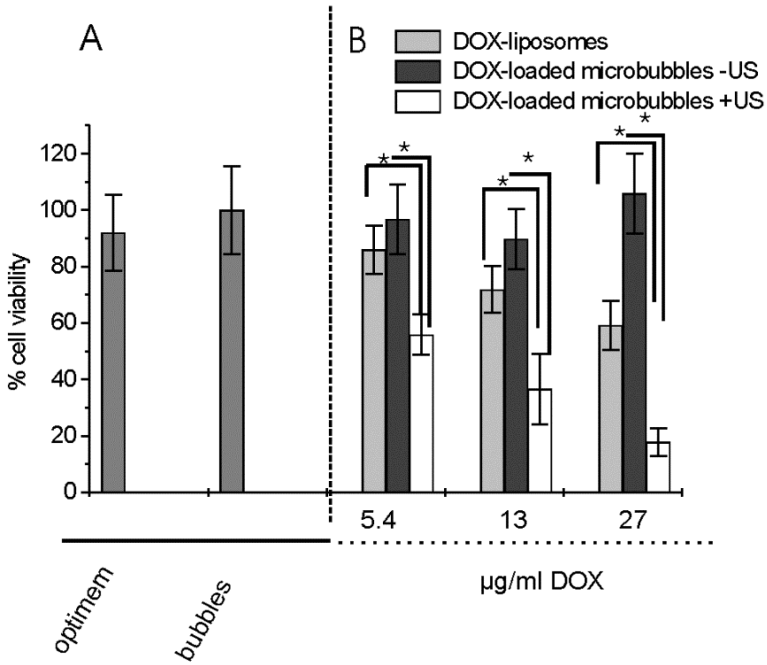


Figure 7: Viability measurements on melanoma cells: (A) Effect of microbubbles alone in presence of ultrasound on melanoma cell viability compared to no treatment (optimum). (B) Viability of melanoma cells after treatment with DOX-liposome loaded microbubbles, with ultrasound treatment (light gray bars), DOX-liposome loaded microbubbles without ultrasound treatment (dark gray bars) and DOX-liposomes alone were measured using augmenting amounts of DOX-liposomes in an Opticell™ plate.

Can dose reduction be achieved with DOX-liposome loaded microbubbles?

In the experiments in Figure 7 the DOX-liposome loaded microbubble dispersions did still contain an amount of free DOX-liposomes as it was experimentally difficult to separate free liposomes from the microbubbles. We were especially interested in the cell killing properties of the DOX-liposome loaded microbubbles themselves. We described above that between 600 and 1300 liposomes can be bound per microbubble. Therefore we prepared a DOX-liposome microbubble dispersion using an amount of DOX-liposomes which is expected to become fully loaded on the microbubbles. One can calculate that, when the microbubbles are loaded with this amount of liposomes, approximately 5 μg of DOX is loaded on the microbubbles present in 1 mL dispersion. Under these conditions we performed the cytotoxicity measurements, which results in a DOX-concentration of 0.5 $\mu\text{g}/\text{ml}$ in the OpticellsTM after applying the DOX-liposome microbubble dispersion to the cells. Figure 8 compares the cell killing at a DOX concentration of 0.5 $\mu\text{g}/\text{ml}$ in the OpticellsTM, respectively when free DOX and DOX-liposome microbubble dispersion (without free DOX-liposomes) were applied. Despite the very low DOX-concentration in the OpticellsTM, DOX-liposome loaded microbubbles were clearly cytotoxic (in case ultrasound was applied). In contrast, free DOX did not cause any significant tumor cell death. Our results indicate that very low amounts of doxorubicin can become significantly effective when loaded onto microbubbles and exposed to ultrasound. An interesting observation towards the delivery of DOX as a lower dose may become sufficient in the treatment of patients.

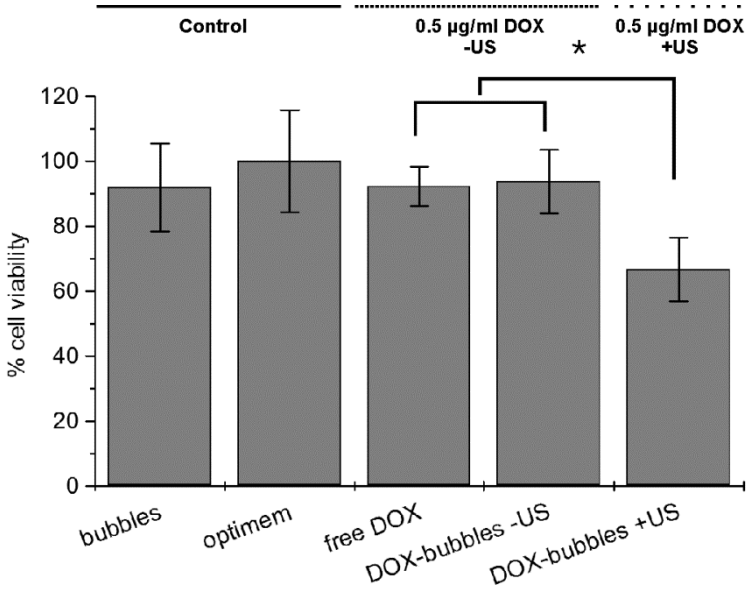


Figure 8: Viability measurements on melanoma cells with reduced dose: Viability of melanoma cells after exposure to respectively DOX-liposome loaded microbubbles (with and without ultrasound (US) treatment) and free DOX. The DOX- concentration in the wells was 0.5 µg/ml. Note that in these experiments we did not expect free DOX-liposomes to be present in the DOX-liposome loaded microbubble dispersion.

DISCUSSION

Here, it is shown that it is possible to design a safe and simple system for ultrasound guided drug delivery and we show that this system is very efficient *in vitro*, even when low amounts of model drug (DOX) are used. However, these *in vitro* experiments were performed in an ideal setting, because microbubbles were contacting the melanoma cells while sonicated, which probably leads to a more efficient sonoporation. In this respect, one could speculate on how to apply this system in an *in vivo* setting. Since microbubbles are relatively large particles, they will not pass the endothelial barrier in the tumor tissue; hence drug release has to occur in the blood vessels. The possible future clinical application of this system will depend on how efficient the drug will penetrate the tissue under ultrasound application. Fortunately it has been recently shown that ultrasound and microbubbles can lead to a permeabilization of the endothelial barrier in (tumor) tissue which causes extravasation of coinjected molecules or drugs [27], other studies prove that ultrasound and microbubbles can even cause a local opening of the Blood Brain Barrier (BBB) [28]. In our measurements we have clearly shown that active compound is released out of the liposomes after implosion of the microbubbles, this release of free DOX can diffuse into the tissue after disruption of the endothelial barrier and can have a fast effect on the tumor cells. Furthermore, it is likely that not every liposome is destructed after ultrasound insonation, but is released in the surrounding environment. These liposomes can also be delivered into the tissue after endothelial barrier disruption. Another mechanism of tumor killing *in vivo* can be the specific killing of the endothelial cell layer directly contacting the microbubbles that are affected by the ultrasound. This mechanism is directly comparable with the *in vitro* experiments performed in this chapter. The specific killing of endothelial cells will impair blood flow in the

tumor and induce necrosis of the tumor. To even improve contact between these endothelial cells and the liposome-loaded microbubble a targeting ligand might be introduced in the system. The use of liposome-loaded microbubbles will in the end allow killing of tumor cells using less drug, because the drug will only be delivered where and when ultrasound is applied. Furthermore, future *in vivo* experiments with this system will have to answer the question whether the efficiency of the therapy will be improved too, if sonoporation allows direct delivery of the drug in endothelial cells and increased uptake in tumor cells.

Another issue which is still prone to discussion is the drug dose which can be maximally loaded on and thus delivered by the microbubbles. A microbubble is relatively small, which limits the space for drug loading. We believe that binding (drug containing) vesicles (like liposomes) on the surface of the bubbles maximizes the amount of drug that can be loaded. From this point of view this strategy may be an advantage when compared with other approaches reported to load microbubbles with drugs, like e.g. ones which load the drug into an inner oil layer or in the bubble shell itself [17,18]. Though we showed that approximately 600 to 1300 liposomes can be bound per single microbubble the amount of DOX which becomes loaded in this way still remains rather limited. The loading may be further improved by applying multiple layers of liposomes around the microbubbles. The materials reported here can only be further clinically evaluated provided one can overcome the low drug loading obstacle. Nowadays cancer patients are treated with a relatively high dose of DOXYL™, i.e. 40-50 mg DOX per injection. Designing drug-loaded microbubbles which would allow such a high DOX dosing is highly likely impossible unless really high amounts of bubbles (in the order of 1×10^{13} bubbles/ml) could be injected. However, considering the targeted and more efficient delivery of DOX when ultrasound

and DOX-liposome loaded bubbles are used, we believe that such high DOX-doses might be no longer necessary, which may also reduce the severe side-effects of DOX-therapy in particular and chemotherapy in general. Since apparatus, that deliver ultrasound into a specific region deep into the tissue, are already under full development [29], the clinical evaluation of the drug-loaded microbubbles reported in this paper will smoothly move on and hopefully make it from bench to bedside.

CONCLUSIONS

This work showed that that DOX-liposome loaded microbubble can be obtained through self-assembly of (functionalized) phospholipids, drug-loaded liposomes and perfluorobutane gas. Importantly, this single step process results in a material which meets all criteria for clinical applicability: (a) no immunogenic compounds are used; (b) sterilization can easily be achieved through straightforward techniques and (c) adequate amounts of liposomes can be stably loaded on the surface of the bubbles. Through flow cytometry and Coulter Counter measurements we showed a maximal loading of the microbubbles with liposomes when the lipid shell of the microbubbles was composed of 35 mol% of DSPE-PEG-SPDP, resulting in approximately 600 to 1300 liposomes bound per single microbubble. Importantly, the liposomes remained bound to the microbubbles' surface upon incubation in plasma, being a clear requirement for clinical application. Ultrasound induced microbubble collapse clearly induced the release of DOX. When compared with free DOX and DOX-liposomes, we observed that DOX-liposome loaded microbubbles in combination with ultrasound showed a significantly stronger killing of cancer cells. It is our opinion

that the DOX-liposome loaded microbubbles described in this paper provide an opportunity for ultrasound targeted cancer therapy.

REFERENCES

- [1] A. Bouakaz, M. Versluis, J.N. de, High-speed optical observations of contrast agent destruction, *Ultrasound Med. Biol.* 31 (2005) 391-399.
- [2] J. Chomas, P. Dayton, D. May, K. Ferrara, Nondestructive subharmonic imaging, *IEEE Trans. Ultrason. Ferroelectr. Freq. Control* 49 (2002) 883-892
- [3] M. Postema, W.A. van, C.T. Lancee, J.N. de, Ultrasound-induced encapsulated microbubble phenomena, *Ultrasound Med. Biol.* 30 (2004) 827-840.
- [4] C.M. Newman, T. Bettinger, Gene therapy progress and prospects: ultrasound for gene transfer, *Gene Ther.* 14 (2007) 465-475.
- [5] K. Ferrara, R. Pollard, M. Borden, Ultrasound microbubble contrast agents: fundamentals and application to gene and drug delivery, *Annu. Rev. Biomed. Eng* 9 (2007) 415-447.
- [6] S. Mehier-Humbert, T. Bettinger, F. Yan, R.H. Guy, Plasma membrane poration induced by ultrasound exposure: implication for drug delivery, *J. Control Release* 104 (2005) 213-222.
- [7] C.D. Ohl, M. Arora, R. Iking, J.N. de, M. Versluis, M. Delius, D. Lohse, Sonoporation from jetting cavitation bubbles, *Biophys. J.* 91 (2006) 4285-4295.
- [8] M.M. Forbes, R.L. Steinberg, W.D. O'Brien, Jr., Examination of inertial cavitation of Optison in producing sonoporation of chinese hamster ovary cells, *Ultrasound Med. Biol.* 34 (2008) 2009-2018.
- [9] A. Rahim, S.L. Taylor, N.L. Bush, G.R. ter Haar, J.C. Bamber, C.D. Porter, Physical parameters affecting ultrasound/microbubble-mediated gene delivery efficiency in vitro, *Ultrasound Med. Biol.* 32 (2006) 1269-1279.
- [10] B.D. Meijering, L.J. Juffermans, W.A. van, R.H. Henning, I.S. Zuhorn, M. Emmer, A.M. Versteilen, W.J. Paulus, W.H. van Gilst, K. Kooiman, J.N. de, R.J. Musters, L.E. Deelman, O. Kamp, Ultrasound and microbubble-targeted delivery of macromolecules is regulated by induction of endocytosis and pore formation, *Circ. Res.* 104 (2009) 679-687.
- [11] A. Yudina, M. Lepetit-Coiffe, C.T. Moonen, Evaluation of the Temporal Window for Drug Delivery Following Ultrasound-Mediated Membrane Permeability Enhancement, *Mol. Imaging Biol.* (2010)
- [12] S. Meairs, A. Alonso, M. Fatar, R. Kern, M. Hennerici, Microbubbles traversing the blood-brain barrier for imaging and therapy, *Med. Biol. Eng Comput.* 47 (2009) 839-849.
- [13] L.H. Treat, N. McDannold, N. Vykhodtseva, Y. Zhang, K. Tam, K. Hynynen, Targeted delivery of doxorubicin to the rat brain at therapeutic levels using MRI-guided focused ultrasound, *Int. J. Cancer* 121 (2007) 901-907.
- [14] Z. Gao, A.M. Kennedy, D.A. Christensen, N.Y. Rapoport, Drug-loaded nano/microbubbles for combining ultrasonography and targeted chemotherapy, *Ultrasonics* 48 (2008) 260-270.
- [15] S. Hernot, A.L. Klibanov, Microbubbles in ultrasound-triggered drug and gene delivery, *Adv. Drug Deliv. Rev.* 60 (2008) 1153-1166.
- [16] I. Lentacker, B.G. De Geest, R.E. Vandenbroucke, L. Peeters, J. Demeester, S.C. De Smedt, N.N. Sanders, Ultrasound-responsive polymer-coated microbubbles that bind and protect DNA, *Langmuir* 22 (2006) 7273-7278.

- [17] S. Tinkov, G. Winter, C. Coester, R. Bekeredjian, New doxorubicin-loaded phospholipid microbubbles for targeted tumor therapy: Part I - Formulation development and in-vitro characterization, *J. Control Release* (2010)
- [18] K. Kooiman, M.R. Bohmer, M. Emmer, H.J. Vos, C. Chlon, W.T. Shi, C.S. Hall, S.H. de Winter, K. Schroen, M. Versluis, N. de Jong, A. van Wamel, Oil-filled polymer microcapsules for ultrasound-mediated delivery of lipophilic drugs, *J. Control Release* 133 (2009) 109-118.
- [19] M.R. Bohmer, A.L. Klibanov, K. Tiemann, C.S. Hall, H. Gruell, O.C. Steinbach, Ultrasound triggered image-guided drug delivery, *Eur. J. Radiol.* 70 (2009) 242-253.
- [20] I. Lentacker, S.C. De Smedt, N.N. Sanders, Drug loaded microbubble design for ultrasound triggered delivery, *Soft Matter* 5 (2009) 2161-2170.
- [21] I. Lentacker, B. Geers, J. Demeester, S.C. De Smedt, N.N. Sanders, Design and evaluation of doxorubicin-containing microbubbles for ultrasound-triggered doxorubicin delivery: cytotoxicity and mechanisms involved, *Mol. Ther.* 18 (2010) 101-108.
- [22] I. Lentacker, S.C. De Smedt, J. Demeester, V. Van Marck, M. Bracke, N.N. Sanders, Lipoplex-loaded microbubbles for gene delivery: A Trojan horse controlled by ultrasound, *Advanced Functional Materials* 17 (2007) 1910-1916.
- [23] R.E. Vandenbroucke, I. Lentacker, J. Demeester, S.C. De Smedt, N.N. Sanders, Ultrasound assisted siRNA delivery using PEG-siPlex loaded microbubbles, *J. Control Release* 126 (2008) 265-273.
- [24] I. Lentacker, R.E. Vandenbroucke, B. Lucas, J. Demeester, S.C. De Smedt, N.N. Sanders, New strategies for nucleic acid delivery to conquer cellular and nuclear membranes, *J. Control Release* 132 (2008) 279-288.
- [25] C. Brancewicz, D.H. Rasmussen, B. Papahadjoulos-Sternberg, Hydrophobic gas bubble formation in definity (R): A freeze fracture electron microscopy study, *Journal of Dispersion Science and Technology* 27 (2006) 761-765.
- [26] A.L. Klibanov, T.I. Shevchenko, B.I. Raju, R. Seip, C.T. Chin, Ultrasound-triggered release of materials entrapped in microbubble-liposome constructs: A tool for targeted drug delivery, *J. Control Release* (2010)
- [27] M.R. Bohmer, C.H. Chlon, B.I. Raju, C.T. Chin, T. Shevchenko, A.L. Klibanov, Focused ultrasound and microbubbles for enhanced extravasation, *J. Control Release* (2010)
- [28] K. Hynynen, Ultrasound for drug and gene delivery to the brain, *Adv. Drug Deliv. Rev.* 60 (2008) 1209-1217.
- [29] R. Seip, C.T. Chin, C.S. Hall, B.I. Raju, A. Ghanem, K. Tiemann, Targeted ultrasound-mediated delivery of nanoparticles: on the development of a new HIFU-based therapy and imaging device, *IEEE Trans. Biomed. Eng* 57

Chapter 3

Cell specific ultrasound-triggered drug delivery

Bart Geers¹, Olivier De Wever², Joseph Demeester¹, Marc Bracke², Stefaan C. De Smedt¹, Ine Lentacker¹

This chapter is accepted for publication in *Small*

¹Ghent Research Group on Nanomedicines, Laboratory of General Biochemistry and Physical Pharmacy, Faculty of Pharmaceutical Sciences, Ghent University, Harelbekestraat 72, 9000 Ghent, Belgium

²Laboratory of Experimental Cancer Research, Ghent University Hospital (UZ Gent), De Pintelaan 185, 9000 Ghent, Belgium

One of the main problems in cancer treatment is disease-relapse through metastatic colonization which is caused by circulating tumor cells (CTCs). This work reports on liposome-loaded microbubbles targeted to N-cadherin, a cell-cell adhesion molecule expressed by CTCs. It is shown that such microbubbles can indeed bind to N-cadherin at the surface of HMB2 cells; interestingly, in a mixture of cells with and without N-cadherin expression, binding of the liposome-loaded microbubbles mainly occurs to the N-cadherin expressing cells. Importantly, applying ultrasound results in the intracellular delivery of a model drug (loaded in the liposomes) in the N-cadherin expressing cells only. As described in this chapter, such liposome-loaded microbubbles may find applications as theranostics and in devices aimed for the specific killing of CTCs in blood.

INTRODUCTION

One of the main problems in cancer is disease-relapse due to metastases. Metastases cause most cancer deaths and originate from invasive cells that are formed in the primary tumor. Invasive cells can enter the bloodstream or the lymphatic system and spread out, to finally colonize a distant organ. Recently, new insights in the molecular processes that cause cancer have defined the switch of a non-invasive into an invasive phenotype as a hallmark of cancer [1,2].

The reason why cancer cells obtain this invasive phenotype may relate to a process called Epithelial-Mesenchymal Transition (EMT) [3]. Epithelial cells are characterized by a tight cell-cell adhesion, which involves specific adhesion molecules such as E-cadherin [4,5]. When such cells become invasive, E-cadherin expression becomes downregulated while other types of cadherins, namely the N-cadherins or mesenchymal cadherins, become upregulated [6]. Although a lot of debate on this matter is still ongoing, mesenchymal cadherins can be one of the key components that induce cell motility [7] and invasiveness [8]. Indeed, CTCs from patients with advanced solid tumors express mesenchymal markers including N-cadherin [9,10]. Consequently, mesenchymal cadherins may become ideal targets for selective drug delivery to Circulating Tumor Cells (CTCs). The idea of identifying such CTCs via (N-cadherin) antibody coated materials [11] inspired us to try to design N-cadherin targeted microbubbles aiming to selectively deliver therapeutic molecules (loaded on the microbubbles) to CTCs.

As shown in previous chapter and in more work by our group [12-14] and others [15-17], microbubbles show potential for ultrasound induced time- and space-controlled drug release. For this purpose, microbubbles can be coated with drug-

loaded nanoparticles that are associated with the shell of the bubbles. Their mechanism of action relies upon their specific interactions with the ultrasound wave. If a gas bubble encounters such a wave it will start to resonate due to the pressure fluctuations exerted by the ultrasound (named cavitation) [18]. If higher acoustic pressures are used, cavitation will result in a microbubble collapse (inertial cavitation) which can result in the release of the drugs or nanoparticles attached to or incorporated in the microbubbles. It has been observed that when microbubble collapse occurs in the vicinity of cell membranes, a transient opening of the cell membrane can be induced (“sonoporation”), which may improve drug uptake by cells [19,20].

Recently, microbubbles coated with antibodies [21] or nanobodies [22] directed against specific antigens have been reported as molecular imaging agents. As mentioned above and envisioned in Figure 1, in this paper we aim to evaluate whether a) it is possible to design a targeted drug-loaded microbubble, b) targeted microbubbles are able to selectively adhere to N-cadherin positive cells and c) whether (small) molecules can be selectively delivered to N-cadherin positive cells upon binding with N-cadherin targeted liposome-loaded microbubbles followed by exposure of ultrasound.

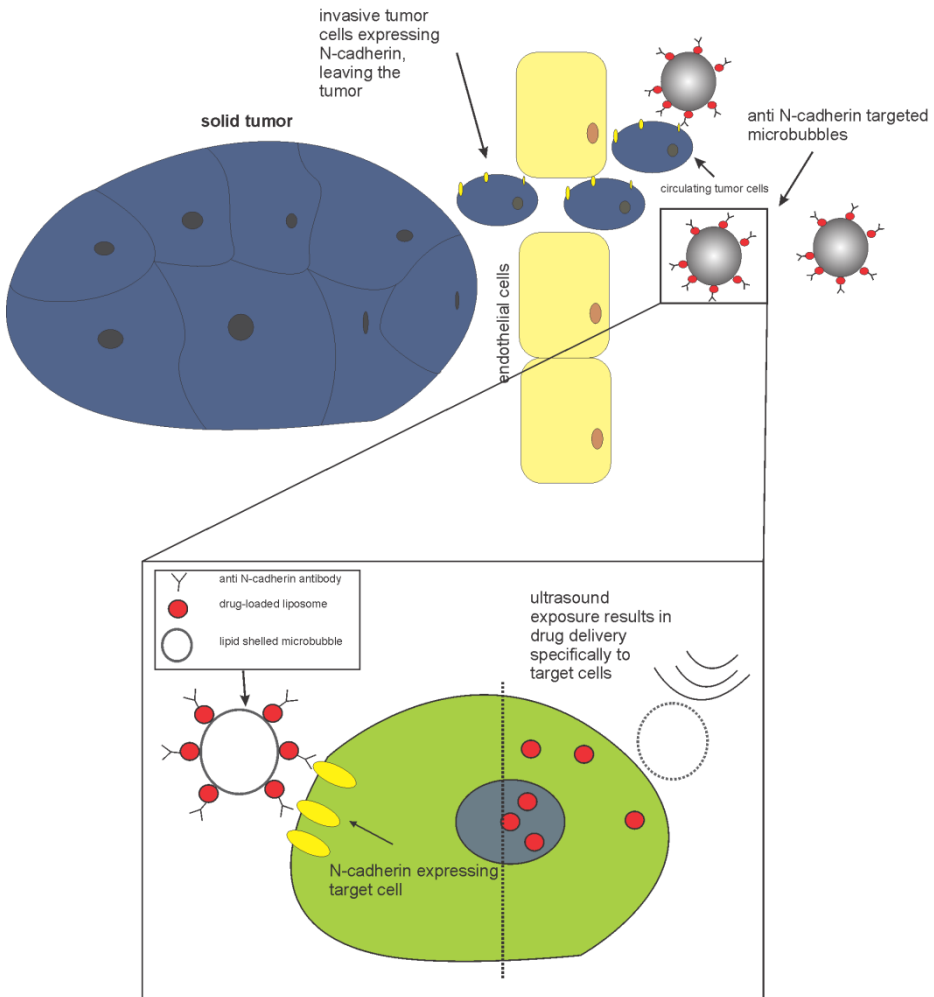


Figure 1: Schematic representation of the envisioned concept: drug loaded microbubbles, targeted through the use of N-cadherin antibodies, specifically adhere to circulating tumor cells expressing N-cadherin; subsequent ultrasound exposure may induce selective drug delivery to the circulating tumor cells.

MATERIALS AND METHODS

Preparation of functionalized liposomes

Liposomes were prepared as described earlier [12,14]. Briefly, 1,2-dipalmitoyl-*sn*-glycero-3-phosphocholine (DPPC), 1,2-distearoyl-*sn*-glycero-3-phosphoethanolamine-N- [maleimide(polyethylene glycol)-2000] (DSPE-PEG-maleimide) (Avanti polar lipids, Alabaster, AL) and cholesterol (Sigma-alldrich, Bornem, Belgium) dissolved in CHCl_3 were mixed in a round bottom flask. After solvent evaporation, the remaining lipid film was dissolved in HEPES-buffer (50 mM, pH 7.4, Sigma-alldrich, Bornem, Belgium), to obtain a liposome dispersion with a lipid concentration of 16mg/ml. This dispersion was extruded through a 200 nm filter with a mini-extruder at 60°C (Avanti-polar lipids, Alabaster, AL). Finally all produced batches were characterized with a Zetasizer (Nano-zs, Malvern, Worcestershire, UK) to evaluate the size-distribution.

Preparation of functionalized antibodies and targeted liposomes

Antibodies were functionalized with 2-imminothiolane or Traut's reagent (Thermo-scientific, Bornem, Belgium). 200 μl of aqueous solution containing N-cadherin (Mouse N-cadherin, Clone GC4, Sigma-alldrich, Bornem, Belgium) with a protein concentration of 3 mg/ml were mixed with 48 μl of Traut's reagent (1 mg/ml in HEPES-buffer). The mixture was allowed to react for 20 min in presence of the reducing agent dithiotreitol. (DTT) (Sigma-alldrich, Bornem, Belgium). Subsequently, reaction aliquots of this mixture were added to 100 μl of functionalized liposomes to obtain targeted liposomes.

Preparation of fluorescently labeled non-targeted and targeted liposomes

Fluorescently labeled targeted or non-targeted liposomes were prepared by adding the green- or red-fluorescent dyes: respectively cholesteryl-bodipy or 1,1'-dioctadecyl-3,3,3',3'-tetramethylindodicarbocyanine (DiD) (life-technologies, Merelbeke, Belgium) to the lipid mixture. DPPC, DSPE-PEG-maleimide and cholesterol dissolved in CHCl_3 were mixed with the fluorescent dye in a molar ratio of respectively 49:15:35:1.

Preparation of propidium iodide (PI)-loaded liposomes

Liposomes were prepared as described above by mixing DPPC, DSPE-PEG-maleimide and cholesterol dissolved in CHCl_3 in a round bottom flask. After solvent evaporation the lipid film was rehydrated with a 2 mg/ml PI (life technologies, Merelbeke, Belgium) solution dissolved in HEPES (50 mM, pH7.2). Subsequently, the liposomes were extruded through a 200 nm filter with a mini-extruder. After extrusion the resulting liposomes were centrifuged (Beckman L8-70M, Beckman-coulter, Brea, CA) at $109000 \times g$ for 1h to remove unencapsulated PI. After centrifugation the supernatant was removed and the remaining PI-loaded liposomes were dissolved in HEPES buffer.

Preparation of functionalized microbubbles

Microbubbles were prepared via the method earlier described by our group [12]. Briefly, these microbubbles were prepared starting from a mixture of DPPC and 1,2-distearoyl-sn-glycero-3-phosphoethanolamine-N- [PDP(polyethylene glycol)-2000] (DSPE-PEG-PDP) (Avanti polar lipids, Alabaster, AL) in a 1:2:7 glycerine:propyleneglycol:H₂O mixture. DPPC and DSPE-PEG-PDP were dissolved in this mixture with a molar ratio of 95:5. The lipid solution was prepared by mixing the different lipids dissolved in CHCl_3 in a round bottom

flask. After solvent evaporation, the remaining lipid film was dissolved in the glycerine:propyleneglycol:H₂O mixture. 1 ml aliquots of the lipid solution were transferred in glass vials and the headspaces of the vials were subsequently filled with C₄F₁₀ gas (F2 chemicals, Preston, UK). Microbubbles are obtained by mechanical activation of this solution in a Capmix™ (3M-ESPE, Diegem, Belgium) mechanical shaker.

Preparation and characterization of targeted liposome-loaded microbubbles

Targeted liposome-loaded microbubbles were prepared by adding targeted liposomes to the lipid solution. This mixture was transferred into glass vials and the headspace of the vials was filled with C₄F₁₀ gas. Targeted liposome-loaded microbubbles were then obtained by mechanical activation of the vials with a Capmix™ mechanical shaker. The constructs were characterized by confocal scanning laser microscopy (CSLM) (Nikon EZC1, Nikon, Brussels, Belgium) equipped with a 60 x oil immersion lens with a numerical aperture of 1.2. Subsequently, we labeled the liposomes with cholesteryl-bodipy as described above, antibodies were labeled by adding 30 μl of allophycocyanin (APC) labeled goat anti-mouse secondary antibodies (BD-pharmingen, Erembodegem, Belgium) to 1 ml of the targeted liposome-loaded microbubble dispersion. After reaction (10 min) and a short centrifugation step (300 x g for 1 min) to separate unbound secondary antibody from the microbubble dispersion, the microbubbles were imaged with CSLM using a Ar-ion laser with an excitation wavelength of 488 nm and a diode-pumped solid state laser with an excitation wavelength of 632 nm. Fluorescence was detected at emission wavelengths of 551 nm and 660 nm respectively. Non-targeted (without antibodies) liposome-loaded microbubbles were prepared via the same method.

Quantification of antibody-loading of the microbubbles

Targeted liposomes were prepared by adding 25, 50, 100 and 200 μl of functionalized N-cadherin antibodies (2.14 $\mu\text{g}/\mu\text{l}$) to 100 μl of liposomes. Targeted liposome-loaded microbubbles were subsequently prepared as described above. Antibody-loading was characterized with flow cytometry (BD FACScalibur, Beckton Dickinson, Erembodegem, Belgium) after labeling the targeted liposomes with secondary allophycocyanin-(APC) labeled goat anti-mouse antibodies. Again, the microbubble dispersion was centrifuged shortly (300 \times g, 1 min) to remove unbound secondary antibodies before flow cytometry analysis. The APC-label was excited using a 630nm red diode laser installed on the flow cytometer and fluorescence was detected at 670nm. All measurements were performed in triplicate.

Cell cultures

HMB2, BLM and H1299 cells were cultured in different media. HMB2 cells were cultured in F12-supplemented Dulbecco's modified Eagles medium (DMEM) containing 1% penicillin/streptomycin; 2 mmol/ml L-glutamine and 10% Fetal bovine serum (all purchased from Life Technologies, Merelbeke, Belgium). H1299 cells were cultured in Roswell Park Memorial Institute (RPMI) 1640 phenol red supplemented medium additionally supplemented with 1% penicillin/streptomycin; 2mmol/ml L-glutamine and 10% fetal bovine serum. BLM cells were cultured in F12-supplemented Dulbecco's modified Eagles medium (DMEM) containing 1% penicillin/streptomycin; 2mmol/ml L-glutamine and 10% Fetal bovine serum and 100 mmol/l HEPES pH 7.2. All cell types were cultured in 75cm² flasks in a humidified incubator at 37°C under 5% CO₂ atmosphere

Evaluation of targeting efficiency to HMB2 cells *in vitro*

Targeting efficiency was determined on HMB2 cells labeled with an aspecific green dye Cell Tracker™ bodipy (life technologies, Merelbeke, Belgium). HMB2 cells cultured in 75cm² flasks as described above were washed with phosphate buffered saline (PBS, life technologies, Merelbeke, Belgium). Subsequently, 10 ml optimem (life technologies, Merelbeke Belgium) was added to the cells together with 50 µl of Cell Tracker™ bodipy reagent (dissolved in DMSO 1mg/ml, life technologies, Merelbeke, Belgium). The cells were cultured for 15 min and afterwards washed with PBS. Subsequently the cells were detached with calcium supplemented trypsin prepared according to the protocol by *Boterberg et al. [33]*. The detached cells were resuspended in cell culture medium and centrifuged at 300 x g during 7 min. Finally the cells were resuspended in 4 ml PBS. 200 µl aliquots of the cell suspension were transferred into eppendorf tubes and 100 and 250 µl of targeted or non-targeted liposome-loaded microbubbles (1 x 10⁷ microbubbles/ml) labeled with a red-fluorescent dye (DiD) as described earlier were added to the eppendorf tubes containing the suspension of HMB2 cells. The resulting mixtures were analyzed with flow cytometry (BD FACScalibur, Beckton Dickinson, Erembodegem, Belgium) in triplicate. The Cell Tracker label was excited with the 488nm laser and detected in the 530 nm channel, the DiD-labeled microbubbles were excited with the 635 nm laser and fluorescence was detected in the 660nm channel. Events that showed significant fluorescence in both channels were regarded as cells with adherent microbubbles due to antibody-antigen interactions. The percentage of targeting was determined via quadrant analysis of the plots showing green against red fluorescence and were calculated via equation (1).

(1)

$$\begin{aligned} & \% \text{ HMB2 cells carrying microbubbles} \\ &= \frac{\text{number of events in quadrant } b}{\text{number of events in quadrant } c + \text{number of events in quadrant } b} \end{aligned}$$

Evaluation of N-cadherin expression on HMB2 cells

Cells were cultured as described above in 75 cm² cells and upon washing with PBS incubated with anti-N-cadherin antibody for 10 min at 37°C. Subsequently, unbound antibodies were removed and upon a second washing step (PBS) secondary goat anti-mouse Alexa-488-labeled antibodies (BD, Erembodegem, Belgium) were added to the cells. Upon incubation at 37°C the medium was removed and cells were detached with calcium supplemented trypsin and resuspended in PBS. Finally, flow cytometry was performed using with a BD FacsCalibur using the 488 nm excitation laser.

Evaluation of specific targeting in a mixture of cell types with flow cytometry

HMB2 and BLM cells were cultured in 75 cm² flasks and cells were washed with PBS before the experiments. HMB2 cells were stained with the green-fluorescent Cell Tracker™ dye as described in the previous section, washed and cells were detached with calcium supplemented trypsin. BLM cells were detached with 0.05% Trypsin-EDTA (life-technologies, Merelbeke, Belgium). After detachment of the cells, trypsin was inactivated with their respective cell culture media and centrifuged at 300 x g for 7min. After centrifugation cells were resuspended in 2 ml PBS and 200 µl aliquots of each cell type were transferred into eppendorf tubes. 250 µl of non-targeted and targeted liposome-loaded microbubbles (1 x 10⁷ microbubbles/ml) with a red-fluorescent DiD label, were added to this cell suspension and subsequently analyzed with flow cytometry by plotting green

against red fluorescence in density plots. These density plots were divided in quadrants (a,b,c and d) based upon measurements of cells and microbubbles only. All measurements were performed in triplicate.

Microscopic evaluation of specific targeting in a mixture of cell types

HMB2 and H1299 cells stably expressing enhanced green-fluorescent protein (EGFP) were used for these experiments. Again, cells were cultured in 75 cm² cell culture flasks and washed with PBS before experiment. HMB2 cells were detached with calcium supplemented trypsin and 0.25% trypsin-EDTA was used to detach the H1299 cells. Afterwards, trypsin was inactivated with the respective cell culture media and cells were centrifuged at 300 x g for 7min. After centrifugation the supernatant was removed and cells were resuspended in PBS. 200 µl aliquots were transferred into eppendorf tubes and 250 µl DiD-labeled targeted or non-targeted microbubbles (1 x 10⁷ microbubbles/ml) were added to the aliquots. The suspensions were transferred to slides to be analyzed with CSLM (Nikon EZC1, Nikon, Brussels Belgium) equipped with a 60 x water immersion objective with a numerical aperture of 1.2. EGFP was excited with the 488 nm Ar-ion laser and fluorescence was detected at 550 nm. DiD was excited with the 630 nm diode pumped laser and fluorescence was detected at 660 nm.

Ultrasound enhanced cell specific small molecule delivery

HMB2 and BLM cells were cultured in 75 cm² cell culture flasks and washed with PBS before experiment. HMB2 cells were labeled with Cell Tracker™ bodipy, afterwards detached with calcium supplemented trypsin and centrifuged as described above. BLM cells were detached with 0.05% Trypsin-EDTA (life technologies, Merelbeke, Belgium), trypsin was inactivated with cell culture medium and the cells were centrifuged as described above. After centrifugation

250µl aliquots were transferred into eppendorf tubes and 250 µl targeted- or non-targeted PI-liposome-loaded microbubbles (1×10^7 microbubbles/ml) were added to the cell suspension. The eppendorf tubes were submerged in a warm water bath (37°C) with an absorbing rubber and ultrasound was delivered during 20 s with a sonitron device (Artison Corporation, Inola, OK). The ultrasound frequency was 1 MHz, with a duty cycle of 50 %. Corresponding to measurements with a needle hydrophone, a maximum acoustic pressure of 600 kPa was obtained in the focus of the transducer. Samples were analyzed in triplicate by means of flow cytometry. Cell Tracker™ and PI were excited with the 488nm laser, and fluorescence was detected at respectively 530 nm and 670 nm. The percentage of PI positive cells was evaluated by quadrant analysis of plots, plotting Cell tracker™- against PI-fluorescence. Quadrants were chosen analogue with the analysis of the measurements described in section 5.11 and the percentage of HMB2 and BLM cells positive for PI was respectively calculated via equations (2) and (3).

(2)

% HMB2 cells positive for PI =

$$\frac{\text{number of events in quadrant } b}{\text{number of events in quadrant } d + \text{number of events in quadrant } b}$$

(3)

% BLM cells positive for PI =

$$\frac{\text{number of events in quadrant } a}{\text{number of events in quadrant } c + \text{number of events in quadrant } a}$$

Statistics

All data are presented as means +/- one standard deviation. A student's t-test was performed to determine whether datasets differed significantly. A p-value smaller than 0.05 was regarded significant.

RESULTS

Preparation and characterization of targeted liposome-loaded microbubbles

As described above [12], liposome-loaded microbubbles can be formed via mechanical activation of a solution of lipids (DPPC and DSPE-PEG-SPDP) in the presence of (chemically functionalized) liposomes and a hydrophobic (C_4F_{10}) gas. In this paper we use the same procedure, the only difference being the use of targeted (antibody containing) functionalized liposomes. First, free thiol (SH) groups were introduced on N-cadherin antibodies with Traut's reagent (2-Iminothiolane-HCl). Subsequently, targeted liposomes were made by addition of the SH enriched antibodies to maleimide-containing liposomes. The SH/maleimide ratio was kept low, leaving enough free maleimide groups available on the liposomes for coupling them to the microbubbles. The maleimide-containing liposomes were subsequently added to a vial containing a lipid solution composed of DPPC and DSPE-PEG-SPDP and covered with C_4F_{10} gas. In this way, the remaining free maleimide-groups on the surface of the liposome are able to form a stable bond with the DSPE-PEG-SPDP lipids. Subsequent mechanical activation of this dispersion (containing lipids and liposomes) results in the formation of targeted liposome-loaded microbubbles, as envisioned in Figure 2A, and as evidenced from confocal microscopy images (Figure 2 C-E) which clearly show co-localization of bodipy-labeled liposomes and secondary antibodies (against the N-cadherin antibodies). A detailed description of the preparation method can be found in the materials and methods section.

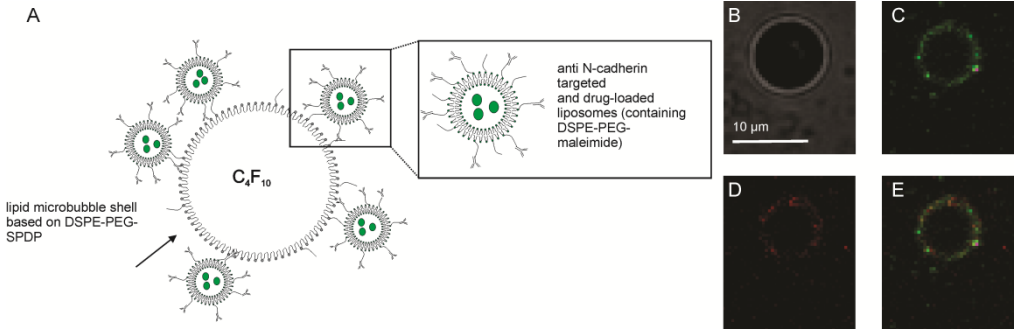


Figure 2: Schematic depiction of a targeted liposome-loaded microbubble (A) and corresponding microscopy images (B-E). Transmission (B) and confocal fluorescent images (C-E) of a microbubble loaded with (green fluorescent labeled) N-cadherin targeted liposomes. (C) Shows green fluorescence while (D) shows red fluorescence due to red-labeled secondary antibodies (against the N-cadherin antibodies). (E) is a merged image.

Optimal antibody-loading

As explained above, the same functionalized lipid in the liposomal bilayer (DSPE-PEG-maleimide) is used to a) equip the liposomal surface with N-cadherin antibodies and b) couple the targeted liposomes to the microbubbles (see **Figure 2A**). Therefore it was crucial to determine the maximal amount of antibodies that could be attached to the liposomal membrane without compromising microbubble coupling. To evaluate the amount of antibodies on the surface of the liposome-loaded microbubbles, we performed flow cytometry with red-fluorescent secondary antibodies (against the N-cadherin antibodies). **Figure 3** shows that the addition of 25 to 50 μl of thiol-activated antibody to 100 μl liposomes results in a maximal amount of antibodies loaded *per microbubble* (**Figure 3A**). Higher amounts of antibody might result in a higher antibody load *per liposome* but limits the amount of liposomes loaded *per microbubble*. To verify this, we used green- (cholesteryl-bodipy) labeled liposomes to measure the

amount of targeted liposomes loaded on the surface of the microbubbles with flow cytometry. Figure 3B shows that the use of higher amounts of N-cadherin antibodies indeed hampers liposome loading of the microbubbles. Based upon the data in figure 3A we decided to use 50 μl of N-cadherin antibody per 100 μl liposomes in the continuation of this work, corresponding to 107 μg of N-cadherin antibody added to 100 μl liposomes.

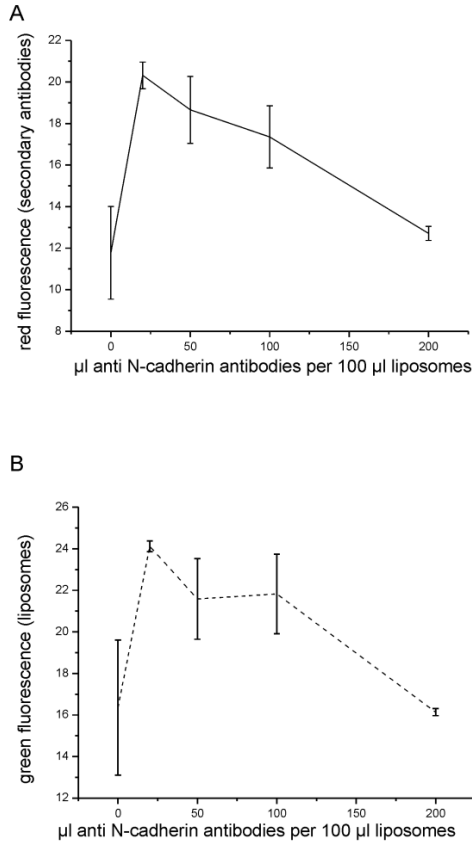


Figure 3: Quantitative flow cytometry analysis showing: (A) the red fluorescence (amount of N-cadherin antibodies) *per microbubble* and (B) the green fluorescence (amount of liposomes) *per microbubble*, as a function of the amount of N-cadherin antibodies added to the liposomes.

Selectivity of the concept: targeting-efficiency to N-cadherin expressing HMB2 cells

To evaluate the ability of the designed microbubbles to adhere to N-cadherin expressing metastatic tumor cells we performed flow cytometry and quantified the number of HMB2 cells (melanoma cell line derived from lymph node metastases) containing adhered microbubbles. Earlier, *Van Marck et al.* [23] showed that the HMB2 cell line is distinguished by a strong expression of the N-cadherin protein. For this experiment, we prepared red-labeled liposomes by incorporating the red-fluorescent lipophilic dye DiD (1,1'-dioctadecyl-3,3',3'-tetramethylindodicarbocyanine) in the liposomal membrane. Subsequently, these red-fluorescent N-cadherin targeted liposomes were coupled onto the microbubble surface resulting in red-labeled microbubbles. HMB2 cells were labeled in green by loading them with the aspecific intracellular dye Cell Tracker™ bodipy.

Figure 4 shows the number of HMB2 cells with and without microbubbles at their surface; note that in the experiments a) respectively 100 μ L and 250 μ L microbubble suspension (1×10^7 bubbles/ml) was added per 1×10^6 cells, b) targeted and non-targeted liposomes were used. In figure 4A, microbubble red fluorescence intensity is plotted on the Y-axis against the green fluorescence intensity coming from the HMB2 cells (X-axis). As a result, microbubbles can be found in the upper left quadrant a, HMB2 cells are seen in the lower right quadrant c while HMB2 cells with adhered microbubbles will be observed in quadrant b. Figure 4A shows a significant increase in events in quadrant b if targeted microbubbles are used, indicating adherence of the N-cadherin targeted microbubbles to the HMB2 cells. Adherence of non-targeted liposome-loaded

microbubbles to HMB2 cells is significantly lower, although some aspecific binding was observed. This may be caused by thiol-groups present on the surface of the cells interacting with some free maleimide-groups on the surface of the liposomes [24].

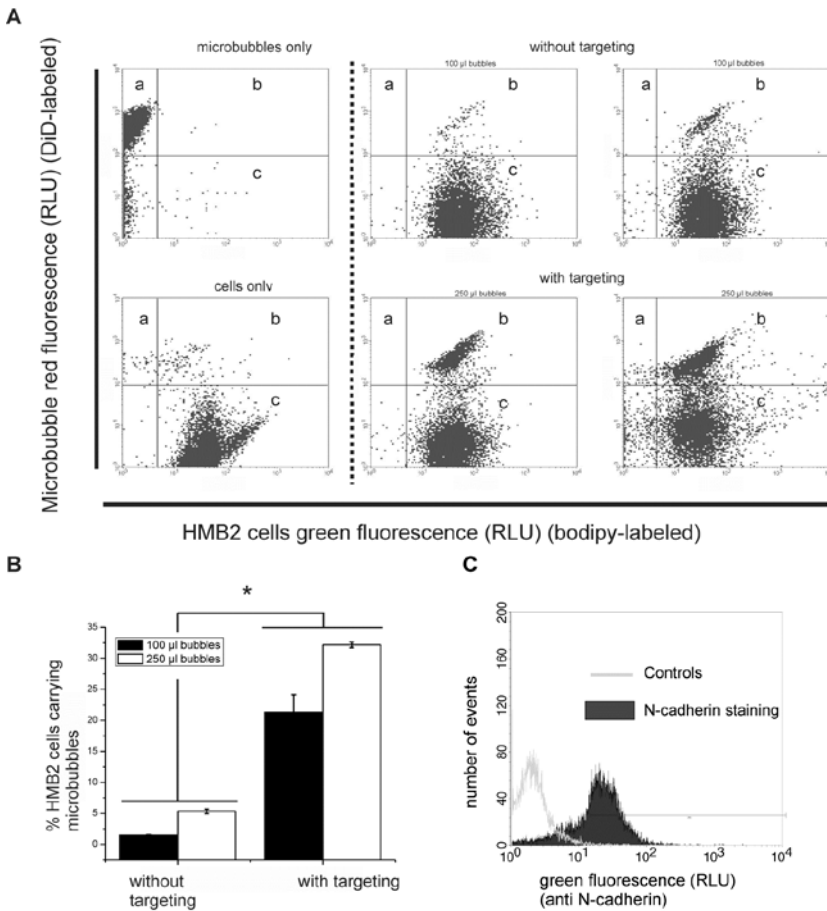


Figure 4: (A) Red (DiD)-labeled microbubbles (y-axis) and green (bodipy)-labeled HMB2 cells (x-axis) 'only' were used to define the quadrants (a,b,c). Binding of N-cadherin targeted liposome-loaded microbubbles to green HMB-2 cells was compared with the aspecific adherence of non-targeted

liposome-loaded microbubbles to the HMB-2 cells. (B) Percentage of HMB2 cells carrying microbubbles (as calculated from the number of events in quadrants b and c in (A)). (C) Green fluorescence intensity plot of HMB2 cells after exposing them to N-cadherin antibodies and subsequent staining with green-fluorescent secondary antibodies (HMB2 cells without N-cadherin staining were used as controls).

Subsequently, we measured the percentage of HMB2 cells carrying microbubbles, in case targeted and non-targeted liposomes were used. Figure 4B clearly shows that using targeted liposomes, the percentage of HMB2 cells carrying microbubbles is significantly higher. At the highest microbubble concentration used (which corresponds to approximately 2.5 microbubbles/cell, see materials and methods) up to 32% of the cells carried microbubbles targeted to N-cadherin. Without targeting maximally 5% of the HMB2 cells were “microbubble positive”. To have a more accurate view on microbubble targeting we measured which percentage of the HMB2 cells indeed expressed N-cadherin. Flow cytometry (Figure 4C) revealed that approximately 70% of the HMB2 cells expressed significant amounts of N-cadherin. Hence, we concluded that, under the experimental conditions used, about 1 out of 2 N-cadherin expressing cells was ‘found’ by the targeted liposome-loaded microbubbles.

Specificity of the concept: do targeted microbubbles specifically bind to N-cadherin expressing cells in a mixture of cells?

The next aim was to get an idea on the binding specificity of N-cadherin targeted liposome-loaded microbubbles in a mixture of different cell types. Therefore we analyzed to which extent targeted liposome-loaded microbubbles were able to bind specifically to HMB2 cells in a cell suspension composed of HMB2 cells

(with a significant expression of N-cadherin) and BLM melanoma cells which show only limited N-cadherin expression (*Van Marck et al* [23]).

HMB2 cells were labeled with the aspecific green dye Cell Tracker™ bodipy (as described above) while BLM cells were not fluorescently labeled, targeted and non-targeted microbubbles were red-labeled with DiD. **Figure 5A** shows density plots in which the red-fluorescent events, originating from DiD-labeled microbubbles, are plotted on the y-axis against the green fluorescent events from the green-labeled HMB 2 cells in the mixture of HMB2 and BLM cells. These plots were divided in quadrants based upon measurements with cells and microbubbles 'only'. Quadrant a represents events positive for red fluorescence (microbubbles) only, quadrant b represents events positive for both red and green fluorescence (microbubbles bound to HMB2 cells), quadrant c represents non-fluorescent events (BLM cells) and quadrant d represents events positive for green fluorescence only (HMB2 cells). Note that in Figure 5A the darker colored areas within the plots represent areas with a higher number of events occurring. In Figure 5A one can clearly observe that there is a shift in the number of events from quadrant a to quadrant b upon loading microbubbles with N-cadherin targeted liposomes (with targeting), indicating specific binding of targeted microbubbles to green-labeled HMB2 cells and not to BLM cells as this would result in an increase in events in quadrant a. Figure 5B shows the green fluorescent intensity plot obtained on a mixture of green-labeled HMB2 cells and non-labeled BLM cells, with indication of the two cell populations and corresponding quadrants in the density plots.

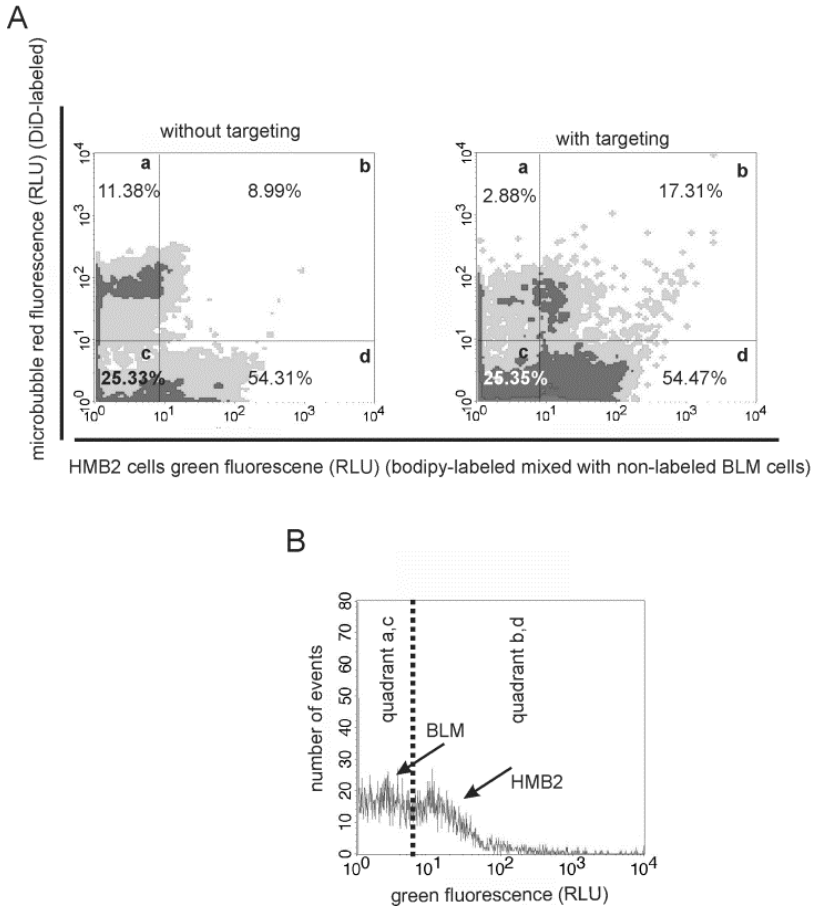


Figure 5: (A) shows flow cytometry density plots of green fluorescence (from HMB2 cells) against red fluorescence (from microbubbles) after addition of respectively non-targeted and N-cadherin targeted liposome-loaded microbubbles to a mixture of green-labeled HMB2 cells and non-labeled BLM cells (1:1). (B) Histogram showing the number of green fluorescent events in the mixture of green-labeled HMB2 cells and non-labeled BLM cells (without microbubbles). BLM cells only were used as a reference for quadrant analysis.

The flow cytometry observations described above were subsequently confirmed by confocal microscopy, using H1299 [25] lung carcinoma cell with impaired N-cadherin expression but expressing EGFP which allows to distinguish them under the microscope from the HMB2 cells; note that the H1299 cells were trypsin-EDTA treated which reduces the amount of surface proteins (including N-cadherin) significantly (data not shown). Figure 6 shows confocal images of a cell suspension with non-labeled HMB2 cells and EGFP expressing H1299 cells. We observed that the HMB2 cells have red-fluorescent (DiD-labeled) targeted liposome-loaded microbubbles closely bound to their surface while the microbubbles did not attach to the surface of the green H1299 cells.

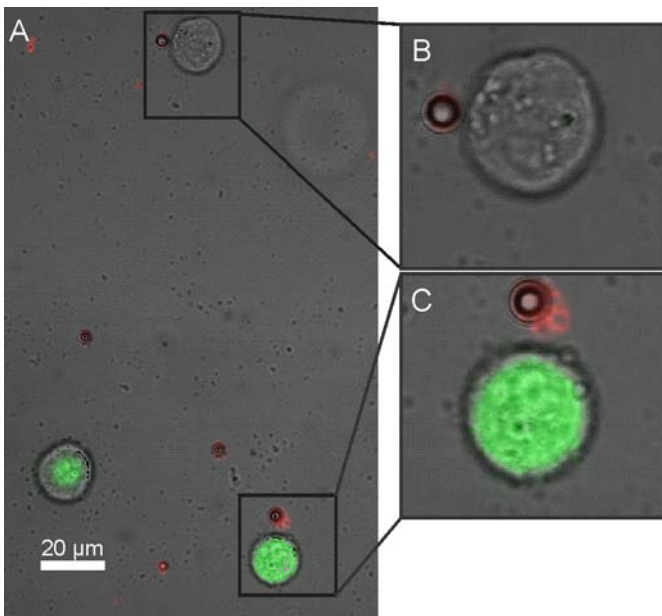


Figure 6: (A) Overlay of confocal fluorescent images of a cell suspension composed of EGFP expressing H1299 cells (lacking N-cadherin), HMB2 cells (expressing N-cadherin) and DiD-labeled

(red-fluorescent) targeted liposome-loaded microbubbles. (B and C) Show detailed zooms of both cell types.

Drug delivery to a specific cell type

To evaluate specific drug delivery to cells expressing N-cadherin as a metastatic marker, we loaded the targeted liposomes with propidium iodide (PI) as a model compound, as depicted in Figure 7A. PI is not able to spontaneously diffuse through cell membranes under normal conditions unless sonoporation and subsequent pore formation occurs [26,27].

Figure 7 gives an overview of the results obtained by flow cytometry. For this experiment, N-cadherin targeted PI liposome-loaded microbubbles were added to a mixture of green-labeled HMB2 cells and unlabeled BLM cells. The mixture contained 25% of HMB2 cells and 75% of BLM cells and was exposed to ultrasound, as described in the materials and methods section. We calculated the percentage of respectively HMB2 cells and BLM cells that showed PI uptake upon applying ultrasound by analyzing the events that were positive for both PI and bodipy fluorescence; the results are shown in Figure 7B. When targeted bubbles were used up to 20 % of the HMB2 cells were PI positive, while only 5% PI positive HMB2-cells were observed when non-targeted microbubbles were used. The BLM cells did not show any significant PI uptake (+/- 1%). These results indeed show that, under the given experimental conditions, drug delivery to specific cell types can be enhanced using targeted liposome-loaded microbubbles.

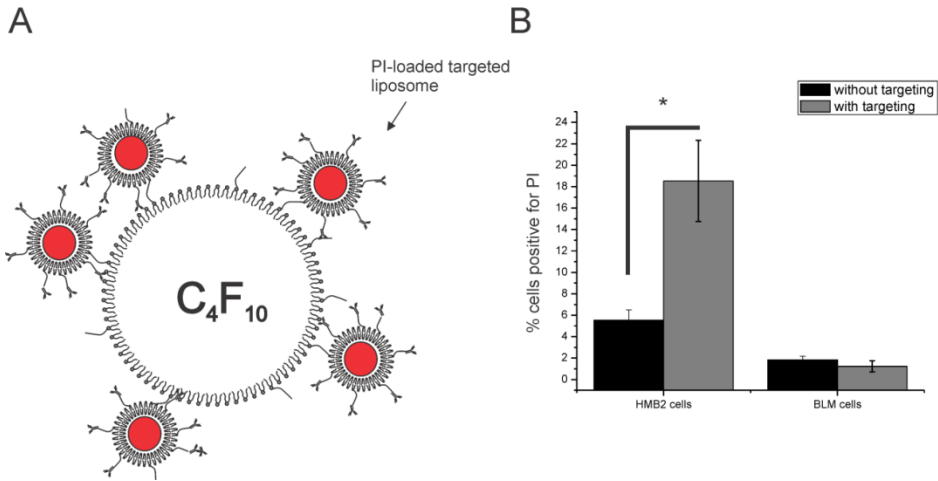


Figure 7: (A) Schematic representation of propidium iodide (PI)-loaded targeted liposomes loaded on lipid microbubbles. (B) Quantitative analysis of flow cytometry experiments on delivery of PI to green-fluorescent labeled HMB2 mixed with non-labeled BLM cells.

DISCUSSION

Above it is shown that a) coupling of N-cadherin antibodies to liposomes and subsequent loading of such constructs to lipid-shelled microbubbles via thiol-maleimide linkages is feasible, b) such targeted liposome-loaded microbubbles can adhere to N-cadherin expressing HMB2 cells, c) in a mixture of N-cadherin expressing HMB2 cells with BLM cells or H1299 cells, the microbubbles specifically adhere to the HMB2 cells and d) that microbubbles can deliver a small molecule (PI) into the target (HMB2) cells.

Clearly, a major question remains whether the concept introduced above has indeed the potential to kill circulating tumor cells *in vivo*. In this study a simplified experimental setup was used, i.e. only two cell types (dispersed in cell

medium) were mixed at high concentrations of target cells, while no flow was applied. *In vivo*, one can expect that only few circulating tumor cells present in a huge pool of blood cells have to be targeted. Hence, the ideal technology should not only be cell specific but also sufficiently sensitive.

To work under conditions as used in this study, and hence make the proposed system applicable in practice, cells should be isolated from blood *ex vivo*. Indeed, microfluidic devices are currently under full development to filter CTCs from blood [28-30]. Targeted (liposome-loaded) microbubbles might be applied in such devices allowing specific capturing and subsequent ultrasound induced killing of CTCs.

As introduced above, microbubbles are used clinically as imaging agents. In this regard the materials reported could be promising as a theranostic [31]. For example, microbubbles could be covered with drug-loaded liposomes and targeted to the Vascular Endothelial Growth Factor Receptor (VEGFR) which is involved in angiogenesis, a process of abnormal vessel growth that occurs in inflammation but also occurs when solid tumors are formed [32]. Such targeted microbubbles might adhere to the expressed VEGF receptors thereby enhancing tumor contrast, subsequently, upon using destructive ultrasound settings the delivery of anticancer drugs into the tumor could become promoted, through enhanced extravasation and sonoporation of the cancer cells. Targeting microbubbles to tumor endothelial cells would allow closer contact between microbubbles and these cells as well, increasing drug-delivery efficiency to these endothelial cells and hence tumor killing due to a loss of blood supply.

ACKNOWLEDGEMENTS

This research was funded by the EU FP7 collaborative project SONODRUGS (NMP-4-LA-2008-213706) and the FWO-flanders research project G.0187.11. Ine Lentacker is a post-doctoral fellow of the FWO flanders the financial support of this institute is thanked. Bram Clement is thanked for technical support.

REFERENCES

- [1] D. Hanahan and R.A. Weinberg, The hallmarks of cancer, *Cell*, 100 (2000) 57-70.
- [2] D. Hanahan and R.A. Weinberg, Hallmarks of cancer: the next generation, *Cell*, 144 (2011) 646-674.
- [3] M.W. Klymkowsky and P. Savagner, Epithelial-mesenchymal transition: a cancer researcher's conceptual friend and foe, *Am. J. Pathol.*, 174 (2009) 1588-1593.
- [4] G. Bex and R.F. van, Involvement of members of the cadherin superfamily in cancer, *Cold Spring Harb. Perspect. Biol.*, 1 (2009) a003129.
- [5] H. Semb and G. Christofori, The tumor-suppressor function of E-cadherin, *Am. J. Hum. Genet.*, 63 (1998) 1588-1593.
- [6] R.B. Hazan, R. Qiao, R. Keren, I. Badano, and K. Suyama, Cadherin switch in tumor progression, *Ann. N. Y. Acad. Sci.*, 1014 (2004) 155-163.
- [7] M.J. Wheelock, Y. Shintani, M. Maeda, Y. Fukumoto, and K.R. Johnson, Cadherin switching, *J. Cell Sci.*, 121 (2008) 727-735.
- [8] W.O. De, W. Westbroek, A. Verloes, N. Bloemen, M. Bracke, C. Gespach, E. Bruyneel, and M. Mareel, Critical role of N-cadherin in myofibroblast invasion and migration in vitro stimulated by colon-cancer-cell-derived TGF-beta or wounding, *J. Cell Sci.*, 117 (2004) 4691-4703.
- [9] P. Balasubramanian, J.C. Lang, K.R. Jatana, B. Miller, E. Ozer, M. Old, D.E. Schuller, A. Agrawal, T.N. Teknos, T.A. Summers, M.B. Lustberg, M. Zborowski, and J.J. Chalmers, Multiparameter Analysis, including EMT Markers, on Negatively Enriched Blood Samples from Patients with Squamous Cell Carcinoma of the Head and Neck, *Plos One*, 7 (2012).
- [10] A.J. Armstrong, M.S. Marengo, S. Oltean, G. Kemeny, R.L. Bitting, J.D. Turnbull, C.I. Herold, P.K. Marcom, D.J. George, and M.A. Garcia-Blanco, Circulating Tumor Cells from Patients with Advanced Prostate and Breast Cancer Display Both Epithelial and Mesenchymal Markers, *Molecular Cancer Research*, 9 (2011) 997-1007.
- [11] V. Sivagnanam, B. Song, C. Vandevyver, J.C. Bunzli, and M.A. Gijs, Selective breast cancer cell capture, culture, and immunocytochemical analysis using self-assembled magnetic bead patterns in a microfluidic chip, *Langmuir*, 26 (2010) 6091-6096.
- [12] B. Geers, I. Lentacker, N.N. Sanders, J. Demeester, S. Meairs, and S.C. De Smedt, Self-assembled liposome-loaded microbubbles: The missing link for safe and efficient ultrasound triggered drug-delivery, *J. Control Release*, 152 (2011) 249-256.
- [13] I. Lentacker, R.E. Vandenbroucke, B. Lucas, J. Demeester, S.C. De Smedt, and N.N. Sanders, New strategies for nucleic acid delivery to conquer cellular and nuclear membranes, *J. Control Release*, 132 (2008) 279-288.

- [14] I. Lentacker, B. Geers, J. Demeester, S.C. De Smedt, and N.N. Sanders, Design and evaluation of doxorubicin-containing microbubbles for ultrasound-triggered doxorubicin delivery: cytotoxicity and mechanisms involved, *Mol. Ther.*, 18 (2010) 101-108.
- [15] M.R. Bohmer, C.H. Chlon, B.I. Raju, C.T. Chin, T. Shevchenko, and A.L. Klibanov, Focused ultrasound and microbubbles for enhanced extravasation, *J. Control Release*, 148 (2010) 18-24.
- [16] K. Kooiman, M.R. Bohmer, M. Emmer, H.J. Vos, C. Chlon, W.T. Shi, C.S. Hall, S.H. de Winter, K. Schroen, M. Versluis, J.N. de, and W.A. Van, Oil-filled polymer microcapsules for ultrasound-mediated delivery of lipophilic drugs, *J. Control Release*, 133 (2009) 109-118.
- [17] S. Tinkov, C. Coester, S. Serba, N.A. Geis, H.A. Katus, G. Winter, and R. Bekeredjian, New doxorubicin-loaded phospholipid microbubbles for targeted tumor therapy: in-vivo characterization, *J. Control Release*, 148 (2010) 368-372.
- [18] E.P. Stride and C.C. Coussios, Cavitation and contrast: the use of bubbles in ultrasound imaging and therapy, *Proc. Inst. Mech. Eng H*, 224 (2010) 171-191.
- [19] B. Geers, I. Lentacker, A. Alonso, N.N. Sanders, J. Demeester, S. Meairs, and S.C. De Smedt, Elucidating the mechanisms behind sonoporation with adeno-associated virus-loaded microbubbles, *Mol. Pharm.*, 8 (2011) 2244-2251.
- [20] A. Van Wamel, K. Kooiman, M. Hartevelde, M. Emmer, F.J. ten Cate, M. Versluis, and N. de Jong, Vibrating microbubbles poking individual cells: drug transfer into cells via sonoporation, *J. Control Release*, 112 (2006) 149-155.
- [21] A.L. Klibanov, Ligand-carrying gas-filled microbubbles: ultrasound contrast agents for targeted molecular imaging, *Bioconjug. Chem.*, 16 (2005) 9-17.
- [22] S. Hernot, S. Unnikrishnan, Z. Du, T. Shevchenko, B. Cosyns, A. Broisat, J. Toczek, V. Cavelliers, S. Muyldermans, T. Lahoutte, A.L. Klibanov, and N. Devoogdt, Nanobody-coupled microbubbles as novel molecular tracer, *J. Control Release*, (2011).
- [23] V. Van Marck, C. Stove, K. Van Den Bossche, V. Stove, J. Paredes, H.Y. Vander, and M. Bracke, P-cadherin promotes cell-cell adhesion and counteracts invasion in human melanoma, *Cancer Res.*, 65 (2005) 8774-8783.
- [24] M.T. Stephan, J.J. Moon, S.H. Um, A. Bershteyn, and D.J. Irvine, Therapeutic cell engineering with surface-conjugated synthetic nanoparticles, *Nat. Med.*, 16 (2010) 1035-1041.
- [25] F.L. Fonseca, L.A. Azzalis, D. Feder, E. Nogoceke, V.B. Junqueira, V.E. Valenti, and L.C. de Abreu, Adhesion molecules affected by treatment of lung cancer cells with epidermal growth factor, *Lung*, 189 (2011) 383-389.
- [26] K. Kooiman, M. Foppen-Hartevelde, and N. de Jong, Ultrasound-mediated targeted microbubble sonoporation of endothelial cells, *J. Control Release*, 148 (2010) e62-e63.
- [27] K. Kooiman, M. Foppen-Hartevelde, A.F. van der Steen, and N. de Jong, Sonoporation of endothelial cells by vibrating targeted microbubbles, *J. Control Release*, 154 (2011) 35-41.
- [28] A.A. Adams, P.I. Okagbare, J. Feng, M.L. Hupert, D. Patterson, J. Gottert, R.L. McCarley, D. Nikitopoulos, M.C. Murphy, and S.A. Soper, Highly efficient circulating tumor cell isolation from whole blood and label-free enumeration using polymer-based microfluidics with an integrated conductivity sensor, *J. Am. Chem. Soc.*, 130 (2008) 8633-8641.
- [29] S.L. Stott, C.H. Hsu, D.I. Tsukrov, M. Yu, D.T. Miyamoto, B.A. Waltman, S.M. Rothenberg, A.M. Shah, M.E. Smas, G.K. Korir, F.P. Floyd, Jr., A.J. Gilman, J.B. Lord, D. Winokur, S. Springer, D. Irimia, S. Nagrath, L.V. Sequist, R.J. Lee, K.J. Isselbacher, S. Maheswaran, D.A. Haber, and M. Toner, Isolation of circulating tumor cells using a microvortex-generating herringbone-chip, *Proc. Natl. Acad. Sci. U. S. A.*, 107 (2010) 18392-18397.
- [30] S. Nagrath, L.V. Sequist, S. Maheswaran, D.W. Bell, D. Irimia, L. Ulkus, M.R. Smith, E.L. Kwak, S. Digumarthy, A. Muzikansky, P. Ryan, U.J. Balis, R.G. Tompkins, D.A. Haber, and

M. Toner, Isolation of rare circulating tumour cells in cancer patients by microchip technology, *Nature*, 450 (2007) 1235-1239.

[31] S. Fokong, B. Theek, Z. Wu, P. Koczera, L. Appold, S. Jorge, U. Resch-Genger, Z.M. van, G. Storm, F. Kiessling, and T. Lammers, Image-guided, targeted and triggered drug delivery to tumors using polymer-based microbubbles, *J. Control Release*, (2012).

[32] M. Potente, H. Gerhardt, and P. Carmeliet, Basic and therapeutic aspects of angiogenesis, *Cell*, 146 (2011) 873-887.

[33] T. Boterberg, M.E. Bracke, E.A. Bruyneel, and M.M. Mareel, Cell aggregation assays, *Methods Mol. Med.*, 58 (2001) 33-45.

Chapter 4

The influence of microbubble shell and the type of liposome loaded

Bart Geers¹, Ine De Cock¹, Heleen Dewitte¹, Ceciel Chlon², Marcel Böhmer², Joseph Demeester¹, Stefaan C. De Smedt¹, Ine Lentacker¹

Manuscript in preparation

¹ Lab of General Biochemistry and Physical Pharmacy, Faculty of Pharmaceutical Sciences, Ghent University, Harelbekestraat 72, 9000 Ghent, Belgium

²Philips Research Eindhoven, High Tech Campus 11, 5656 AE Eindhoven, The Netherlands

Microbubbles indeed, show great potential for time-and space-controlled drug delivery. In this work we wanted to evaluate the impact of shell composition and liposomal membrane composition on ultrasound induced drug-release from liposome-loaded microbubbles *in vitro* and the biophysical mechanisms behind it. We observe that liposome-loaded lipid-shelled microbubbles release more anticancer drug doxorubicin (DOX) and kill more cells *in vitro* upon ultrasound application, than when microbubbles are composed out of a polymer shell (poly-L-lactic acid-pentadecafluoro-octanol PLLA-PFO). Moreover, if thermosensitive liposomes are loaded at the surface of the microbubbles drug-release and *in vitro* cell killing is even more efficient. Fluorescence microscopy during ultrasound application reveals that upon loading microbubbles with thermosensitive liposomes free drug may be released from the microbubble instead of the particulate materials that is released from “standard” liposome-loaded microbubbles. This study hence reveals that (thermosensitive) liposome-loaded lipid-shelled microbubbles might be the most suitable carriers for further *in vivo* evaluation of ultrasound-triggered drug-delivery with liposome-loaded microbubbles.

INTRODUCTION

Microbubbles are stabilized by a (lipid, polymer or protein) shell. As shown in previous work [1-6], such microbubbles show potential for ultrasound induced time- and space-controlled drug release. Their mechanism of action relies upon their specific interactions with the ultrasound wave. If a gas bubble encounters such a wave it will start to resonate due to the pressure fluctuations exerted by the ultrasound (called cavitation) [7]. If higher acoustic pressures are used, cavitation will result in a microbubble collapse (inertial cavitation) which can result in the release of the drugs or nanoparticles attached to or incorporated in the microbubbles. It has been observed that when microbubble collapse occurs in the vicinity of cell membranes a transient opening of the cell membrane can be induced (“sonoporation”), which can improve drug uptake by the sonoporated cells [8,9]. In the past it is shown [10-13] that the concept of nanoparticle loaded microbubbles can be beneficial to induce local drug *release* and *uptake* at the same time.

Microbubbles made from stiffer shell materials, like e.g. polymers, respond differently to ultrasonic pressure fluctuations than the more elastic lipid-shelled microbubbles [14,15]. This suggests that the composition of the microbubble shell could have an influence on drug-delivery efficiency when drug-loaded liposomes or other nanoparticles are loaded on their surface.

Additionally, not only the microbubble shell itself but the liposomes’ phospholipid membrane can be tuned for more efficient drug-release as well. It has been shown that microbubble cavitation induces temperature changes of up to a 4°C and thus causes mild hyperthermia (41-42 °C) in the vicinity of an

oscillating microbubble [16,17]. Microbubble oscillations have as well been shown to induce a temperature increase of 1000°K in the vicinity of the microbubble [18,19]. Hence loading microbubbles with temperature sensitive liposomes may enhance the percentage of free drug released from these carriers. Liposomes can be made sensitive to temperature by incorporating phospholipids with a T_m around 40°C in their membranes (1,2-dipalmitoyl-sn-glycero-3-phosphocholine or DPPC), additional incorporation of so-called lysolipids (1-palmitoyl-2-hydroxy-sn-glycero-3-phosphocholine or MPPC) [20-22] may improve destabilization of the liposomal membrane at higher temperatures.

As schematically depicted in figure 1, this study aims to estimate the impact of microbubble shell composition (polymer or lipid) and liposome composition (standard or thermosensitive) on the drug-delivery efficiency from drug-loaded microbubbles upon ultrasound application.

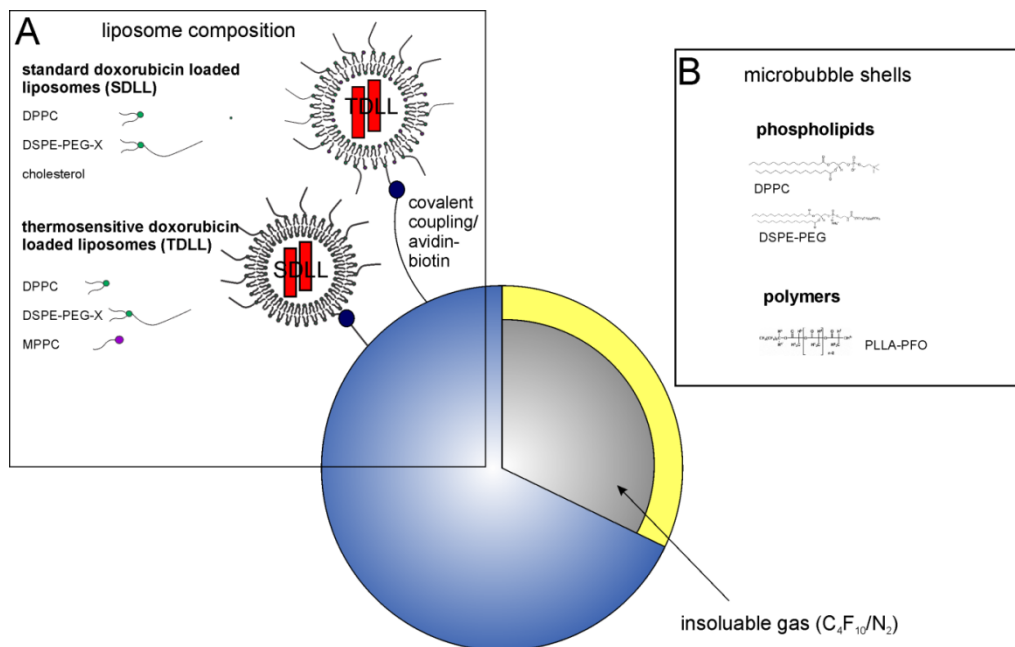


Figure 1: Schematic representation of the studied liposome loaded microbubbles. Microbubbles loaded with two different liposome types (standard or thermosensitive) (A) and with two different types of microbubble shells (polymer or lipid) are investigated (B).

MATERIALS AND METHODS

Preparation and characterization of Standard Doxorubicin (DOX) Loaded Liposomes (SDLL)

SDLL were prepared via the method described in earlier publications by our group [23,24]. Briefly, 1,2-dipalmitoyl-sn-glycero-3-phosphocholine (DPPC), 1,2-distearoyl-sn-glycero-3-phosphoethanolamine-N-[maleimide(polyethylene glycol)-2000] (DSPE-PEG-maleimide) or 1,2-distearoyl-sn-glycero-3-phosphoethanolamine-N-[biotinyl(polyethylene glycol)-2000] (DSPE-PEG-biotin) and cholesterol dissolved in CHCl_3 at a concentration of 20 mg/ml and 10 mg/ml respectively, were transferred in a round bottom flask in a 49:15:36 molar ratio. After evaporation, the remaining lipid film was rehydrated with buffer $(\text{NH}_4)_2\text{SO}_4$ (250 mM) to obtain a liposomal dispersion with a final lipid concentration of 16 mg/ml. The resulting liposome dispersion was extruded through a 200 nm filter using a mini-extruder at 60 °C. After extrusion the excess of ammonium sulfate was removed by ultracentrifugation at 109000 x g (Ultrafuge, Beckman-Coulter, Brea, CA). Hereafter the liposomal dispersion was aliquoted into 450 μl aliquots and liposomes were loaded with DOX by adding 50 μl of a doxorubicin.HCl (Sigma-alldrich, Bornem, Belgium) 10 mg/ml solution, afterwards this mixture was incubated at 50°C for 2hrs. Non-encapsulated DOX was removed in a second ultracentrifugation step at 109000 x g (Ultrafuge, Beckman-Coulter, Brea, CA). Final DOX concentration was evaluated using absorbance spectrometry (500 nm) using an Envision plate-reader and reached between 0.5 and 0.8 mg/ml (Perkin-elmer, Waltham, MA)

Preparation and characterization Thermosensitive Doxorubicin (DOX) Loaded Liposomes (TDLL)

TDLL were prepared using a method adapted from de Smet et al. [25]. 2-dipalmitoyl-sn-glycero-3-phosphocholine (DPPC), 1,2-distearoyl-sn-glycero-3-phosphoethanolamine-N-[maleimide(polyethylene glycol)-2000] (DSPE-PEG-maleimide) or 1,2-distearoyl-sn-glycero-3-phosphoethanolamine-N-[biotinyl(polyethylene glycol)-2000] (DSPE-PEG-biotin) dissolved in CHCl_3 at a concentration of 20 mg/ml and 10 mg/ml respectively and 1-palmitoyl-2-hydroxy-sn-glycero-3-phosphocholine (MPPC) dissolved in a CHCl_3 :EtOH (1:1) mixture at a concentration of 13.3 mg/ml were mixed in a round bottom flask in a molar ratio (DPPC:DSPE-PEG-maleimide:MPPC) of 82:10:8. After solvent evaporation the remaining lipid film was rehydrated with a 250 mM $(\text{NH}_4)_2\text{SO}_4$ buffer solution. The final lipid concentration of the liposomal dispersion in the flask was 32 mg/ml. The resulting dispersion was extruded through a 200 nm filter using a mini-extruder at 60 °C. After extrusion the excess of ammonium sulfate was removed by ultracentrifugation at 109000 x g (Ultrafuge, Beckman-Coulter, Brea, CA). Hereafter the dispersion was aliquoted into 400 μl aliquots and 100 μl of Doxorubicin.HCl (10 mg/ml) was added to the liposomal dispersion and was allowed to incubate at 37°C for 3 hrs. Upon incubation, the remaining unencapsulated doxorubicin was removed via ultracentrifugation at 109000 x g (Ultrafuge, Beckman-Coulter, Brea, CA). Final DOX concentration was evaluated using absorbance spectrometry (500 nm) using an Envision plate-reader and reached between 0.5 and 0.8 mg/ml (Perkin-elmer, Waltham, MA).

Evaluation of temperature induced Doxorubicin release from SDLL and TDLL

Both liposomal dispersions (SDLL and TDLL) were dissolved in HEPES buffer (50 mM, Sigma-alldrich, Bornem, Belgium) until a final concentration of 0.5 mg DOX/ml was reached. Samples were incubated at room temperature (25°C), 37°C and 43°C respectively for 20 mins. Upon incubation sample fluorescence (excitation wavelength 480 nm, emission wavelength 590 nm) was measured with an Envision plate reader (Perkin-elmer, Waltham, MA). Subsequently, the percentage of DOX-release was determined based on equation (1), Triton X-100 treated samples (TDLL and SDLL 0.5 mg DOX/ml) were measured as 100 % release controls.

$$\% \text{ DOX - release} = \frac{\text{sample fluorescence (43/25}^\circ\text{C)} - \text{sample fluorescence (37}^\circ\text{C)}}{\text{sample fluorescence (Triton X - 100)} - \text{sample fluorescence (37}^\circ\text{C)}}$$

Preparation and characterization of lipid-shelled microbubbles

Lipid-shelled microbubbles were prepared as described earlier by our group (Geers *et al.* 2011[23]). Briefly, microbubbles were prepared starting from a lipid solution being a mixture of 1,2-dipalmitoyl-*sn*-glycero-3-phosphocholine (DPPC) and 1,2-distearoyl-*sn*-glycero-3-phosphoethanolamine-N-[PDP(polyethylene glycol)-2000] (DSPE-PEG-PDP) (Avanti polar lipids, Albaster, AL) in a 1:2:7 glycerine-propyleneglycol-H₂O solvent (Sigma-alldrich, Bornem, Belgium), the molar ratio of the lipids in the lipid solutions was 95:5. Aliquots of this lipid solution were transferred into 2.5 ml chromatography vials, which headspace was filled with C₄F₁₀ gas (F2 chemicals, Preston, UK). Finally, functionalized microbubbles (with an average size of 3µm) were obtained by high speed shaking of the lipid solution in a Capmix™ device (3M-ESPE, Diegem, Belgium) during 15

sec. The size and the concentration of the microbubbles in the dispersion (i.e. number of microbubbles per mL) were determined with a Beckman-coulter Multisizer 4 (Beckman-coulter, Brea, CA).

Preparation of green-fluorescent labeled lipid-shelled microbubbles

Green-fluorescent labeled lipid-shelled microbubbles were prepared via the same procedure as non-labeled lipid-shelled microbubbles. A lipid solution was prepared containing DPPC, DSPE-PEG-SPDP, cholesteryl-bodipy (molecular probes, Merelbeke, Belgium) in a 1:2:7 glycerine-propyleneglycol-H₂O solvent.

Preparation and characterization of neutravidin coated poly-L-lactic acid-pentadecafluoro-octanol (PLLA-PFO) microbubbles

PLLA-PFO neutravidin coated bubbles were prepared as earlier described by *Chlon et al.* [26]. First, the polymers PLLA-PFO containing 10% w/w PLLA-biotin (synthesized at Philips Research Eindhoven) were dissolved in dichloromethane at 5% w/w. 250 mg of this solution was added to 100 mg of cyclodecane and 0.9 mg of dichloromethane and subsequently emulsified in 20 g of a 0.3% (w/w) PVA in H₂O solution. The obtained premix was passed through an acrodisk glass filter (1 μ m) 10 times. Subsequently the emulsion was stirred for 1 h to allow the dichloromethane to dissolve. Afterwards the remaining emulsion was centrifuged at 968 x g and the top fraction was retrieved and washed with a 5% Polyethyleneglycol (PEG MW= 3400) in H₂O solution containing neutravidin. Subsequently the obtained samples were rapidly frozen at -80°C o precooled glass vials. To remove ice and the cyclodecane fraction the samples were subsequently freeze dried in a Christ Epsilon 2-6 freeze drier (Martin Christ Gefriertrocknungsanlagen GmbH, Osterode am Harz, Germany). Samples were subjected to 2 freeze dry cycles at 1.98mbar for 20 hrs and at 0.03mbar for 20 hrs

respectively at a shelf temperature of -10°C . After freeze drying the system was filled with nitrogen and samples were stored at 4°C . Particle size and concentrations were measured using a Multisizer 4 (Beckman Coulter, Brea, CA).

Preparation of liposome loaded lipid and polymer-shelled microbubbles

To prepare liposome-loaded lipid-shelled microbubbles adequate amounts of SDLL or TDLL containing 15 mol% DSPE-PEG-maleimide were added to the lipid solution prior to adding C_4F_{10} and shaking of the vials. To obtain ideal concentrations for in vitro experiments (10^7 microbubbles/ml) HEPES buffer was added to the solution. PLLA-PFO capsules were loaded with liposomes by adding adequate amounts of DSPE-PEG-biotin containing SDLL or TDLL to the capsules dispersed in HEPES buffer (microbubble concentration 2×10^7 bubbles per ml)

***In vitro* evaluation of ultrasound induced drug release**

Liposome-loaded microbubbles (lipid or polymer-shelled) with a microbubble concentration of approximately 10^7 microbubbles per ml were dispersed in Opticell™ plates containing 9 ml of phosphate buffered saline (PBS) (Gibco, Merelbeke, Belgium) with a final doxorubicin concentration of approximately $5\mu\text{g/ml}$. Subsequently the Opticell™ plates were submerged in a water bath and samples were subjected to ultrasound during 15 s using the Sonitron device (Artison Corporation, Inola, OK, USA) equipped with a 2 cm ultrasound probe. This probe was used with an ultrasound frequency of 1 MHz with 50 % duty cycle at an ultrasound intensity of 2 W/cm^2 . The transducers' beam profile was evaluated with a needle hydrophone and the ultrasound settings used in these experiments correspond with a maximal acoustic pressure of 600 kPa. Negative control samples weren't subjected to ultrasound and positive control samples

were prepared by adding a 1:1 propyleneglycol:H₂O mixture to negative control samples. Dynamic Light Scattering (DLS) shows that application of this solvent to the samples dissolves the liposomal structures in the sample upon ultrasound application 100 µl aliquots of the samples were diluted with 100 µl PBS and fluorescence (excitation wavelength 480, emission wavelength 590 nm) was evaluated with an Envision plate reader. There were no differences in fluorescence of DOX at the concentrations used between the different solvents. Subsequently the % DOX-release was calculated via equation (2)

(2)

% DOX – release =

$$\frac{\text{Fluorescence (US subjected samples)} - \text{Fluorescence (negative control samples)}}{\text{Fluorescence (positive control samples)} - \text{Fluorescence (negative control samples)}}$$

Cell culture

BLM cells (melanoma cells) were cultured in F12-supplemented Dulbecco's modified Eagles medium (DMEM-F12) which contained 1% Penicillin/Streptomycin, 2mmol/l glutamine, 10 % Fetal bovine serum (FBS) (all purchased from Gibco, Merelbeke, Belgium) and 100 mmol/l HEPES pH 7.2. Cells were grown in a humidified incubator at 37°C in a 5 % CO₂ atmosphere.

In vitro evaluation of inherent toxicity of SDLL and TDLL

BLM cells were seeded in 12-well plates (1 × 10⁵ cells per well) and were grown to 90% confluence, which was reached two days after seeding. Cells were washed with PBS and subsequently 1ml of optimem (Gibco, Merelbeke, Belgium) mixed with SDLL or TDLL (5 µg DOX/ml) was added to the cells. After 24 hours cells were washed and the MTT reagent (Cell proliferation kit I, Roche diagnostics, Leuven, Belgium) was added for 4 hours. Subsequently, the solubilization

reagent was added and cells were incubated overnight to allow cell lysis at 37°C. The next day, the absorbance of each plate was measured in an absorbance plate reader at respectively 590 nm (OD₅₉₀) to determine the formed formazan and at 690 nm (OD₆₉₀) as a reference. The results of the cytotoxicity measurements are expressed as percentages; the viability of the cells which were only treated with optimum was considered to be 100 %, while the viability of cells exposed to a concentrated DMSO in H₂O solution was considered to be 0 %. Experiments were performed at least in triplicate.

***In vitro* evaluation ultrasound induced cell killing**

BLM cells were seeded in Opticell™ plates (1.3 × 10⁶ cells per Opticell™) and were grown to 90 % confluency, which was reached two days after seeding. Before experiments were performed, cells were washed with PBS. Subsequently, liposome loaded microbubbles were added to the cells. The following samples were prepared for the cytotoxicity experiments. A) Lipid microbubbles loaded with SDLL or TDLL were prepared by adding adequate amounts of TDLL or SDLL liposomes to 700 µl of lipid solution was added until a final volume of 1 ml and a DOX concentration of 60 µg/ml was reached. After shaking in the Capmix™ device. The 1 ml microbubble dispersion was added to 10 ml of optimum and this mixture was added to the cells in Opticell™ plates. PLLA-PFO shelled bubbles loaded with SDLL or TDLL were prepared by adding adequate amounts of DSPE-PEG-biotin containing liposomes to a dispersion of capsules in HEPES buffer until a final concentration of 120 µg/ml was reached with bubble concentration (2 × 10⁷ microbubbles per ml). 500 µl of the obtained dispersion was added to 10 ml of optimum and this mixture was added to the cells in the opticell plates. Subsequently, these plates were submerged in a warm water bath (37°C)

with a bottom of ultrasound absorbing rubber. Ultrasound was delivered by moving the Sonitron ultrasound probe over the whole plate during 10-15 sec. We used 1 MHz ultrasound with a 20 % duty cycle with an ultrasound intensity of 2 W/cm², as described above; the acoustic pressure exerted by the transducer at these settings was calculated to be 600 kPa. During ultrasound application cells were located on the top membrane of the Opticell™, in this way microbubbles are directly contacting the cells during sonication. After ultrasound application cell displacement was evaluated by means of microscopy and was always minimal with the microbubble concentrations used for these experiments. After 4 hours of incubation, microbubbles were removed; cells were washed with PBS and incubated in fresh culture medium. After 24 hours cells were washed and the MTT reagent (Cell proliferation kit I, Roche diagnostics, Leuven, Belgium) was added for 4 hours. Subsequently, the solubilization reagent was added and cells were incubated overnight to allow cell lysis at 37°C. The next day, the absorbance of each plate was measured in an absorbance plate reader at respectively 590 nm (OD₅₉₀) to determine the formed formazan and at 690 nm (OD₆₉₀) as a reference. The results of the cytotoxicity measurements are expressed as percentages; the viability of the cells which were only treated with optimem was considered to be 100 %, while the viability of cells exposed to a concentrated DMSO in H₂O solution was considered to be 0 %. Experiments were performed at least in triplicate.

Microscopy setup

Microscopy experiments were performed using a custom built setup that allows ultrasound application during microscopic imaging. This setup is comparable with the setup used in the experiments performed by *Van Wamel* [27,28] and

Kooiman et al. [29], but allows fluorescent imaging during ultrasound application. A Nikon EZC1 (Nikon, Brussels, Belgium) confocal inverted microscope equipped with an LSM tech objective inverter (LSM tech, Etters, PA) and a 40 x objective, was mounted with a water tank equipped with a panametrics A303 transducer. This single element transducer emits an ultrasound beam focused on the Opticell™ plate which is installed on the top-side the water tank. The ultrasound is generated by an Agilent 33210A arbitrary waveform generator (Agilent, Diegem, Belgium) and the signal produced by the waveform generator is amplified using an AR 100A400 amplifier (Amplifier Research, Hazerswoude Dorp, The Netherlands). The emitted signal is monitored with an oscilloscope.

Microscopic confocal fluorescence cell and microbubble (loaded with SDLL or TDLL) imaging during ultrasound application

BLM cells were seeded in Opticell™ plates (1.3×10^6 cells per Opticell™) and were grown to 90 % confluency, which was reached two days after seeding. Before experiments were performed, cell membranes were stained by adding 7 μ l of Cell Mask™ deep red (Life technologies, Merelbeke, Belgium) (2 mg/ml) to the cell medium and were subsequently washed with PBS and filled with 10 ml of optimem (Gibco, Merelbeke, Belgium). 100 μ l of a 1 in 10 dilution (solvent: PBS) of green-fluorescent labeled microbubbles loaded with SDLL or TDLL with a DOX concentration of 60 μ g/ml and a microbubble concentration of 10^8 microbubbles/ml or polymer-shelled microbubbles loaded with SDLL (identical DOX concentrations) were added to the cells. Afterwards the Opticell™ containing the experimental mixture was placed in the microscopy setup for microscopic confocal fluorescence imaging during ultrasound application. Excitation of the cell mask dye was performed with a diode laser at 630 nm;

emitted fluorescence was detected at 660 nm. Both cholesteryl-bodipy and DOX were excited with a diode laser at 488 nm; emitted laser light was detected at 550 and 590 nm respectively. Fluorescent time-lapse images were acquired starting 4 seconds before ultrasound application and lasted for 20s upon ultrasound application. Ultrasound was applied by triggering the arbitrary wave generator to emit a sinusoidal wave with a frequency of 1MHz, amplitude of 1.6 Vpp (peak to peak). The wave was emitted as a burst of 2000 cycles with a burst period of 8 ms. The measured signal after amplification was measured with the oscilloscope and equaled 220 V which corresponds with an acoustic pressure of 400 kPa at the focus of the transducer as determined with a needle hydrophone. Images were analyzed using ImageJ software by defining the intracellular space of at least ten cells per acquired time-lapse frame as a ROI. The amount of DOX fluorescence (ex: 488 nm, em: 590 nm) was afterwards measured per ROI and determined in function of time.

Statistic analysis

All measurements were performed at least in triplicate unless otherwise stated, presented as means +/- one standard deviation and statistical significance was determined using a students t-test or ANOVA analysis when multiple samples were compared. A p-value smaller than 0.05 was regarded as statistically significant.

RESULTS

As mentioned before, the aim of this paper is to evaluate the influence of microbubble type and liposome type on (a) the ultrasound induced cell killing (b) the ultrasound induced DOX-release and finally (c) we aim to evaluate the mechanisms of drug-release of the most efficient formulation with fluorescence microscopy during ultrasound application.

Analysis of temperature induced DOX-release from SDLL and TDLL

To estimate the impact of liposome formulation on ultrasound induced drug release from the microbubbles we prepared two different DOX-loaded microbubble formulations a) standard DOX-containing liposomes (SDLL) containing DPPC, DSPE-PEG and cholesterol (formulation used in previous studies) and b) thermosensitive DOX-containing liposomes (TDLL) containing DPPC, DSPE-PEG and MPPC. The latter is based on formulations described earlier [20].

To verify whether the developed TDLL were indeed thermosensitive, we measured the temperature-induced DOX-release from both SDLL and TDLL without microbubbles by means of fluorescence measurements as shown in figure 2. The presence of DOX precipitates in the intraliposomal space significantly quenches DOX fluorescence. In contrast, DOX fluorescence increases when the liposomes break up (under the influence of surfactants or when temperature is increased) and release the encapsulated DOX. This increase was used to estimate the % of DOX release from both liposome types as explained in the materials and methods section. For the TDLL we observed an increase in DOX fluorescence intensity of approximately 60% when liposomes were incubated at 43°C (using

37°C as a reference). SDLL on the other hand showed no temperature induced DOX release since fluorescence did not increase upon heating the liposomes to 43°C. We compared DOX fluorescence intensity from both SDLL and TDLL at 37°C and 25°C as well, but no significant differences between samples were found, indicating that both liposome formulations were stable at room temperature.

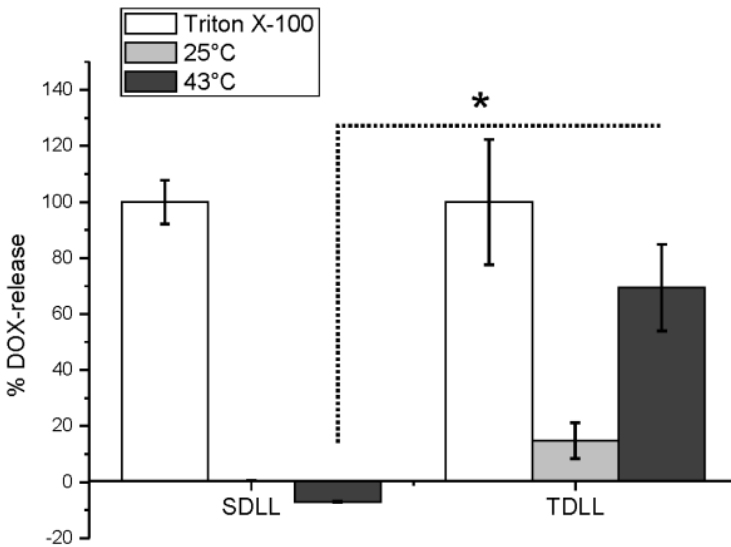


Figure 2: temperature induced % DOX-release based upon fluorescence intensity measurements of SDLL and TDLL upon incubation of the samples at 25°C and 43°C. Fluorescence intensity of Triton X-100 treated liposomes was regarded as 100% release there where liposomes incubated at 37°C were regarded as negative controls.

Influence of microbubble shell and liposomal composition on the ultrasound induced tumor cell killing efficiency.

We evaluated the inherent toxicity of the liposomal formulations (SDLL and TDLL) at 2 different DOX concentrations (5 μ g and 10 μ g DOX per well). As shown in figure 3A TDLL induce more cytotoxicity at both incubation times (45 min and 4 h), most likely this cytotoxicity will be caused by leakage of free DOX out of the liposome as described by *Tagami et al.* [30]. However, if the incubation time is limited to 45 min and if low DOX concentrations are used, the effect of external events (like ultrasound) will be maximal. Hence, we selected these particular incubation times and concentrations for the continuation of this work.

Next, we determined the ultrasound-triggered cell killing effect of DOX-liposome (6 μ g DOX/ml) loaded microbubbles (10⁷ microbubbles/ml) composed of different shell (PLLA-PFO or lipids) materials and loaded with SDLL or TDLL. As shown in figure 3B, we observe significant ultrasound-triggered cell killing when using lipid-shelled microbubbles. Especially, when TDLL are loaded on the surface of these microbubbles the highest cell killing effect is achieved (only 45 % of the treated cells remain viable). PLLA-PFO shelled microbubbles (loaded with both types of liposomes) on the other hand, didn't show significant ultrasound induced cell killing compared to the unloaded ultrasound treated PLLA-PFO control microbubbles.

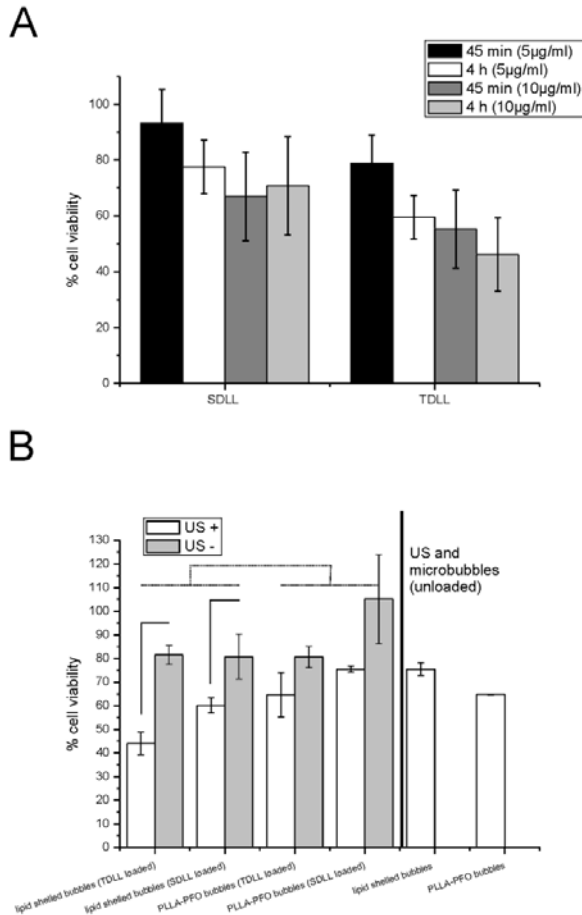


Figure 3: (A) Cytotoxicity measurements (MTT) on melanoma cells comparing the inherent cytotoxicity of SDLL and TDLL with two different DOX concentrations (5 and 10 µg DOX per ml) and two different incubations times (45 min and 4h). (B) Cytotoxicity measurements (MTT) of ultrasound-triggered cell killing on melanoma cells. The ultrasound induced cell killing (white bars) of lipid-shelled and PLLA-PFO shelled microbubbles loaded with TDLL or SDLL (6 µg/ml DOX and 10⁷ microbubbles/ml), was compared to samples that were not ultrasound treated with ultrasound (gray bars). Unloaded ultrasound treated microbubbles were measured as control samples.

Influence of microbubble shell and liposomal composition on the ultrasound induced drug release.

To evaluate our hypothesis that an increased DOX release is responsible for the observed differences in tumor cell killing, we compared the ultrasound induced DOX-release from DOX-liposome loaded microbubbles composed out of different shell materials (PLLA-PFO or lipid) and loaded with different liposomal formulations (SDLL or TDLL). To calculate the % DOX-release, DOX fluorescence intensity after ultrasound exposure of DOX-liposome loaded microbubbles was compared to loaded microbubbles without ultrasound application (negative controls) and samples treated with a 1:1 propyleneglycol:H₂O mixture (positive controls). As shown in figure 4 ultrasound application induces a 50% DOX-release from PLLA-PFO-shelled microbubbles loaded with SDLL. Ultrasound application on lipid-shelled microbubbles loaded with SDLL on the other hand induces more DOX-release (65%). Indeed, these results indicate that ultrasound-triggered drug release is more efficient when lipid-shelled microbubbles are used compared to PLLA-PFO polymer bubbles. We analyzed ultrasound-triggered DOX-release from lipid-shelled microbubbles loaded with TDLL as well and here we observed that almost all DOX was released from the microbubbles. This indicates that loading lipid-shelled microbubbles with TDLL results in a more efficient ultrasound-triggered drug release compared to SDLL loading.

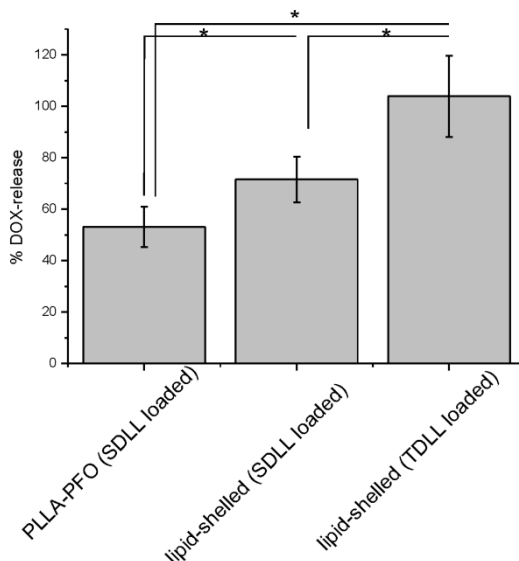


Figure 4: % Ultrasound induced DOX-release from PLLA-PFO shelled microbubbles loaded with SDLL and lipid-shelled microbubbles loaded with SDLL or TDLL (5 $\mu\text{g/ml}$ DOX and 10^7 microbubbles/ml in all samples) based on DOX fluorescence intensity measurements. Liposome loaded microbubbles without ultrasound treatment were regarded as 0% controls while propyleneglycol:H₂O treated samples were regarded as 100% controls.

Microscopic evaluation during ultrasound application

We further wanted to evaluate the mechanisms behind ultrasound induced drug-release from lipid-shelled microbubbles. Hence, we investigated the differences in ultrasound-triggered drug release in function of the type of liposome (TDLL or SDLL) loaded on lipid-shelled microbubbles as visualized with confocal fluorescent imaging during ultrasound application. As schematically shown in figure 5, a customized setup was installed on a confocal scanning laser microscope (as explained in detail in the materials and methods section) allowing

synchronized fluorescent cell and microbubble imaging while the cells were in the focus of a single element ultrasound transducer.

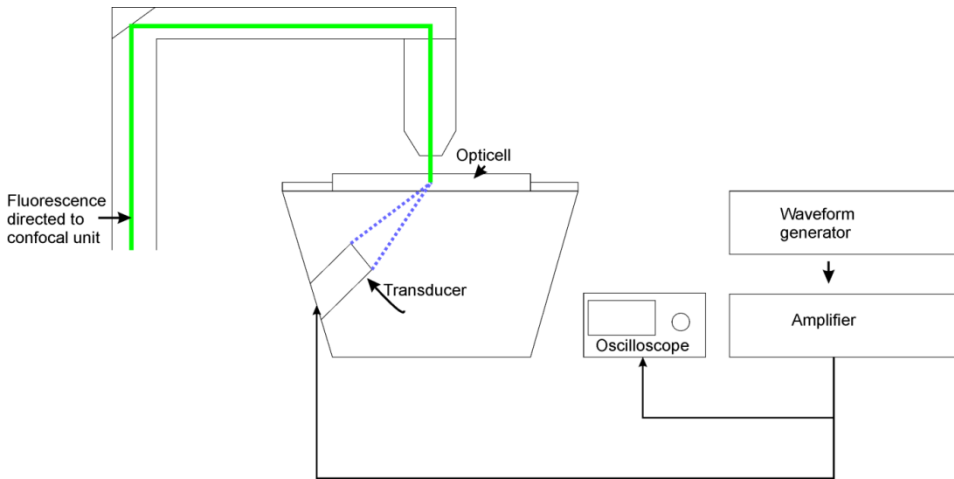


Figure 5: Schematic depiction of the microscopy setup used for confocal fluorescent cell imaging during ultrasound application.

Figure 6 shows overlays of confocal fluorescent images of ultrasound-triggered drug release from lipid-shelled bubbles loaded with TDLL (figure 6A) or loaded with SDLL (figure 6B). One can observe a difference in microbubble implosion and subsequent drug release between both types of formulations. It appears that ultrasound induces a direct release of free DOX from microbubbles loaded with TDLL. The lipid material of the microbubble (green-fluorescent) seems to be released in the form of a mist. Looking upon the images of the SDLL loaded bubbles one can observe that clumpy material adheres to the cells or is delivered into the cytoplasm of the cells upon ultrasound application. Indeed, these data suggest that loading lipid-shelled microbubbles with TDLL induces direct homogenous release of free DOX upon ultrasound application, there where

loading with SDLL results in a release of vesicular material from the microbubbles.

We were not able to investigate polymer-shelled microbubbles with a green-fluorescent labeled shell. However, we've included quantitative data obtained by fluorescence microscopy during ultrasound application in the next section.

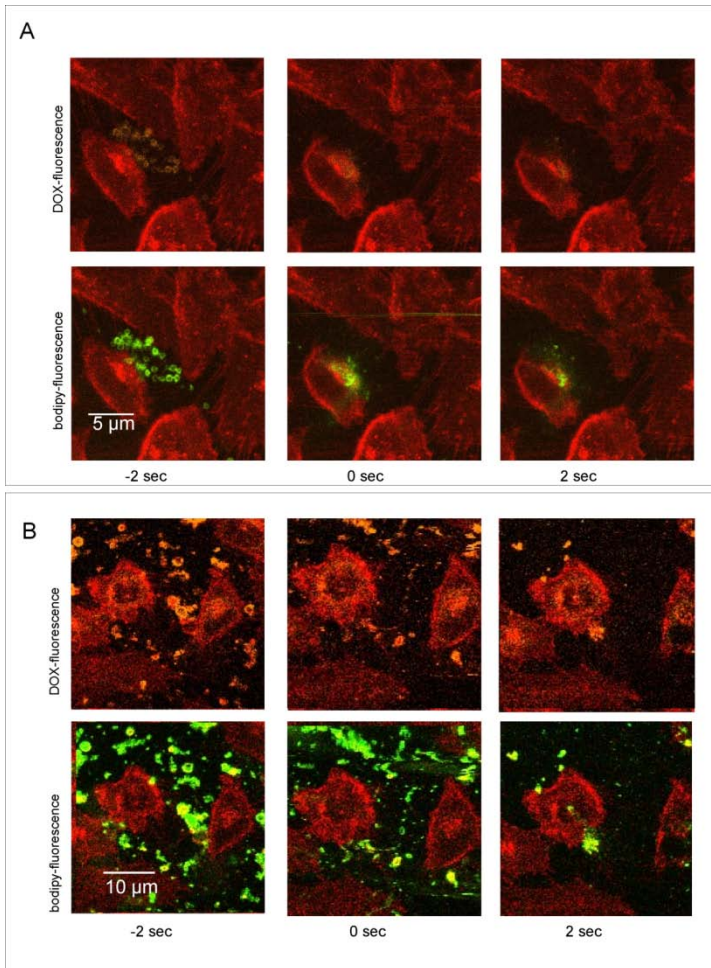


Figure 6: Overlay of confocal fluorescent images of BLM cells exposed to TDLL liposome loaded lipid microbubbles (A) and SDLL liposome loaded lipid microbubbles (B) acquired during ultrasound application. BLM cell membranes were labeled with Cell Mask™ deep red, microbubble (lipid) shells were labeled with cholesteryl-bodipy and DOX-liposomes were visualized by their inherent fluorescence. (A) Shows images obtained with TDLL loaded microbubbles before (-2 sec) and during (0 sec and 2 sec) ultrasound application. (B) Shows images obtained with SDLL loaded microbubbles at the same time points. Images are shown as merged images of red fluorescence with DOX fluorescence (top row) and merged images of red-fluorescence with green- (bodipy) fluorescence (bottom row).

Quantitative analysis of confocal fluorescent images during ultrasound application of lipid-shelled microbubbles in function of type of liposome loaded

To verify the assumptions on drug-release made in the previous section and to analyze DOX-release from polymer-shelled microbubbles, we performed quantitative image processing on the fluorescent images in function of time post ultrasound application. We defined the intracellular space of (at least) 10 BLM cells with red-fluorescent labeled cell membranes as ROIs and we subsequently analyzed the DOX fluorescence intensity of these ROIs frame per frame (as a function of time). The results of this analysis (shown as relative values to be able to compare different results) are shown in figure 7. Here, one can clearly observe a significant increase in the mean DOX fluorescence per cell if TDLL are loaded on the surface of the lipid-shelled microbubbles. In contrast, SDLL coupling on the microbubble shell caused a much slower rise in DOX fluorescence per cell. Quantitative image processing hence reveals that a release of free DOX might be involved in ultrasound triggered drug delivery from lipid-shelled microbubbles loaded with TDLL. Another type of drug-release is clearly involved upon loading microbubbles with SDLL, which may relate to the release of vesicles and not free

DOX molecules upon ultrasound application. Polymer-shelled microbubbles loaded with TDLL don't show any uptake of DOX upon ultrasound application. Instead we observe a decrease in the relative DOX fluorescence per cell which may be caused by photo bleaching. Hence, we can conclude that drug release from polymer-shelled liposome-loaded microbubbles will be minimal.

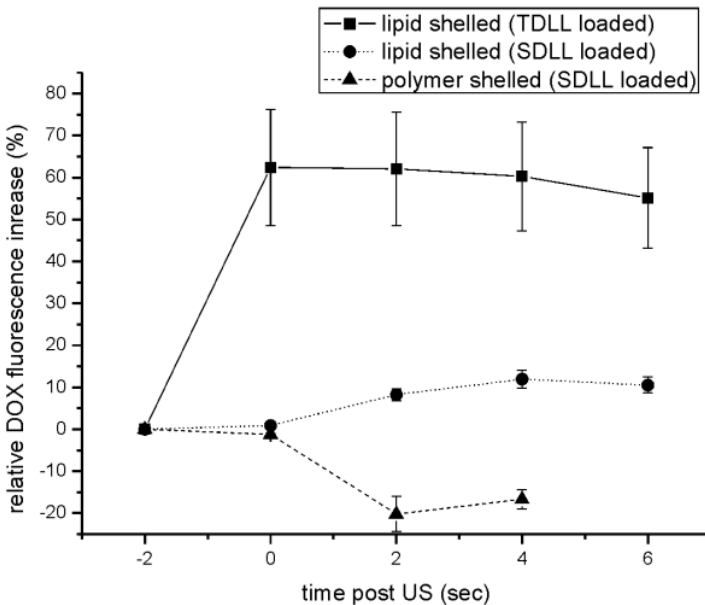


Figure 7: Quantitative analysis of DOX fluorescence per cell (based on cell ROIs in time-lapse microscopic images) in function of time post ultrasound application. Results are shown as relative increase of fluorescence compared with cell fluorescence before ultrasound application (-2 sec).

DISCUSSION

Above is shown that a) ultrasound induces more drug release from lipid-shelled drug-loaded microbubbles than from PLLA-PFO shelled drug-loaded microbubbles; b) ultrasound induces more drug-release from lipid-shelled microbubbles loaded with TDLL than from lipid-shelled microbubbles loaded with SDLL; c) in vitro tumor cell killing is significantly higher with lipid-shelled TDLL loaded microbubbles and finally; d) these observations may be explained by a release of free DOX from TDLL loaded lipid-shelled microbubbles upon ultrasound application as shown by confocal fluorescence microscopy during ultrasound application.

The observed differences in drug-delivery efficiency may be due to a difference in response to ultrasound between polymer- and lipid-shelled microbubbles. As depicted in figure 8A polymer coated microbubbles show gas-release only at the weakest point in the polymer coating (so-called “cracking [14]), leaving the other parts of the polymer shell and the liposomes loaded on their surface intact. This may indeed be caused by cracking of the polymer shell. In contrast to this, lipid coatings are damaged more homogeneously (so-called fragmentation [31,32]) during microbubble implosion. This fragmentation affects nearly all loaded liposomes (figure 8B) and hence drug-release from lipid-shelled microbubble will be higher compared to polymer-shelled microbubbles.

Loading these lipid-shelled microbubbles with thermosensitive liposomes enhances drug-delivery efficiency even more. Indeed, this can be due to a local and short increase in temperature upon microbubble cavitation as explained in the introduction section This sudden increase in temperature might cause the

liposomal membrane to melt, releasing the encapsulated drug in free form instantaneously (as shown by confocal microscopy during ultrasound application). Standard liposomes containing a significant percentage of the stabilizing agent cholesterol, are not sensitive for this increase in temperature, which explains the release of clumpy material (liposome aggregates) upon ultrasound application.

Releasing free DOX will indeed result in a direct and more efficient uptake of the drug by the cells. This will induce more effect because free DOX is more potent than DOX encapsulated in a liposome. However, if cells will be incubated for a longer period of time, liposomes or liposome-like structures will be taken up by the cells and induce effect as well. Depending on the type of drug used and the timeframe in which an effect is needed, both types of liposomes loaded on the surface of a microbubble may hence be suitable for drug-delivery applications.

This work shows that the composition of the microbubble shell and the loaded liposomes do have a significant influence on ultrasound-induced drug-release from liposome-loaded microbubbles. Further evaluation of liposome-loaded PLLA-PFO shelled microbubbles *in vivo*, can be excluded due to inefficient drug release and cell killing *in vitro*, there where lipid-shelled microbubbles loaded with TDLL may be promising. However, further *in vivo* evaluation is needed to confirm the observations made in this work.

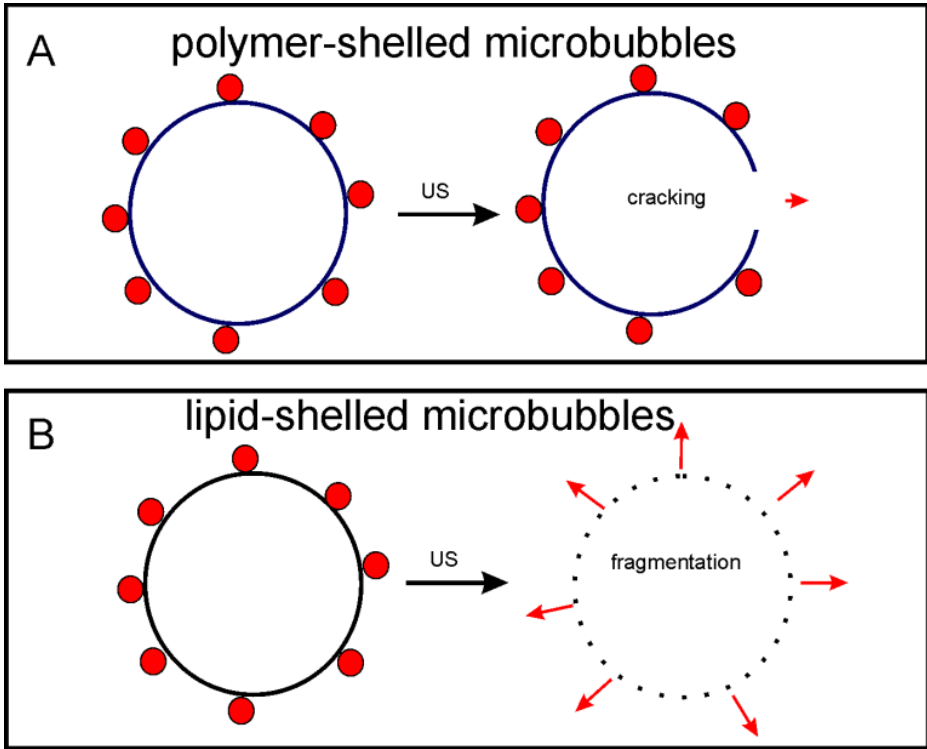


Figure 8: Schematic depiction of drug release mechanisms upon ultrasound application. (A) shows cracking of polymer-shelled microbubbles leaving a significant part of the liposomes intact. (B) shows fragmentation and subsequent homogenous liposome-destruction and subsequent drug-release from lipid-shelled microbubbles.

ACKNOWLEDGEMENTS

This research was funded by the EU FP7 collaborative project SONODRUGS (NMP-4-LA-2008-213706) and the FWO-Flanders research project G.0187.11. Ine Lentacker is a post-doctoral fellow of the FWO Flanders, the financial support of this institute is thanked. Ine De Cock and Heleen Dewitte are fellows of the Flemish institute for innovation in technology (IWT); the financial support of this institute is thanked. Katrien Van Holle is thanked for technical support. We would also like to thank Prof. Nico de Jong and Ying Luan for the help with the ultrasound and microscopy setup.

REFERENCES

- [1] B. Geers, I. Lentacker, N.N. Sanders, J. Demeester, S. Meairs, and S.C. De Smedt, Self-assembled liposome-loaded microbubbles: The missing link for safe and efficient ultrasound triggered drug-delivery, *J. Control Release*, 152 (2011) 249-256.
- [2] I. Lentacker, R.E. Vandenbroucke, B. Lucas, J. Demeester, S.C. De Smedt, and N.N. Sanders, New strategies for nucleic acid delivery to conquer cellular and nuclear membranes, *J. Control Release*, 132 (2008) 279-288.
- [3] I. Lentacker, B. Geers, J. Demeester, S.C. De Smedt, and N.N. Sanders, Design and evaluation of doxorubicin-containing microbubbles for ultrasound-triggered doxorubicin delivery: cytotoxicity and mechanisms involved, *Mol. Ther.*, 18 (2010) 101-108.
- [4] M.R. Bohmer, C.H. Chlon, B.I. Raju, C.T. Chin, T. Shevchenko, and A.L. Klibanov, Focused ultrasound and microbubbles for enhanced extravasation, *J. Control Release*, 148 (2010) 18-24.
- [5] K. Kooiman, M.R. Bohmer, M. Emmer, H.J. Vos, C. Chlon, W.T. Shi, C.S. Hall, S.H. de Winter, K. Schroen, M. Versluis, N. de Jong, and A. Van Wamel, Oil-filled polymer microcapsules for ultrasound-mediated delivery of lipophilic drugs, *J. Control Release*, 133 (2009) 109-118.
- [6] S. Tinkov, C. Coester, S. Serba, N.A. Geis, H.A. Katus, G. Winter, and R. Bekeredjian, New doxorubicin-loaded phospholipid microbubbles for targeted tumor therapy: in-vivo characterization, *J. Control Release*, 148 (2010) 368-372.
- [7] E.P. Stride and C.C. Coussios, Cavitation and contrast: the use of bubbles in ultrasound imaging and therapy, *Proc. Inst. Mech. Eng H*, 224 (2010) 171-191.
- [8] B. Geers, I. Lentacker, A. Alonso, N.N. Sanders, J. Demeester, S. Meairs, and S.C. De Smedt, Elucidating the mechanisms behind sonoporation with adeno-associated virus-loaded microbubbles, *Mol. Pharm.*, 8 (2011) 2244-2251.

- [9] A. Van Wamel, K. Kooiman, M. Hartevelde, M. Emmer, F.J. ten Cate, M. Versluis, and N. de Jong, Vibrating microbubbles poking individual cells: drug transfer into cells via sonoporation, *J. Control Release*, 112 (2006) 149-155.
- [10] B. Geers, I. Lentacker, A. Alonso, N.N. Sanders, J. Demeester, S. Meairs, and S.C. De Smedt, Elucidating the mechanisms behind sonoporation with adeno-associated virus-loaded microbubbles, *Mol. Pharm.*, 8 (2011) 2244-2251.
- [11] I. Lentacker, N. Wang, R.E. Vandenbroucke, J. Demeester, S.C. De Smedt, and N.N. Sanders, Ultrasound exposure of lipoplex loaded microbubbles facilitates direct cytoplasmic entry of the lipoplexes, *Mol. Pharm.*, 6 (2009) 457-467.
- [12] S. Mehier-Humbert, T. Bettinger, F. Yan, and R.H. Guy, Plasma membrane poration induced by ultrasound exposure: implication for drug delivery, *J. Control Release*, 104 (2005) 213-222.
- [13] B.D. Meijering, L.J. Juffermans, W.A. van, R.H. Henning, I.S. Zuhorn, M. Emmer, A.M. Versteilen, W.J. Paulus, W.H. van Gilst, K. Kooiman, N. de Jong, R.J. Musters, L.E. Deelman, and O. Kamp, Ultrasound and microbubble-targeted delivery of macromolecules is regulated by induction of endocytosis and pore formation, *Circ. Res.*, 104 (2009) 679-687.
- [14] K. Kooiman, M.R. Bohmer, M. Emmer, H.J. Vos, C. Chlon, W.T. Shi, C.S. Hall, S.H. de Winter, K. Schroen, M. Versluis, N. de Jong, and A. van Wamel, Oil-filled polymer microcapsules for ultrasound-mediated delivery of lipophilic drugs, *J. Control Release*, 133 (2009) 109-118.
- [15] M.R. Bohmer, C.H. Chlon, B.I. Raju, C.T. Chin, T. Shevchenko, and A.L. Klibanov, Focused ultrasound and microbubbles for enhanced extravasation, *J. Control Release*, 148 (2010) 18-24.
- [16] E. Stride and N. Saffari, The potential for thermal damage posed by microbubble ultrasound contrast agents, *Ultrasonics*, 42 (2004) 907-913.
- [17] J. Wu, J.D. Chase, Z. Zhu, and T.P. Holzapfel, Temperature rise in a tissue-mimicking material generated by unfocused and focused ultrasonic transducers, *Ultrasound Med. Biol.*, 18 (1992) 495-512.
- [18] S. Mitragotri, Healing sound: the use of ultrasound in drug delivery and other therapeutic applications, *Nat. Rev. Drug Discov.*, 4 (2005) 255-260.
- [19] P. Riesz and C.L. Christman, Sonochemical free radical formation in aqueous solutions, *Fed. Proc.*, 45 (1986) 2485-2492.
- [20] D. Needham, G. Anyarambhatla, G. Kong, and M.W. Dewhirst, A new temperature-sensitive liposome for use with mild hyperthermia: characterization and testing in a human tumor xenograft model, *Cancer Res.*, 60 (2000) 1197-1201.
- [21] D. Needham and M.W. Dewhirst, The development and testing of a new temperature-sensitive drug delivery system for the treatment of solid tumors, *Adv. Drug Deliv. Rev.*, 53 (2001) 285-305.
- [22] T. Tagami, M.J. Ernsting, and S.D. Li, Efficient tumor regression by a single and low dose treatment with a novel and enhanced formulation of thermosensitive liposomal doxorubicin, *J. Control Release*, 152 (2011) 303-309.
- [23] B. Geers, I. Lentacker, N.N. Sanders, J. Demeester, S. Meairs, and S.C. De Smedt, Self-assembled liposome-loaded microbubbles: The missing link for safe and efficient ultrasound triggered drug-delivery, *J. Control Release*, 152 (2011) 249-256.
- [24] I. Lentacker, B. Geers, J. Demeester, S.C. De Smedt, and N.N. Sanders, Design and evaluation of doxorubicin-containing microbubbles for ultrasound-triggered doxorubicin delivery: cytotoxicity and mechanisms involved, *Mol. Ther.*, 18 (2010) 101-108.
- [25] M. de Smet, S. Langereis, S. van den Bosch, and H. Grull, Temperature-sensitive liposomes for doxorubicin delivery under MRI guidance, *Journal of Controlled Release*, 143 (2010) 120-127

- [26] C. Chlon, C. Guedon, B. Verhaagen, W.T. Shi, C.S. Hall, J. Lub, and M.R. Bohmer, Effect of molecular weight, crystallinity, and hydrophobicity on the acoustic activation of polymer-shelled ultrasound contrast agents, *Biomacromolecules.*, 10 (2009) 1025-1031.
- [27] A. van Wamel, A. Bouakaz, M. Versluis, and N. de Jong, Micromanipulation of endothelial cells: ultrasound-microbubble-cell interaction, *Ultrasound Med. Biol.*, 30 (2004) 1255-1258
- [28] A. van Wamel, K. Kooiman, M. Hartevelde, M. Emmer, F.J. ten Cate, M. Versluis, and N. de Jong, Vibrating microbubbles poking individual cells: drug transfer into cells via sonoporation, *J. Control Release*, 112 (2006) 149-155.
- [29] K. Kooiman, M. Foppen-Hartevelde, A.F. van der Steen, and J.N. de, Sonoporation of endothelial cells by vibrating targeted microbubbles, *J. Control Release*, 154 (2011) 35-41.
- [30] T. Tagami, J.P. May, M.J. Ernsting, and S.D. Li, A thermosensitive liposome prepared with a Cu²⁺ gradient demonstrates improved pharmacokinetics, drug delivery and antitumor efficacy, *Journal of Controlled Release*, 161 (2012) 142-149.
- [31] C. Sonne, F. Xie, J. Lof, J. Oberdorfer, P. Phillips, E.E. Carr, and T.R. Porter, Differences in definity and optison microbubble destruction rates at a similar mechanical index with different real-time perfusion systems, *J. Am. Soc. Echocardiogr.*, 16 (2003) 1178-1185.
- [32] M.A. Borden, D.E. Kruse, C.F. Caskey, S. Zhao, P.A. Dayton, and K.W. Ferrara, Influence of lipid shell physicochemical properties on ultrasound-induced microbubble destruction, *IEEE Trans. Ultrason. Ferroelectr. Freq. Control*, 52 (2005) 1992-2002.

Chapter 5

Delivery of small molecules with liposome-loaded microbubbles to tumors *in vivo*: a pilot study

Bart Geers¹, Steven K. Cool², Joseph Demeester¹, Stefaan C. De Smedt¹, Niek N. Sanders², Ine Lentacker¹

¹ Ghent Research Group on Nanomedicines, Laboratory of General Biochemistry and Physical Pharmacy, Faculty of Pharmaceutical Sciences, Ghent University Harelbekestraat 72, 9000 Ghent, Belgium

² Laboratory of Veterinary Gene Therapy, Department of ethology and genetics, Faculty of Veterinary Sciences, Ghent University, Heidestraat 19, 9800 Merelbeke, Belgium

Microbubbles have been shown to be potentially useful in drug-delivery applications especially when loaded with drug-containing nanoparticles. Up to now we succeeded in optimizing a formulation which allows safe, easy and stable production of drug-containing liposome-loaded microbubbles, however it wasn't tested *in vivo* yet. In this work we evaluate the efficiency of indocyanine green (ICG) uptake with ultrasound and ICG liposome-loaded microbubbles into tumors in mice and compared this with standard ICG liposomes. We observed that all experimental groups show ICG uptake into tumors, however standard ICG liposomes show the highest uptake.

INTRODUCTION

Microbubbles show potential for ultrasound induced time- and space-controlled drug release *in vitro* [1]. Their mechanism of action relies upon their response to the alternating acoustic pressure field exerted by the ultrasound wave. If a gas bubble encounters high intensities of acoustic pressure, microbubbles will collapse which can result in the release of drugs or nanoparticles attached to or incorporated in the microbubbles [2,3]. In the past it has been shown [4-6] that the concept of nanoparticle loaded microbubbles can be beneficial to induce local drug *release and uptake* at the same time *in vitro*.

Up to now we succeeded in the design of a) an easy to store, to produce and safe microbubble formulation loaded with doxorubicin-containing liposomes [7], b) we were able to attach antibodies to liposomes loaded on the surface of the microbubbles enabling cell type specific drug-delivery *in vitro* and c) we have optimized ultrasound induced drug-release from microbubbles by loading them with thermosensitive liposomes.

In this chapter we will evaluate whether or not optimized liposome-loaded microbubbles in combination with localized ultrasound application can induce uptake of the small molecule indocyanine green (ICG) into tumors *in vivo* compared to the clinically used liposomal formulations. ICG is a near infrared fluorescent dye that does not leave the bloodstream under normal conditions [8] and hence is an ideal molecule to study tumor uptake *in vivo* via near infrared biofluorescent imaging [9].

MATERIALS AND METHODS

Preparation of functionalized indocyanine green (ICG)-loaded liposomes

Functionalized ICG-loaded liposomes were prepared via the method described earlier. Briefly, 1,2-dipalmitoyl-sn-glycero-3-phosphocholine (DPPC), 1,2-distearoyl-sn-glycero-3-phosphoethanolamine-N-[maleimide(polyethylene glycol)-2000] (DSPE-PEG-maleimide) and cholesterol dissolved in CHCl_3 at a concentration of 20 mg/ml and 10 mg/ml respectively, were transferred in a round bottom flask in a 49:15:36 molar ratio. After solvent evaporation, the remaining lipid film was rehydrated with a solution of indocyanine green (ICG) (sigma-alldrich, Bornem, Belgium) in H_2O (5 mg/ml) to obtain a liposomal dispersion with a final lipid concentration of 16 mg/ml. The resulting liposome dispersion was extruded through a 200 nm filter using a mini-extruder at 60 °C. After extrusion the excess of ICG was removed by ultracentrifugation at 109000 x g (Ultrafuge, Beckman-Coulter, Brea, CA). Final ICG concentration was evaluated using absorbance spectrometry (680 nm) using an Envision plate-reader (Perkin-elmer, Waltham, MA).

Preparation of functionalized thermosensitive ICG-loaded liposomes

Thermosensitive ICG-loaded liposomes were prepared as follows. 2-dipalmitoyl-sn-glycero-3-phosphocholine (DPPC), 1,2-distearoyl-sn-glycero-3-phosphoethanolamine-N-[maleimide(polyethylene glycol)-2000] (DSPE-PEG-maleimide) dissolved in CHCl_3 at a concentration of 20 mg/ml and 10 mg/ml respectively and 1-palmitoyl-2-hydroxy-sn-glycero-3-phosphocholine (MPPC) dissolved in a CHCl_3 :EtOH (1:1) mixture at a concentration of 13.3 mg/ml were mixed in a round bottom flask in a molar ratio (DPPC:DSPE-PEG-

maleimide:MPPC) of 82:10:8. After solvent evaporation the remaining lipid film was rehydrated 5 mg/ml ICG solution as described in the previous section. The final lipid concentration of the liposomal dispersion in the flask was 32 mg/ml. The resulting dispersion was extruded through a 200 nm filter using a mini-extruder at 60 °C. After extrusion the excess of ammonium sulfate was removed by ultracentrifugation at 109000 × g (Ultrafuge, Beckman-Coulter, Brea, CA). Final ICG concentration was evaluated using absorbance spectrometry (680 nm) using an Envision plate-reader (Perkin-elmer, Waltham, MA).

Preparation of liposome-loaded microbubbles

Microbubbles were prepared as described previously. Briefly, microbubbles were prepared starting from a lipid solution being a mixture of 1,2-dipalmitoyl-*sn*-glycero-3-phosphocholine (DPPC) and 1,2-distearoyl-*sn*-glycero-3-phosphoethanolamine-N-[PDP(polyethylene glycol)-2000] (DSPE-PEG-PDP) (Avanti polar lipids, Alabaster, AL) in a 1:2:7 glycerine-propyleneglycol-H₂O solvent (Sigma-aldrich, Bornem, Belgium), the molar ratio of the lipids in the lipid solutions was 95:5. Aliquots of this lipid solution were transferred into 2.5 ml chromatography vials, together with 100 μl of freshly made (targeted, thermosensitive or standard) ICG liposomes, which headspace was filled with C₄F₁₀ gas (F2 chemicals, Preston, UK). Finally, functionalized microbubbles (with an average size of 3 μm) were obtained by high speed shaking of the lipid solution in a Capmix™ device (3M-ESPE, Diegem, Belgium) during 15 sec. The size and the concentration of the microbubbles in the dispersion (i.e. number of microbubbles per mL) were determined with a Beckman-coulter Multisizer 4 (Beckman-coulter, Brea, CA).

Animal model and xenograft tumor implants

6 weeks old nude athymal NMRI mice (Harlan, Boxmeer, The Netherlands) were kept in individual ventilated cages under constant temperature (22-25°C) and humidity (45-65%). Xenograft tumors were implanted when the animals were 7 weeks old by injecting 100 µl of a suspension of BLM cells [12,13] (1×10^6 cells per ml) in PBS at the dorsal side of the animal subcutaneously. Prior to injection these cells were cultured in 75cm² cell culture flasks in Dulbecco's modified eagles medium (DMEM) F12 supplemented, and additionally supplemented with 1 % penicillin-streptomycin, 10% Fetal Bovine Serum (FBS), L-glutamine and 100 mM HEPES buffer (all purchased from Gibco, Merelbeke, Belgium) under 5% CO₂ at 37°C. Tumors were allowed to grow for 5 weeks upon implantation.

Animal experiments and ultrasound application

When tumor volume reached approximately 500 mm³-1 cm³ experiments were performed. 100 µl of pure ICG liposome or microbubble (loaded with standard or thermosensitive ICG liposomes) (1×10^7 microbubbles/ml) dispersion containing 120 µg ICG was injected via the tail vein of the animal. Before experiment, the concentration of ICG in all experimental materials was evaluated with the IVIS, in order to make sure that the materials injected contained comparable amounts of ICG. Per group at least 3 animals were treated. During all experimental procedures the animals were anesthetized with isoflurane (O₂ 1 l/ min), 5% isoflurane was used for induction and 1.5% during the procedure. Animals were imaged directly after the injection and 24 h after injection using an IVIS lumina II system (Caliper Life sciences, Zaventem, Belgium). The 780 nm line was used to excite ICG, where the 820 nm line was detected in the emission channel. Tumors from animals injected with microbubbles were treated with a commercially

available sonidel SP100 ultrasound sonoporation device (5 W/cm² for 2 min). Therefore, tumors were covered with gel and gradually insonified as depicted in figure 2. 24 h post injection, the animals were sacrificed by cervical dislocation; tumors were excised and imaged with the IVIS lumina II to analyze the exact amount of ICG in the tumor. The amount of fluorescence in the tumors was corrected for tumor size. All animal experiments were approved by the ethical committee of the faculty of veterinary sciences of Ghent University

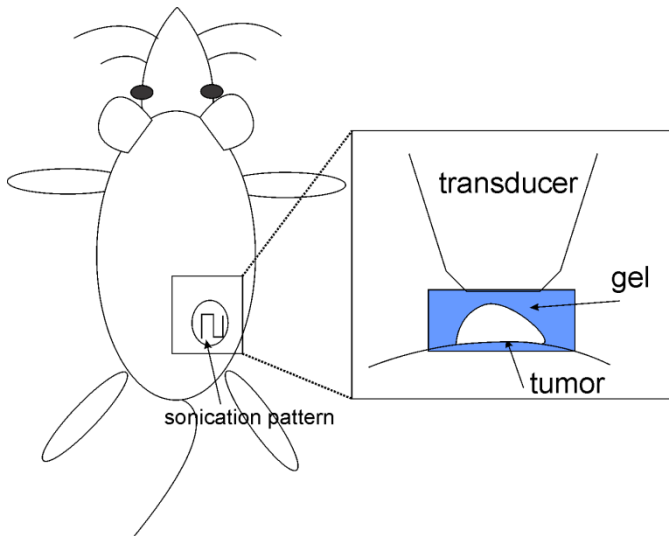


Figure 1: Schematic overview of ultrasound application in implanted tumors.

Statistical analysis

All data are presented as means \pm one standard deviation. A student's t-test was performed to determine whether datasets differed significantly. A p-value smaller than 0.05 was regarded significant

RESULTS

This work gives an overview of the behavior of the materials developed for ultrasound-triggered drug-delivery by our group in tumor bearing mice. Tumor uptake of ICG will be evaluated as a function of the drug-delivery vehicle used, namely: a) standard liposomes, b) liposome-loaded microbubbles in combination with ultrasound, and c) thermosensitive liposome-loaded microbubbles in combination with ultrasound.

Kinetics

As shown in figure 2, directly after injection of the liposomes or liposome-loaded microbubbles combined with ultrasound application, a strong accumulation of ICG fluorescence in the liver is observed. However, the accumulated liver and overall fluorescence in animals treated with liposomes is much higher. Indeed, if ICG is delivered via ultrasound assisted drug-delivery from liposome-loaded microbubbles less ICG will initially accumulate in the liver because more molecules are delivered in the tumor where ultrasound is applied. However this tumor uptake is still much lower than liver uptake. Free liposomes however, will distribute throughout the animal with maximal liver uptake directly after injection.

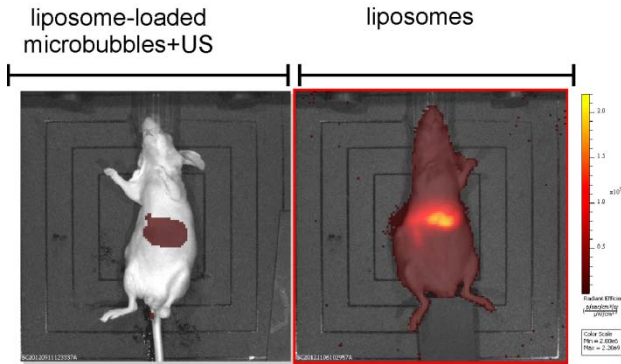


Figure 2: Fluorescent images (IVIS lumina II) of BLM tumor bearing mice directly upon injection of liposomes only or liposome-loaded microbubbles in combination with ultrasound (US).

After 24 hours fluorescence has distributed over the complete animal. However, upon injection of liposomes a strong accumulation of fluorescence in the tumor area can be observed as shown in figure 3. Liposome-loaded microbubbles show less accumulation in the tumor, as well as upon ultrasound application. Because it is hard to distinguish tumor ICG accumulation into the tumor from ICG, which is excreted via biliary excretion [14] into the intestines of the animals, we decided to excise tumors.

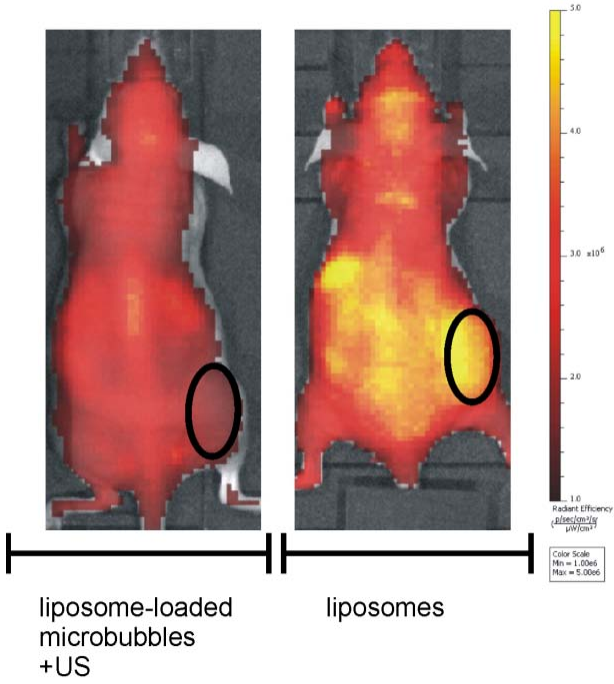


Figure 3: Fluorescent images (IVIS lumina II) of BLM tumor bearing mice 24 h upon injection of liposomes only or liposome-loaded microbubbles in combination with ultrasound (US). Circles indicate the location of the tumors.

Tumor accumulation and quantitative results

Upon excision and subsequent imaging of the tumors (figure 4) one can clearly observe significant ICG accumulation in tumors treated with ICG-loaded liposomes only. ICG accumulation can be observed in the other experimental groups as well. However, significantly less ICG accumulates in these experimental groups.

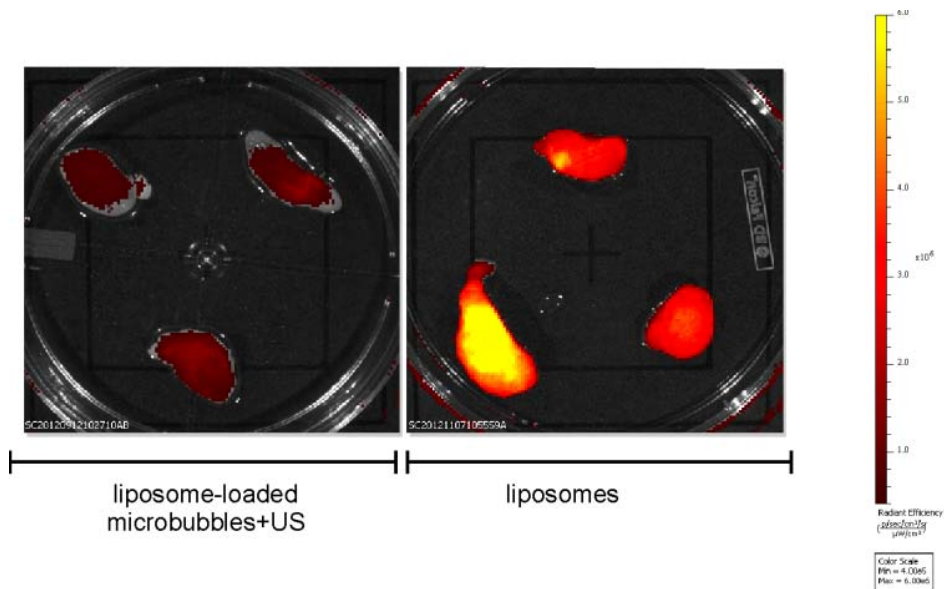


Figure 4: Fluorescent images (IVIS lumina II) of excised tumors 24 h after injection of BLM tumor bearing mice with liposomes or liposome-loaded microbubbles in combination with ultrasound application.

To quantify the amount of ICG delivered into the tumors, we calculated the amount of fluorescence per cm^2 tumor for the different treatment groups in different animals. Additionally we calculated this for tumors treated with ultrasound and *thermosensitive* ICG liposome-loaded microbubbles as well.

Indeed, one can observe significant ICG uptake in tumors treated with liposomes only and a significant uptake of ICG in all other groups compared with PBS treated control tumors. Interestingly, we could observe a slightly higher ICG uptake in ultrasound treated tumors in combination with thermosensitive ICG liposome-loaded microbubbles, although this increase was not statistically significant compared with other ultrasound treated groups.

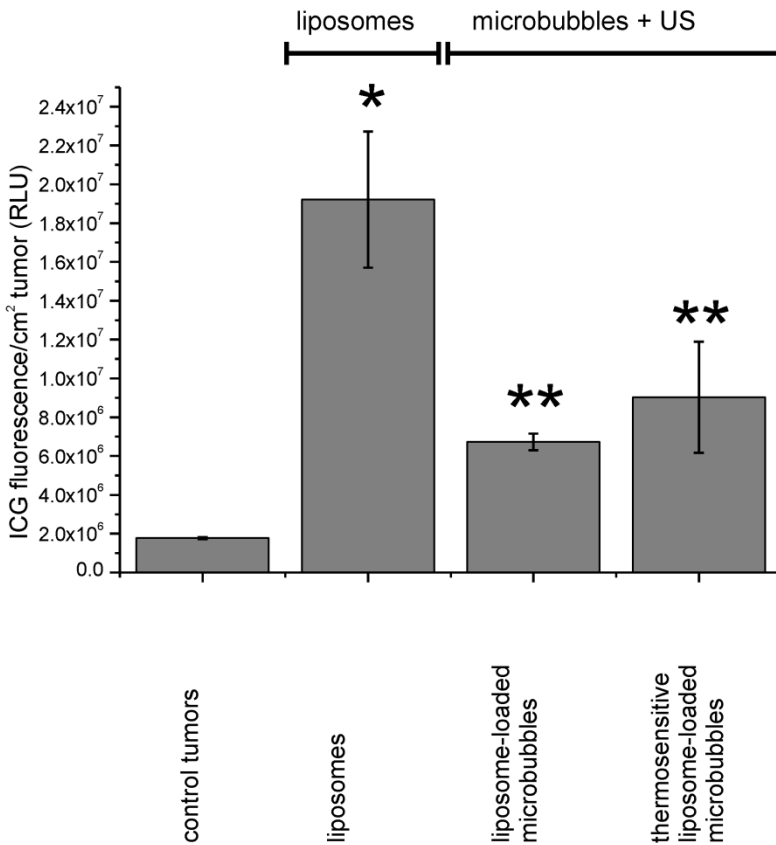


Figure 5: Quantitative analysis of fluorescence intensity per cm² tumor of the different treatment groups in BLM tumor bearing mice.(** significant with regard to control tumors)

CONCLUSIONS AND DISCUSSION

This work shows that ultrasound indeed enables release and subsequent tumor uptake of a molecule (ICG) that is not able to penetrate into tissues via the bloodstream safely (none of the animals endured severe side effects during the intervention). However, standard liposomal formulations still enable a better uptake of these molecules into tumors.

Indeed, standard liposomal formulations will circulate for a significantly longer period of time in the bloodstream [15] allowing constant accumulation of these nanoparticles in the tumor via enhanced permeation and retention (EPR) [16,17], especially in well vascularized tumors. Ultrasound treatment on the other hand only lasts for 2 min and microbubbles only circulate for maximally 10 min [18]. Hence, accumulation over a long period of time by nanoparticles and drug, as with liposomes, will not occur which explains why less ICG uptake was observed in tumors treated with ultrasound and liposome-loaded microbubbles. On the other hand, a slight though statistically insignificant increase in ICG uptake was observed when the microbubbles were loaded with thermosensitive liposomes. This observation correlates nicely with our previous findings (*in vitro*) on ultrasound triggered drug release from microbubbles loaded with these thermosensitive liposomes.

One could argue that these materials aren't suited for small molecule delivery into tumors. However, more research is needed to evaluate the real potential of ultrasound triggered drug-delivery. The tumors used in this study showed to be well vascularized, making them very well suited for liposome accumulation via EPR. Ultrasound assisted drug delivery may hence be more useful in tumors that

are less vascularized. Additionally, we observed significantly less overall distribution and liver accumulation of ICG in mice directly after injection/treatment. This suggests that ultrasound mediated drug-delivery may cause less side-effects because lower drug doses may be delivered more efficiently. Moreover, it may become possible to treat patients multiple times using these lower doses enabling a more efficient therapy.

The type of drug loaded on the microbubbles will have an influence on delivery as well. Macromolecules like pDNA, mRNA or siRNA for example that need to be transported into cells can benefit from ultrasound induced sonoporation [19,20]. The results in this work also point out that microbubbles are still too large (2-3 μm); one should be able to lower the size of the microbubbles or other ultrasound responsive particles to below 200 nm. This will allow tumor accumulation via EPR and subsequent ultrasound application may increase delivery of the drug in the tumor. This can be achieved by a strategy described by *Rapoport and co-workers*. [21-24] making use of drug-loaded perfluorocarbon nano-emulsions, which are phase-convertible small nanoparticles (150 nm), that may become microbubbles upon heating due to liquid-gas phase conversion upon heating (40°C).

REFERENCES

- [1] S. Hernot and A.L. Klibanov, Microbubbles in ultrasound-triggered drug and gene delivery, *Adv. Drug Deliv. Rev.*, 60 (2008) 1153-1166.
- [2] M.R. Bohmer, C.H. Chlon, B.I. Raju, C.T. Chin, T. Shevchenko, and A.L. Klibanov, Focused ultrasound and microbubbles for enhanced extravasation, *J. Control Release*, 148 (2010) 18-24.
- [3] S. Mehier-Humbert, T. Bettinger, F. Yan, and R.H. Guy, Plasma membrane poration induced by ultrasound exposure: implication for drug-delivery, *J. Control Release*, 104 (2005) 213-222.
- [4] I. Lentacker, N. Wang, R.E. Vandenbroucke, J. Demeester, S.C. De Smedt, and N.N. Sanders, Ultrasound exposure of lipoplex loaded microbubbles facilitates direct cytoplasmic entry of the lipoplexes, *Mol. Pharm.*, 6 (2009) 457-467.
- [5] I. Lentacker, B. Geers, J. Demeester, S.C. De Smedt, and N.N. Sanders, Design and evaluation of doxorubicin-containing microbubbles for ultrasound-triggered doxorubicin delivery: cytotoxicity and mechanisms involved, *Mol. Ther.*, 18 (2010) 101-108.
- [6] S. Tinkov, C. Coester, S. Serba, N.A. Geis, H.A. Katus, G. Winter, and R. Bekeredjian, New doxorubicin-loaded phospholipid microbubbles for targeted tumor therapy: in-vivo characterization, *J. Control Release*, 148 (2010) 368-372.
- [7] B. Geers, I. Lentacker, N.N. Sanders, J. Demeester, S. Meairs, and S.C. De Smedt, Self-assembled liposome-loaded microbubbles: The missing link for safe and efficient ultrasound triggered drug-delivery, *J. Control Release*, 152 (2011) 249-256.
- [8] R. Weissleder, A clearer vision for in vivo imaging, *Nat. Biotechnol.*, 19 (2001) 316-317.
- [9] J.V. Frangioni, In vivo near-infrared fluorescence imaging, *Curr. Opin. Chem. Biol.*, 7 (2003) 626-634.
- [10] P. Carmeliet and R.K. Jain, Angiogenesis in cancer and other diseases, *Nature*, 407 (2000) 249-257.
- [11] S. Fokong, B. Theek, Z. Wu, P. Koczera, L. Appold, S. Jorge, U. Resch-Genger, Z.M. van, G. Storm, F. Kiessling, and T. Lammers, Image-guided, targeted and triggered drug-delivery to tumors using polymer-based microbubbles, *J. Control Release*, 163 (2012) 75-81.
- [12] K. Jacobs, L. Feys, B. Vanhoecke, M. Van, V, and M. Bracke, P-cadherin expression reduces melanoma growth, invasion, and responsiveness to growth factors in nude mice, *Eur. J. Cancer Prev.*, 20 (2011) 207-216.
- [13] Van Marck, V, C. Stove, K. Jacobs, G. Van den Eynden, and M. Bracke, P-cadherin in adhesion and invasion: opposite roles in colon and bladder carcinoma, *Int. J. Cancer*, 128 (2011) 1031-1044.
- [14] P. Recknagel, R.A. Claus, U. Neugebauer, M. Bauer, and F.A. Gonnert, In vivo imaging of hepatic excretory function in the rat by fluorescence microscopy, *J. Biophotonics*, 5 (2012) 571-581.
- [15] Y.C. Barenholz, Doxil(R) - The first FDA-approved nano-drug: Lessons learned, *J. Control Release*, (2012).
- [16] H. Maeda, L.W. Seymour, and Y. Miyamoto, Conjugates of Anticancer Agents and Polymers - Advantages of Macromolecular Therapeutics In vivo, *Bioconjugate Chemistry*, 3 (1992) 351-362.
- [17] H. Maeda, J. Wu, T. Sawa, Y. Matsumura, and K. Hori, Tumor vascular permeability and the EPR effect in macromolecular therapeutics: a review, *Journal of Controlled Release*, 65 (2000) 271-284.

[18] C.C. Chen, S.R. Sirsi, S. Homma, and M.A. Borden, Effect of surface architecture on in vivo ultrasound contrast persistence of targeted size-selected microbubbles, *Ultrasound Med. Biol.*, 38 (2012) 492-503.

[19] B. Geers, I. Lentacker, A. Alonso, N.N. Sanders, J. Demeester, S. Meairs, and S.C. De Smedt, Elucidating the mechanisms behind sonoporation with adeno-associated virus-loaded microbubbles, *Mol. Pharm.*, 8 (2011) 2244-2251.

[20] B.D. Meijering, L.J. Juffermans, A. van Wamel, R.H. Henning, I.S. Zuhorn, M. Emmer, A.M. Versteilen, W.J. Paulus, W.H. van Gilst, K. Kooiman, N. de Jong, R.J. Musters, L.E. Deelman, and O. Kamp, Ultrasound and microbubble-targeted delivery of macromolecules is regulated by induction of endocytosis and pore formation, *Circ. Res.*, 104 (2009) 679-687.

[21] Z. Gao, A.M. Kennedy, D.A. Christensen, and N.Y. Rapoport, Drug-loaded nano/microbubbles for combining ultrasonography and targeted chemotherapy, *Ultrasonics*, 48 (2008) 260-270.

[22] N. Rapoport, W.G. Pitt, H. Sun, and J.L. Nelson, Drug-delivery in polymeric micelles: from in vitro to in vivo, *J. Control Release*, 91 (2003) 85-95.

[23] N. Rapoport, Z. Gao, and A. Kennedy, Multifunctional nanoparticles for combining ultrasonic tumor imaging and targeted chemotherapy, *J. Natl. Cancer Inst.*, 99 (2007) 1095-1106.

[24] N. Rapoport, K.H. Nam, R. Gupta, Z. Gao, P. Mohan, A. Payne, N. Todd, X. Liu, T. Kim, J. Shea, C. Scaife, D.L. Parker, E.K. Jeong, and A.M. Kennedy, Ultrasound-mediated tumor imaging and nanotherapy using drug loaded, block copolymer stabilized perfluorocarbon nanoemulsions, *J. Control Release*, 153 (2011) 4-15.

Chapter 6

On the mechanisms behind sonoporation

Bart Geers¹, Ine Lentacker¹, Angelika Alonso², Niek N. Sanders³, Joseph Demeester¹, Stephen Mearns², Stefaan C. De Smedt¹

This chapter has been published: *Elucidating the mechanisms behind sonoporation with adeno-associated virus-loaded microbubbles; Molecular Pharmaceutics*, 8 (6), 2011, 2244-2251

¹ Ghent Research Group on Nanomedicines, Lab of General Biochemistry and Physical Pharmacy, Faculty of Pharmaceutical Sciences, Ghent University, Harelbekestraat 72, 9000 Gent, Belgium

² Department of Neurology, Universitätsklinikum Mannheim, Heidelberg University, Theodor-Kutzer-Ufer 1-3, 66167 Mannheim, Germany

³ Laboratory of Gene Therapy, Faculty of Veterinary Medicine, Ghent University, Heidestraat 19, 9820 Merelbeke, Belgium

Microbubbles are FDA approved contrast agents for ultrasound imaging. It has been reported that applying ultrasound on drug loaded microbubbles facilitates drug uptake by cells, due to so named sonoporation. However, the biophysics behind sonoporation is not fully understood. It is believed that sonoporation results in a 'direct' delivery of drugs in the cytoplasm of cells, though, it has been suggested as well that sonoporation facilitates endocytosis which would improve internalization of drugs by cells. To get a better understanding of sonoporation this study reports on the ultrasound assisted delivery of adeno-associated virus (AAV) loaded on the surface of microbubbles. AAV's rely on endocytosis for efficient transduction of cells and are, consequently, an elegant tool to evaluate whether endocytosis is involved in ultrasound induced sonoporation. Applying ultrasound on AAV-loaded microbubbles clearly improved the internalization of AAV's by cells, though transduction of the cells did not occur, indicating that by sonoporation substances become directly delivered in the cytosol of cells.

INTRODUCTION

Since a few years the interest in microbubbles as drug delivery carriers has grown exponentially. A major reason for this is that microbubbles, with some of them being approved by FDA as contrast agents for diagnostic ultrasound, may allow time and space controlled drug delivery upon mechanical activation of the bubbles by ultrasound [1]. Such micron sized bubbles are usually filled with an inert hydrophobic gas while their shell consists out of lipids, polymers or proteins [2,3].

The mechanism of action of these microbubbles is based on the specific response of the bubbles upon exposure to ultrasound [4]. Because of the difference in density between the gas core of the microbubble and the surrounding aqueous fluid, microbubbles start to oscillate once subjected to the pressure fluctuations as exerted by an ultrasonic wave. This process of oscillation is called cavitation [5]. “Stable cavitation” occurs when microbubbles are subjected to an ultrasonic field with a low acoustical pressure; stably cavitating microbubbles expand and contract around a given diameter. “Inertial cavitation” on the other hand involves a more violent process: the bubbles do not longer oscillate around a given diameter, their movement is more violent and ultimately they become destroyed [6]. It has been shown that cell membranes neighboring a cavitating or collapsing microbubble become temporarily permeabilized (“sonoporation”) [7] which is believed to result in a more efficient uptake of the drug by cells.

However, the biophysics behind this mechanism is not yet fully understood. Our group showed that when drug molecules are attached to the microbubble surface microbubble collapse is able to locally release drug molecules, which become

directly delivered into the cytosol of the surrounding cells [8]. However other studies described that sonoporation might facilitate the formation of endosomes which would explain the more efficient drug uptake by the cells [9]. Hence, there is a need to further elucidate the biophysical effects involved in sonoporation. In order to prove if sonoporation involves endocytosis or not, we decided to use a viral gene delivery vector, namely adeno-associated-virus (AAV), which totally relies on receptor mediated endocytosis to achieve cell transduction [10,11]. Especially, we made use of “non-active AAV”, being AAV-vectors chemically modified at their surface with a polyethylene glycol (PEG) brush. This PEGylation strongly reduces the endocytosis of AAV-vectors and, subsequently, lowers their transduction properties [12,13]. Since our research group is mainly focusing on surface-loaded lipid-shelled microbubbles [14-16], we decided to construct PEGylated AAV-loaded lipid-shelled microbubbles. PEGylation of the vectors also allows the straightforward insertion of a biotin group on the capsid by introducing heterofunctional PEGs. As shown in Figure 1a these PEG-biotinylated AAV vectors can easily be attached to the surface of a lipid coated microbubble by means of avidin-biotin linkages.

Consequently, we believe that PEGylated AAV-vectors are an ideal tool to study whether sonoporation enhances endocytosis or not, as a better transduction of the cells upon applying ultrasound and microbubbles will be only observed if sonoporation promotes endocytosis and hereby, we hope to deliver more insight in the interactions between ultrasound and cellular processes.

METHODS AND MATERIALS

Preparation and characterization of biotinylated microbubbles

Microbubbles were prepared following the protocol published by *Lentacker et al* [17]. Briefly, the phospholipids 1,2-dipalmitoyl-*sn*-glycero-3-phosphocholine (DPPC) and 1,2-distearoyl-*sn*-glycero-3-phosphoethanolamine-N-Biotinyl (polyethylene glycol)-2000] (DSPE-PEG-biotin) (Avanti polar lipids, Albaster, AL) both dissolved in CHCl_3 were added in a round bottom flask in an 85:15 molar ratio. After CHCl_3 evaporation, the lipid film was dissolved in HEPES buffer 50 mM, pH 7.4 (Sigma-alldrich, Bornem, Belgium). This mixture was extruded using a 200 nm polycarbonate membrane filter in a mini-extruder (Avanti polar lipids, Albaster, AL) at 60°C to obtain liposomes with a minimal size of 200 nm, as measured by dynamic light scattering (Nano-zs, Malvern, Worcestershire, UK). An aliquot of the liposomal dispersion was transferred into a 15ml tube and subsequently C_4F_{10} gas (MW238 g/mol, F2 chemicals, Preston, UK) was added to this dispersion. Microbubbles could be obtained by ultrasonication of the liposomes with a 20 kHz probe (Branson 250 sonicator, Branson ultrasonics, Danbury, CT). After sonication the microbubbles were centrifuged to remove the remaining liposomes. Microbubbles were washed with 3 ml of HEPES buffer. To allow coupling of biotinylated AAV-vectors, the microbubbles were subsequently incubated with 500 μl of avidin (10 mg/ml). After another washing step with 3 ml HEPES buffer and subsequent centrifugation, microbubbles were incubated with biotinylated AAV-vectors. Microbubble concentration was evaluated using light microscopy in a Burkner chamber and equaled 1×10^7 microbubbles per ml.

Preparation and characterization of PEG--biotinylated AAV-vectors

Recombinant adeno-associated virus serotype 2 (rAAV2) expressing enhanced green fluorescent protein (EGFP) was provided by the German Cancer Research Centre, with a stock concentration of 10^{12} particles/ml. To obtain PEGylated or PEG-biotinylated AAV-vectors, a 100 μ l aliquot of the AAV-vectors was incubated with a desired amount of alpha-methoxy-omega-carboxylic acid succinimidyl ester poly(ethylene glycol) (MW 2000 g/mol, Iris Biotech GmbH, Marktdrewitz, Germany) (NHS-MPEG200) or alpha-biotin-omega-carboxy succinimidyl ester poly(ethylene glycol) (NHS-PEG-biotin) (MW 3000 g/mol, Iris Biotech GmbH, Marktdrewitz, Germany) respectively. Therefore the NHS-MPEG200 and NHS-PEG-biotin were dissolved in HEPES-buffer just before adding to the AAV-vector dispersion. The vectors were incubated with the PEGylation agent during 30 min. Subsequently HEPES buffer was added to obtain a final volume of 200 μ l with a concentration of $5 \cdot 10^{10}$ particles/ml. PEGylation of the AAV was characterized by measuring the electroforetic mobility of the viral particles with a zetasizer (Nano-zs, Malvern, Worcestershire, UK).

Preparation of fluorescent AAV-vectors

AAV-vectors were fluorescently labeled with red- or green-fluorescent labels. For labeling in red, 100 μ l of PEG-biotinylated AAV-vectors (freshly prepared) were incubated with 3-5 μ l of NHS-dyelight633 labeling reagent (2mg/ml, Thermo Scientific, Bornem, Belgium) for 30 min. After incubation the dye excess was removed by dialysis against distilled water (MWCO 15000 Da, Microdispo dialyser, Spectra/Por, Compton, CA). Green-fluorescent AAV-vectors were obtained by labeling 100 μ l of PEG-biotinylated AAV-vectors (freshly prepared)

with 3-5 μ l of NHS-alexa488 (2mg/ml, Invitrogen Molecular probes, Merelbeke, Belgium). The same protocol as described for the labeling of the viruses in red was followed.

Preparation and characterization of AAV-loaded microbubbles

AAV-loaded microbubbles were prepared by mixing 3 ml of PEG-biotinylated microbubbles with 300 μ l of the PEG-biotinylated AAV-vectors. To remove unbound AAV-vectors, microbubbles loaded with the AAV-vectors were washed and centrifuged twice. The percentage of vectors present in the supernatants after every centrifugation step was analyzed with an AAV titration ELISA assay (Progen GmbH, Heidelberg, Germany). The remaining bubble fraction after these washing steps was then dispersed in 3 ml of HEPES and the amount of AAV-vectors bound to the microbubbles was analyzed with the same assay. We quantified the amount of AAV-vectors on the microbubbles to assure that in all experiments the same vector titers were used.

To visualize AAV-loading on the microbubbles, the microbubbles were incubated with alexa488-avidin (Invitrogen Molecular probes, Merelbeke, Belgium) and mixed with red-fluorescent PEG-biotinylated AAV-vectors. Colocalization of (green) avidin and (red) AAV was studied by confocal microscopy, using a Nikon EZC1 confocal microscope (Nikon, Brussels, Belgium) equipped with a 60x lens. Excitation of the alexa488 avidin was done using the 490 nm line while fluorescence was detected at 551 nm. Excitation of the AAV-vectors labeled with the red NHS-dyelight633 dye was done using the 630 nm line while fluorescence was detected at 660 nm.

Cell culture

BLM cells (melanoma cells) were cultured in F12-supplemented Dulbecco's modified Eagles medium (DMEM-F12). This medium also contained 1% Penicillin/Streptomycin, 2 mmol/ml L-glutamine, 10 % Fetal bovine serum (FBS) (all purchased from Gibco, Merelbeke, Belgium) and 100 mmol/l HEPES pH 7.2. Cells were grown in a humidified incubator at 37°C in 5% CO₂ atmosphere.

Transduction of melanoma cells with PEGylated AAV-vectors

BLM melanoma cells were seeded at 1.3×10^6 cells and grown up to 70% confluence in Opticell™ plates (Biocrystal, Westerville, OH). Before the transduction medium was added, cells were washed with phosphate buffered saline (PBS). AAV-vectors were PEGylated as described above using 20, 40, 100 and 200 µg NHS-MPEG200. 200 µl of PEGylated rAAV2 expressing EGFP was added to 9.8 ml of cell culture medium and transferred into the Opticells™, afterwards cells were incubated for 45 min at 37°C. Subsequently cells were washed with PBS, fresh cell culture medium was added and cells were incubated. After 48 hours cells were washed and incubated with 2 ml of a 0.05% trypsin-EDTA solution (GIBCO, Merelbeke, Belgium), after 5 min of incubation trypsin was inactivated with 8 ml of fresh culture medium and centrifuged for 7 min at 1100 rpm. Subsequently medium was removed and cells were resuspended in buffer containing 1% of bovine serum albumin, 0.1% of sodium azide in PBS (chemicals were purchased from Sigma-alldrich, Bornem, Belgium). EGFP expression was measured using flow cytometry with a BD FacsCalibur flow cytometer (Beckton Dickinson, Erembodegem, Belgium). The flow cytometer was equipped with a 488 nm laser and emitted fluorescence was detected in the 530nm channel FL1. Results are expressed as % EGFP positive cells compared

with blank untransduced cells. All experiments were performed at least in triplicate and data are expressed as the mean of all three measurements.

Cytotoxicity assay

BLM melanoma cells were seeded in 12-well plates at 1×10^5 cells and grown up to 70 % confluence. Cells were washed and 10 μ l free AAV or inactive PEGylated AAV with a stock concentration of 10^{12} particles/ml dispersed in cell medium to a final volume of 1 ml was added to the cells. PEGylation occurred via the method described above. Subsequently, cells were incubated for 24 h at 37 °C in a 5 % CO₂ atmosphere. After incubation, cells were washed with PBS and afterwards 50 μ l of MTT-reagent (Roche, Leuven, Belgium) dissolved in cell medium up to 500 μ l was added to the cells and subsequently cells were incubated for 4 h at 37°C in 5 % CO₂ atmosphere. Finally, 500 μ l of solubilization reagent was added. The next day, cell viability was determined by measuring the absorbance of the formed formazan. The absorbance of each plate was measured in an absorbance plate reader at respectively 590 nm to determine the formed formazan and at 690 nm as a reference. The results of the cytotoxicity measurements are expressed as percentages; the viability of the cells which were only treated with cell medium was considered to be 100 %, while the viability of cells exposed to DMSO was considered to be 0 %. Experiments were performed in triplicate.

Transduction of melanoma cells with AAV-loaded microbubbles and ultrasound

BLM melanoma cells were seeded at 1.3×10^6 cells and grown up to 70% confluency in Opticell™ plates as mentioned above. Microbubbles were loaded with rAAV2 vectors expressing EGFP, that were first PEG-biotinylated using 20 or 100 μ g NHS-PEG-biotin, according to the method described above under 2.2.

Control experiments were performed using respectively non-PEGylated AAV-vectors and “free” PEGylated AAV-vectors (i.e. not bound to microbubbles). In each transduction experiment the same AAV concentration was used. After washing the cells, 1ml of AAV-loaded microbubbles, with a concentration of approximately 1×10^7 microbubbles per ml, was mixed with 9ml of fresh culture medium and added to the cells. Subsequently, Opticell™ plates were submerged in a warm water bath (37°C) with a bottom of ultrasound absorbing rubber. Ultrasound was delivered by moving a Sonitron™ ultrasound probe over the whole plate during 10-15 sec. We used 1 MHz ultrasound with a 10% duty cycle, the ultrasound intensity was 2 W/cm^2 . After 45min of incubation, microbubbles were removed; cells were washed with PBS and incubated in fresh culture medium. 48 hrs. later, cells were trypsinized, centrifuged and resuspended in flow buffer for flow cytometry analysis as described above. Results were expressed as % EGFP positive cells compared with untreated cells. All experiments were performed at least in triplicate and data are expressed as the mean of all three measurements.

Internalization of AAV in melanoma cells treated with AAV loaded microbubbles and ultrasound

BLM cells were grown under the conditions as described above. For these experiments microbubbles were loaded with green Alexa488-labeled rAAV2 and PEG-biotinylated using $100 \mu\text{g}$ NHS-PEG-biotin and 1 ml of bubbles (1×10^7 microbubbles/mL). The AAV loaded microbubbles were dispersed in fresh culture medium and added to the Opticells™. Subsequently, Opticell™ plates were subjected to ultrasound as described under 2.7. Cells were washed and fresh culture medium was added. The intracellular localization of the green-fluorescent

AAV-vectors was analyzed by confocal microscopy using the 488nm laser line. The cells were analyzed as well by flow cytometry as described under section 2.5. However, before flow cytometry analysis, cells were incubated with trypan blue to quench extracellular fluorescence.

Colocalization of endosomes with inactive AAV-vectors loaded on microbubbles after ultrasound application

BLM melanoma cells were grown under the conditions described above and transferred in Opticell™ plates. Endosomal labeling was performed by means of transduction with the BacMam™ 2.0 Cellight™ Reagent (Invitrogen, Merelbeke, Belgium). Briefly, the cells were washed with PBS and according to the manufacturers' recommendations, 150 µl of BacMam™ 2.0 reagent together with 9.85 ml of cell medium was subsequently added to the cells. Afterwards the cells were incubated for 24 h at 37°C under 5% CO₂ atmosphere.

Before the ultrasound experiments, microbubbles were prepared as described above and loaded with red-fluorescent labeled inactive PEGylated AAV. PEGylation of the vectors was performed as described in previous sections using 100 µg NHS-PEG-biotin and the vectors were fluorescently-labeled with 2µl of NHS-dyelight633 (2 mg/ml). These fluorescent AAV-loaded microbubbles were suspended in cell medium and this mixture was added to the cells. Subsequently, the Opticell™ plates were subjected to the same ultrasound conditions as used in the other ultrasound experiments. The cells were visualized with confocal microscopy as described above, 15 min post insonation using both the 488 nm laser line and the 633 nm laser line.

Statistical analysis

All data are presented as means +/- one standard deviation. A student's t-test was performed to determine whether datasets differed significantly. A p-value smaller than 0.05 was regarded as significant.

RESULTS

Design of an AAV-loaded microbubble using PEG-biotinylated AAV

Figure 1a schematically shows the structure of the AAV-loaded microbubbles we designed. The microbubbles consist of a lipid shell, composed of the phospholipids DPPC and DSPE-PEG-biotin, which surrounds a perfluorobutane gas core. The presence of biotin-containing lipids allowed the coupling of PEG-biotinylated AAVs through an avidin linker. Therefore the AAV-vectors were chemically modified making use of the NHS-PEG-biotin reagent. As shown in Figure 1b, this occurred via the amine-groups on lysine residues, present on the viral capsid, and the succinimidin ester group of the NHS-PEG-biotin reagent. This reaction leads to the formation of an amide, which should covalently bind the biotinylated PEG-chains to the capsid.

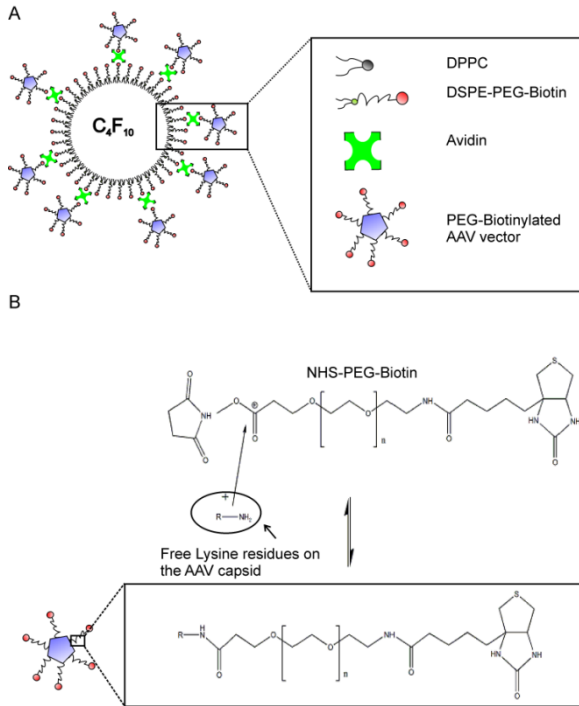


Figure 1: (A) Schematic representation of an AAV-loaded microbubble. The microbubble consists of a pefluorobutane (C_4F_{10}) gas core, surrounded by a lipid monolayer containing 1,2-dipalmitoyl-*sn*-glycero-3-phosphocholine (DPPC) and 1,2-distearoyl-*sn*-glycero-3-phosphoethanolamine-N-biotinyl(polyethylene glycol)-2000] (DSPE-PEG-biotin). Via avidin-biotin bridging, PEG-biotinylated AAV-vectors were loaded on the surface of the microbubbles. (B) Chemical coupling of PEG-biotin molecules to the viral capsid. The alpha-biotin-omega-carboxy succinimidyl ester poly(ethylene glycol) (NHS-PEG-biotin) reagent interacts with amine-groups on lysine residues present on the AAV capsid and binds PEG-biotin molecules onto the viral capsid through an amide bound.

To confirm successful PEGylation of the AAV-vectors, we measured the zeta-potential of the AAV-vectors respectively before and after the PEGylation reaction; Note that NHS-mPEG instead of NHS-PEG-biotin was used in these

experiments. As shown in Figure 2, the PEGylation reaction clearly increased the zeta-potential of the AAV-vectors, indicating that PEG-molecules shielded the negative charges on the viral capsid. As only a (relatively) low amount of NHS-MPEG per amine present on the viral capsid was used, the PEGylation of the AAV-vectors through the NHS coupling strategy seems to be an efficient process.

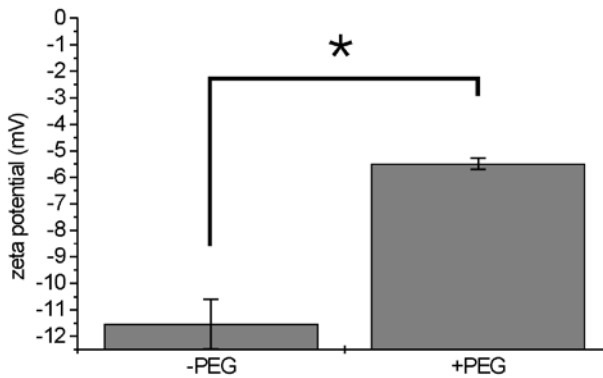


Figure 2: Zeta potential (ζ) measurements on non-PEGylated AAV-vectors (-PEG) And PEGylated AAV-vectors (+PEG). The higher zeta-potential of the PEGylated AAVs indicates a successful coupling of NHS-MPEG to the viral capsid. Experiments were performed using 15 μ g of NHS-MPEG per 5 $\times 10^{10}$ viral particles. (* $p < 0.05$)

In a next step we tried to load the lipid microbubbles with the PEG-biotinylated AAV-vectors. The successful loading of the AAV-vectors on the microbubbles' surface was confirmed by confocal microscopy. Figure 3 shows that green-fluorescent avidin binds to the surface of biotinylated lipid microbubbles (Figures 3b and 3d). Binding of the red-fluorescent PEG-biotinylated AAV-vectors to the microbubbles is shown in Figure 3e. Figure 3f clearly shows colocalization of green-labeled avidin and red-labeled AAV-vectors on the microbubble's surface

proving loading of microbubbles with AAV-vectors through avidin-biotin linkages.

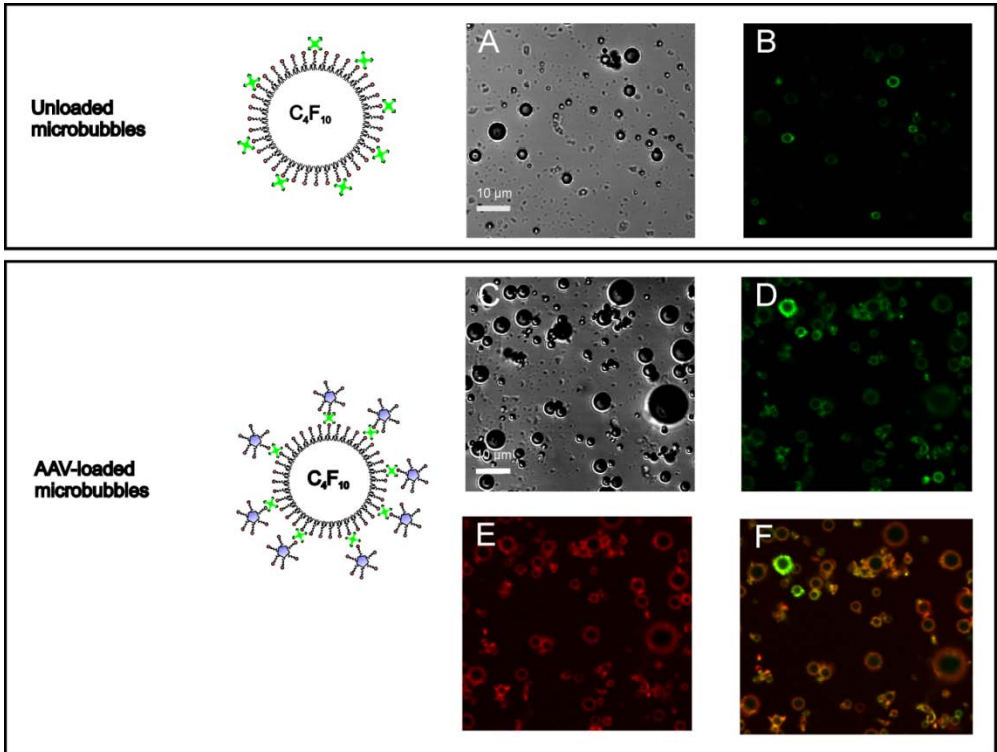


Figure 3: Confocal images of unloaded (A-B) and AAV-loaded (C-F) microbubbles carrying green-labeled avidin (B,D). (A,C) are the corresponding transmission images. Figure (F) shows colocalization of the green labeled avidin and red labeled AAV-vectors onto the shells of the microbubbles.

The influence of PEGylation of AAV-vectors on their transduction properties

To evaluate the influence of PEGylation on the transduction efficiency of the AAV-vectors we performed flow cytometry experiments using EGFP expressing rAAV2 vectors. We measured the percentage of EGFP positive cells as a function of the PEGylation degree of the AAV-vectors. Therefore, AAV-vectors were PEGylated using increasing amounts of PEG, ranging from 20 to 200 μ g NHS-MPEG per 5×10^{10} viral particles. As can be seen in Figure 4, the transduction efficiency of the AAV-vectors became clearly impaired if more than 40 μ g of PEG-reagent was used. Using 20 μ g of NHS-MPEG, the PEGylated AAVs were still able to transduce approximately 10% of the cell population. These results indicate that PEGylation of AAV-vectors clearly hampers their transduction efficiency, which is likely; since the PEG brush is expected to shield the viral capsid proteins thereby preventing optimal interactions with cell membrane components which is essential for their receptor mediated internalization (see below).

Since we wanted to investigate the effect of sonoporation on endocytosis, we considered to perform our further experiments with AAV-vectors that were not able to transduce cells on their own, i.e.: "inactive vectors" (being vectors which were strongly PEGylated through the use of 100 μ g PEG-reagent per 5×10^{10} viral particles). As Figure 4 shows, these inactive and strongly PEGylated vectors are completely incapable to transduce cells, which consequently means no endocytosis could have occurred.

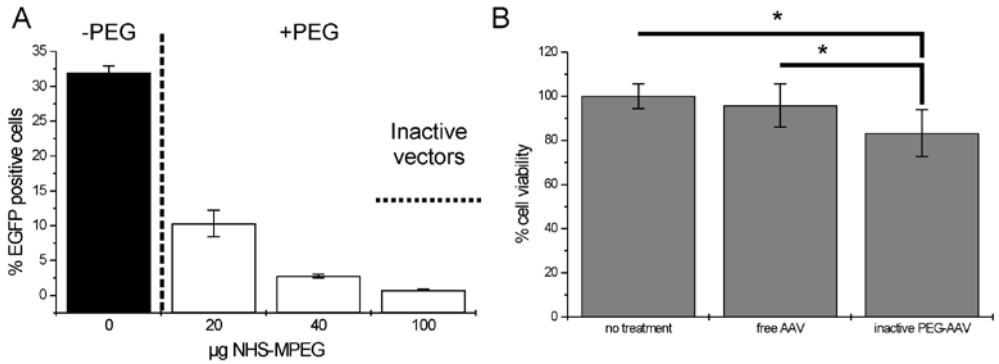


Figure 4: (A) Percentage of EGFP positive cells after transduction with (free) non-PEGylated AAV (black bar) and (free) PEGylated AAV-vectors (white bars). PEGylation of the AAV-vectors was performed with respectively 20, 40, 100 and 200µg of NHS-MPEG per 5×10^{10} particles. (B) Cell viability of melanoma cells after transduction with free AAV and inactive PEGylated AAV compared with no treatment. (* $p < 0.05$)

The influence of ultrasound and microbubbles on transduction of cells by inactive AAV

We measured the transduction efficiencies of AAV-loaded microbubbles, with and without ultrasound exposure. As described in the materials section, we determined the amount of AAV that became loaded on the surface of the microbubble to make sure that in all experiments the amount of vectors was the same. Again, the percentage of transduced cells was estimated by flow cytometry (Figure 5). Experiments were performed using inactive PEGylated vectors (see above), respectively in free form or bound to the microbubbles. We observed that, binding inactive PEGylated AAVs to microbubbles and applying ultrasound did not restore their transduction properties indicating that the mechanism of

internalization cannot involve endocytosis. If endocytosis would have been stimulated by sonoporation, these PEGylated AAV-vectors would have been internalized by endosomes, which would consequently have led to an enhanced transduction if ultrasound was applied. Unfortunately these flow cytometry data did not reveal any significant increase in transduction of the vectors, which can only mean that endocytosis was not enhanced.

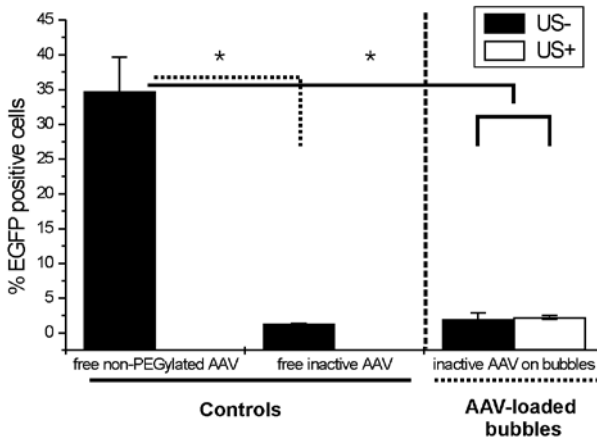


Figure 5: Percentage of EGFP positive cells, as measured by flow cytometry, after transduction of melanoma cells with AAV-loaded microbubbles in the presence (white bars) and absence (black bars) of ultrasound. As a control free non-PEGylated AAV-vectors were used and compared with free PEGylated AAV (black bars). (*p<0.05)

Internalization of AAV in melanoma cells treated with inactive AAV loaded microbubbles and ultrasound

Although these transduction studies prove no enhanced transduction of the vectors, we could not determine whether these vectors were internalized or not. An internalization of the vectors would mean that sonoporation involves a different mechanism compared to endocytosis and that enhanced cytoplasmic

delivery as described by *Lentacker et al.* [8] is really the case. Therefore we aimed to evaluate whether ultrasound and microbubbles enhance the cellular internalization of the inactive AAV-vectors, which showed no transduction as described in the previous section and as shown in Figure 5.

As shown in Figure 6, we quantified the internalization of the vectors with and without ultrasound exposure using flow cytometry: a clear shift in overall fluorescence of the cells could be observed if ultrasound was applied. These results indicate that most cells show a significant internalization of vectors when ultrasound was applied, while there was no internalization without ultrasound. Clearly, Figure 6 shows cellular internalization of the inactive PEGylated AAV-vectors, while the cells did not become transduced (Figure 5). To confirm these internalization data we performed confocal microscopy as a control with green fluorescent inactive PEGylated AAV-vectors loaded on the microbubbles, these experiments confirmed the data obtained by flow cytometry.

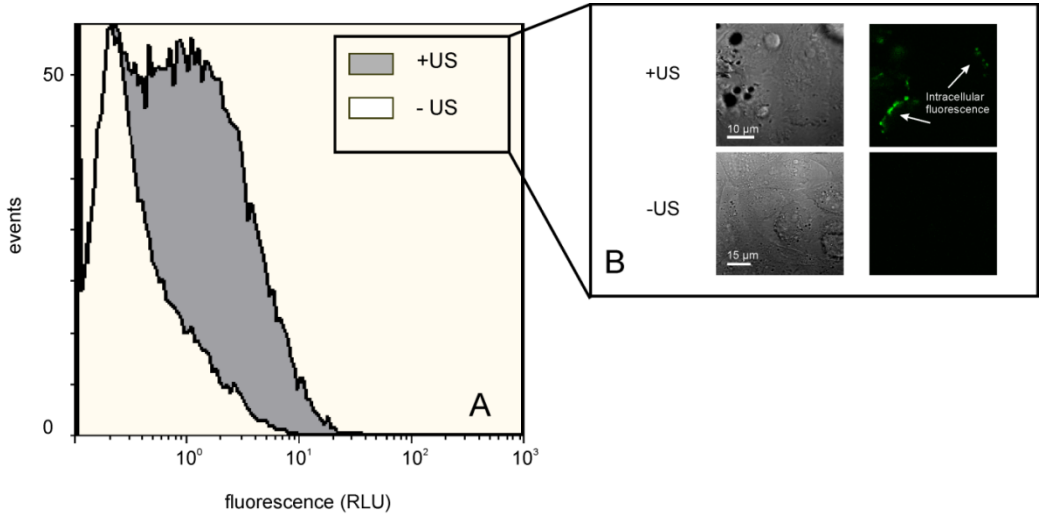


Figure 6: cellular internalization of green fluorescent inactive PEGylated AAV-vectors loaded on microbubbles (A) with (+US) and without ultrasound (-US) radiation, as obtained by flow cytometry. Remark that the extracellular fluorescence was quenched with trypan blue. Results show the fluorescence of the cells (RLU) in function of the number of cells counted by the flow cytometer ('events'). The inset (B) shows confocal and corresponding transmission images of the internalization of green fluorescent non-active PEGylated AAV-vectors loaded on microbubbles respectively with (US+) and without (US-) applying ultrasound measurements were performed 15 minutes after ultrasound exposure.

Endosomal colocalization studies to confirm direct cytoplasmic delivery upon ultrasound

To really confirm the hypothesis that ultrasound evades endocytosis as suggested by the internalization and transduction experiments, confocal microscopy on cells with labeled endosomes needed to be performed. As described in the experimental section, cells were transduced using the BacMam™ 2.0 technique. This technique allows transduction of a GFP-reporter gene targeting the Rab5a sequence which is specific for early endosomes. After staining, the cells were exposed to microbubbles loaded with red-fluorescent labeled inactive AAV-vectors and ultrasound was applied. Directly after ultrasound application we performed microscopy and we specifically checked for any colocalization between red and green fluorescence.

As shown in figure 7 we could not observe any significant colocalization of these red-labeled vectors with the green-labeled endosomes, since no merged green and red (orange) signals could be observed inside the cells. Consequently these data clearly show that ultrasound enables direct delivery of the particles loaded on the surface of the bubbles in the cytosol of the cell without endosomal internalization.

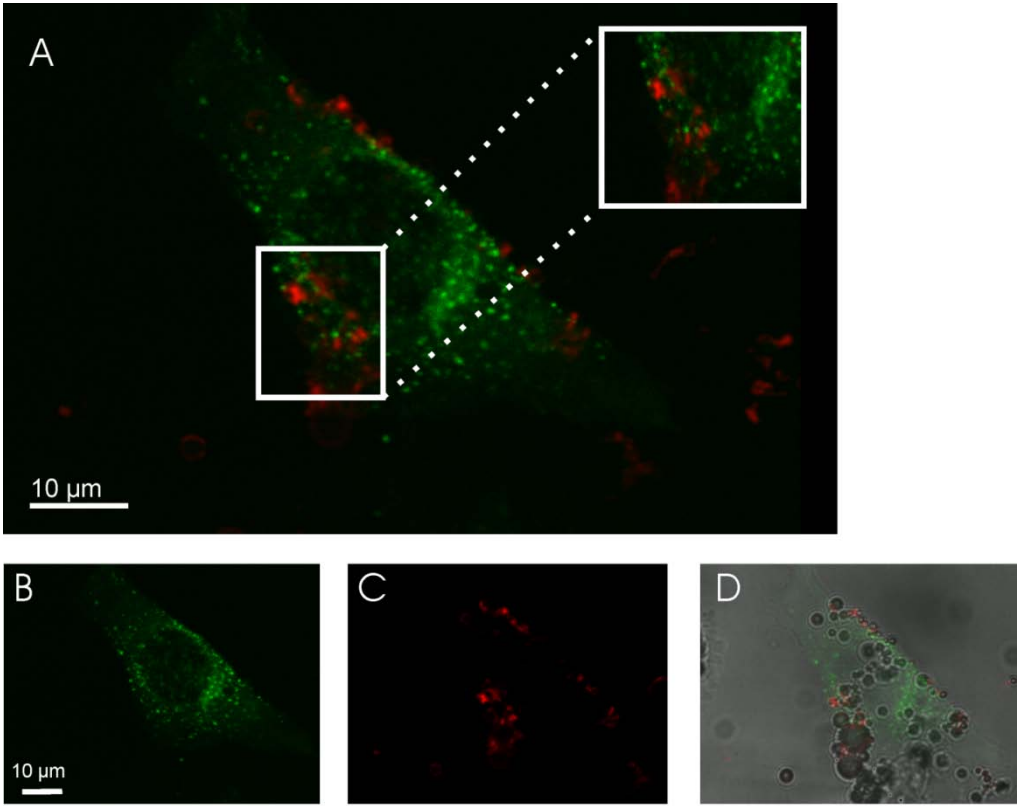


Figure 7: Confocal images of green-labeled endosomes merged with red-labeled inactive AAV-vectors (A) the inset shows a magnification of a region with a high density of red-labeled vectors inside the cell. (B) and (C) respectively show confocal images of green-labeled endosomes inside the cell and red-labeled inactive AAV-vectors. (D) shows a transmission image merged with confocal images of green and red fluorescence. Note that some bubbles remain attached to the cell after insonation.

CONCLUSIONS AND DISCUSSION

Earlier studies indicated that an enhanced deposition of drug molecules in cells through the use of microbubbles and ultrasound relies on the formation of transient pores in the cell membrane which arise upon implosion of the microbubbles. Recently we showed that, due to sonoporation, nanoparticles (like nucleic acid containing lipoplexes) which were attached to the surface of microbubbles become 'directly' delivered in the cytosol of cells upon imploding the bubbles with ultrasound, thus avoiding internalization of the nanoparticles through endosomes [8]. In this study we used PEGylated AAV-loaded microbubbles to elucidate the cellular entrance mechanism behind sonoporation. Shielding the viral capsid with PEG chains, makes it impossible to interact with cell membrane receptors essential to promote receptor mediated endocytosis. This blocks cellular transduction, as the endosomal acidification of the capsid and subsequent increase of its phospholipase activity is not induced [10,18]. As shown in literature, receptor mediated endocytosis is essential to obtain an effective AAV transduction [10,11]. This makes PEGylated AAV vectors an elegant tool to study the contribution of endocytosis to ultrasound induced sonoporation.

PEGylated AAV-vectors were obtained by chemically modifying the AAV capsid with NHS-PEG-biotin. We showed that these PEG-biotinylated AAV-vectors can be linked to lipid-shelled microbubbles via biotin-avidin linkages. This was confirmed with confocal microscopy, where colocalization of the AAV-vectors with avidin-labeled microbubbles was clearly shown. Flow cytometry experiments indeed confirmed that transduction efficiency becomes inhibited, once increasing amounts of PEG polymers are introduced on the AAV's surface. Flow cytometric analysis of the transduction efficiency with PEGylated (EGFP

expressing) AAV-vectors showed that transduction of cells could not be observed when highly PEGylated AAV-vectors (i.e. “inactive AAV-vectors”) were used. Interestingly, flow cytometry measurements revealed that the cellular internalization of inactive AAV-vectors was enhanced upon binding of the vectors to these microbubbles and applying ultrasound.

Figure 8 illustrates what we believe, may happen during and right after microbubble collapse. Ultrasound exposure of AAV loaded microbubbles will cause implosion of the microbubbles thereby releasing the attached vectors. At the same time, microbubble implosion “perforates” the cell membrane enabling the entry of the AAV-vectors, directly in the cytoplasm. Since the only pathway causing efficient transduction of the AAV-vectors is endocytosis and clearly no transduction has been observed by flow cytometry. Sonoporation can only involve a delivery of the vectors directly into the cytoplasm as the internalization studies clearly prove.

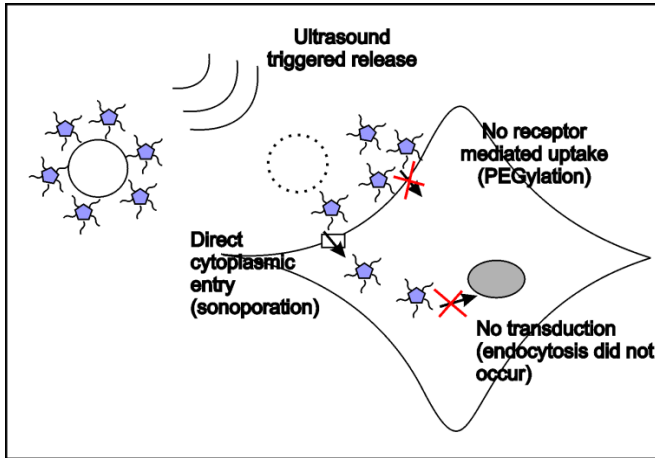


Figure 8: Schematic representation of ultrasound mediated internalization of PEGylated AAV-vectors. Sonoporation will cause direct cytoplasmic entry of the inactive AAV-vectors. These vectors however stay trapped in the cytoplasm.

With the results presented in this chapter, one can conclude that sonoporation enables direct access to the cell cytoplasm. However, we believe that this sonoporation also strongly depends on the ultrasound parameters used, which can be the cause of the different conclusions in other studies. As said before, at lower ultrasound intensities microbubbles will stably oscillate. If this oscillation occurs in the vicinity of cells the movement of the bubbles gently massages the cell membrane. This phenomenon is shown in different studies by *Van Wamel et al.* [19-21] and it is possible that this process induces endocytosis in some cases [9]. However, at higher ultrasound intensities when microbubble collapse occurs in the vicinity of cells, the cell membrane becomes perforated because of microjets and shockwaves produced by the bubble collapse [22], which is the case in this study.

Here, we showed the potential of sonoporation, a mechanism that really perforates the cell membrane which allows an adequate delivery of particles to cells. This type of direct delivery can be very useful, but can also have a negative influence on the outcome of experiments when a particle or vector is used that needs a certain cellular mechanism for its efficiency. We believe that we have made an important step by determining this new cellular delivery mechanism that could be a next step for further research in ultrasound mediated drug delivery.

ACKNOWLEDGEMENTS

This work was funded by the EU FP7 collaborative projects ARISE (which is a part of the European Stroke Network), SONODRUGS (NMP-4-LA-2008-213706) and the FWO-Vlaanderen research project G.0187.11. Ine Lentacker is a post-doctoral fellow of the FWO Flanders research fund (FWO-Vlaanderen).

REFERENCES

- [1] S. Hernot and A.L. Klibanov, Microbubbles in ultrasound-triggered drug and gene delivery, *Advanced Drug Delivery Reviews*, 60 (2008) 1153-1166.
- [2] I. Lentacker, S.C. De Smedt, and N.N. Sanders, Drug loaded microbubble design for ultrasound triggered delivery, *Soft Matter*, 5 (2009) 2161-2170.
- [3] E. Stride, Physical principles of microbubbles for ultrasound imaging and therapy, *Cerebrovasc. Dis.*, 27 Suppl 2 (2009) 1-13.
- [4] V. Sboros, Response of contrast agents to ultrasound, *Advanced Drug Delivery Reviews*, 60 (2008) 1117-1136.
- [5] J. Wu and W.L. Nyborg, Ultrasound, cavitation bubbles and their interaction with cells, *Advanced Drug Delivery Reviews*, 60 (2008) 1103-1116.
- [6] C.M.H. Newman and T. Bettinger, Gene therapy progress and prospects: Ultrasound for gene transfer, *Gene Therapy*, 14 (2007) 465-475.
- [7] S. Mehier-Humbert, T. Bettinger, F. Yan, and R.H. Guy, Plasma membrane poration induced by ultrasound exposure: implication for drug delivery, *J. Control Release*, 104 (2005) 213-222.

- [8] I. Lentacker, N. Wang, R.E. Vandenbroucke, J. Demeester, S.C. De Smedt, and N.N. Sanders, Ultrasound Exposure of Lipoplex Loaded Microbubbles Facilitates Direct Cytoplasmic Entry of the Lipoplexes, *Mol. Pharm.*, (2009).
- [9] B.D. Meijering, L.J. Juffermans, W.A. van, R.H. Henning, I.S. Zuhorn, M. Emmer, A.M. Versteilen, W.J. Paulus, W.H. van Gilst, K. Kooiman, N. de Jong, R.J. Musters, L.E. Deelman, and O. Kamp, Ultrasound and microbubble-targeted delivery of macromolecules is regulated by induction of endocytosis and pore formation, *Circ. Res.*, 104 (2009) 679-687.
- [10] J.S. Bartlett, R. Wilcher, and R.J. Samulski, Infectious entry pathway of adeno-associated virus and adeno-associated virus vectors, *J. Virol.*, 74 (2000) 2777-2785.
- [11] W. Ding, L. Zhang, Z. Yan, and J.F. Engelhardt, Intracellular trafficking of adeno-associated viral vectors, *Gene Ther.*, 12 (2005) 873-880.
- [12] H.T. Le, Q.C. Yu, J.M. Wilson, and M.A. Croyle, Utility of PEGylated recombinant adeno-associated viruses for gene transfer, *J. Control Release*, 108 (2005) 161-177.
- [13] G.K. Lee, N. Maheshri, B. Kaspar, and D.V. Schaffer, PEG conjugation moderately protects adeno-associated viral vectors against antibody neutralization, *Biotechnol. Bioeng.*, 92 (2005) 24-34.
- [14] I. Lentacker, B.G. De Geest, R.E. Vandenbroucke, L. Peeters, J. Demeester, S.C. De Smedt, and N.N. Sanders, Ultrasound-responsive polymer-coated microbubbles that bind and protect DNA, *Langmuir*, 22 (2006) 7273-7278.
- [15] I. Lentacker, S.C. De Smedt, J. Demeester, V. Van Marck, M. Bracke, and N.N. Sanders, Lipoplex-loaded microbubbles for gene delivery: A Trojan horse controlled by ultrasound, *Advanced Functional Materials*, 17 (2007) 1910-1916.
- [16] I. Lentacker, B. Geers, J. Demeester, S.C. De Smedt, and N.N. Sanders, Design and Evaluation of Doxorubicin-containing Microbubbles for Ultrasound-triggered Doxorubicin Delivery: Cytotoxicity and Mechanisms Involved, *Mol. Ther.*, (2009).
- [17] I. Lentacker, S.C. De Smedt, J. Demeester, V. Van Marck, M. Bracke, and N.N. Sanders, Lipoplex-loaded microbubbles for gene delivery: A Trojan horse controlled by ultrasound, *Advanced Functional Materials*, 17 (2007) 1910-1916.
- [18] J. Hansen, K. Qing, and A. Srivastava, Adeno-associated virus type 2-mediated gene transfer: altered endocytic processing enhances transduction efficiency in murine fibroblasts, *J. Virol.*, 75 (2001) 4080-4090.
- [19] A. van Wamel, K. Kooiman, M. Hartevelde, M. Emmer, F.J. ten Cate, M. Versluis, and N. de Jong, Vibrating microbubbles poking individual cells: Drug transfer into cells via sonoporation, *Journal of Controlled Release*, 112 (2006) 149-155.
- [20] A. van Wamel, A. Bouakaz, M. Versluis, and N. de Jong, Micromanipulation of endothelial cells: ultrasound-microbubble-cell interaction, *Ultrasound Med. Biol.*, 30 (2004) 1255-1258.
- [21] A. van Wamel, K. Kooiman, M. Emmer, F.J. ten Cate, M. Versluis, and N. de Jong, Ultrasound microbubble induced endothelial cell permeability, *J. Control Release*, 116 (2006) e100-e102.
- [22] C.D. Ohl, M. Arora, R. Ikin, N. de Jong, M. Versluis, M. Delius, and D. Lohse, Sonoporation from jetting cavitation bubbles, *Biophysical Journal*, 91 (2006) 4285-4295.

General Conclusions and Future Perspectives

Cancer is one of the main causes of death in Europe. Although the scientific community has made significant progress in the understanding of this disease in the past quarter century, no real therapeutic breakthrough has been achieved so far. Cancer therapy (especially chemotherapy) still faces severe side-effects and there is no therapeutic moiety that allows selective targeting of the therapeutic moiety to the tumor. The ideal cancer therapy hence would allow selective treatment of cancer cells without causing damage in healthy cells and tissues.

In **chapter 1** of this thesis we highlight the most important molecular mechanisms behind cancer and their relation with cancer therapy that were elucidated in the past decade. We have seen cancer developing from a group of “out of control” cells to a tissue characterized by cells that express cancer hallmarks and that has a changed communication with the surrounding tissue (i.e. the tumor micro-environment). In this chapter we suggest a novel technique that allows site-specific image-guided drug delivery using ultrasound contrast agents (“microbubbles”) and ultrasound (imaging) in tumors. This technique may allow the delivery of a therapeutic moiety only there where ultrasound is applied. These microbubbles can be loaded with drug-containing nanoparticles that release their (drug) payload upon insonation with a high intensity ultrasound pulse. This type of ultrasound pulse will induce a violent oscillation of the microbubble resulting in implosion of the bubble and hence release of a therapeutic payload attached to the surface of the bubble.

Although substantial evidence was present that these nanoparticle-loaded microbubbles were indeed able to deliver a molecule controlled by ultrasound, the existing materials were mostly not suitable for further preclinical and clinical development. In **chapter 2** we describe the design of a safe, stable and easy to use

formulation of liposome-loaded microbubbles that may be suitable for further clinical development. This formulation is based on the simple self-assembly of the microbubble upon shaking a solution containing all phospholipid constituents of the microbubble and DOX-filled liposomes. We have measured the *in vitro* cell killing activity of this formulation and observed that only upon ultrasound application significant cell killing (concentration dependent) could be observed. Interestingly, we observed significant cell killing at doses that didn't show any cell killing even with free DOX. This shows that ultrasound triggered drug-delivery with microbubbles allows a more efficient delivery of the drug into cells.

We decided to increase the selectivity of our microbubble formulation by introducing a targeting moiety into the drug-filled liposomes loaded on the microbubbles as described in **chapter 3**. Here, we show that liposome-loaded microbubbles targeted against N-cadherin (a protein which is upregulated in invasive tumor cells) are able to adhere specifically to N-cadherin expressing HMB2 cells in a mixture of 2 different cell types. Ultrasound application allows delivery of the model drug propidium iodide to these HMB2 target cells.

In **chapter 4**, we wanted to compare drug-delivery efficiency of our newly developed formulation of liposome-loaded lipid-shelled microbubbles with liposome-loaded microbubbles composed out of (custom-made) polymers. We clearly observe that ultrasound induced cell killing and DOX-release is lower for polymer shelled microbubbles compared with lipid-shelled microbubbles. This could be explained by the different physical response to ultrasound by both types of microbubble shell. The more elastic lipid-shelled microbubbles will be fragmented upon implosion by a high intensity ultrasound pulse, where the polymer coated microbubbles only "crack" upon such ultrasound pulses. This

“cracking” only affects small percentages of the drug-filled liposomes loaded on the surface of the microbubbles, where fragmentation of lipid-shelled microbubbles will affect nearly all loaded liposomes and hence increases drug-release and efficiency. We also loaded the microbubbles with thermosensitive liposomes and saw a significant increase in ultrasound cell killing and DOX-release. This may be explained by an increase in temperature that is induced by microbubble cavitation, which is able to destabilize these thermosensitive liposomes loaded on the surface of the microbubbles and hence induce drug delivery.

Finally the improvements made for optimizing lipid-shelled microbubbles for delivery of small molecules to tumors needed to be put to an (*in vivo*) “acid test”. In **chapter 5** we have tested the efficiency of ultrasound triggered drug-release from (thermosensitive) liposome-loaded microbubbles with different modifications in tumor bearing mice and compared this with standard liposomes. Indocyanine green (ICG) (a small molecule that does normally not diffuse from the bloodstream into tissues) was used as a model drug and was loaded inside the liposomes. We observed significant uptake of ICG into tumors in all treatment groups, however most ICG was taken up in tumors treated with standard liposomes and thermosensitive liposome-loaded microbubbles upon ultrasound application. Indeed, standard liposomes will circulate for a significantly longer period of time, which allows gradual infiltration of the liposomes into the tumor via enhanced permeation and retention (EPR).

In vitro ultrasound assisted drug-delivery is shown very efficient (in chapter 1 we showed that even at very low doses ultrasound assisted drug-delivery was still efficient), which may be caused by the temporal opening of cell membranes upon

microbubble implosion (so-called sonoporation). Unfortunately, the specific biophysical mechanisms behind sonoporation are not yet fully understood. In **chapter 6**, we analyzed the intracellular fate of adeno associated virus (AAV) loaded on the surface of the microbubbles via avidin-biotin chemistry. AAV is a viral vector that needs endocytosis for efficient gene transduction, but upon ultrasound application on AAV-loaded microbubbles AAV particles were detected intracellularly, while no efficient transduction was observed. This indicates that sonoporation does not induce endocytosis (which would have certainly led to efficient gene transduction), but involves direct cytoplasmic delivery of the loaded liposomes.

What are the biggest issues that need to be tackled in future work on ultrasound assisted drug-delivery with microbubbles? As observed, ultrasound-triggered drug-delivery from liposome-loaded microbubbles is very efficient *in vitro* probably due to local sonoporation effects, however as soon as we test the materials *in vivo* standard therapeutic liposomes perform better. This is probably due to the very short circulation time of the bubbles that do not allow accumulation of the drug-filled nanoparticles over a longer period of time. Therefore, further emphasis has to be put on the development of “smaller” drug-filled ultrasound responsive drug-delivery systems. Making these systems smaller will allow longer circulation and hence higher uptake of the particles into tumors via EPR. Ultrasound can in this case be used to make the uptake of anticancer drugs into tumor cells more efficient via sonoporation.

Not only the size of the bubble is an important issue, the type of molecule to deliver and the type of disease to tackle can be important too. Nucleic acids like pDNA, siRNA and mRNA theoretically need only 1 molecule to be efficiently

delivered into the cell cytoplasm to work. In this work we only focus on small molecules (anticancer drugs) which need much higher target cell concentrations to be therapeutically effective. As shown sonoporation helps in delivering molecules intracellularly, this is particularly useful for larger therapeutic molecules like (pDNA, siRNA, mRNA). To conclude, we would advise that research on ultrasound guided drug-delivery and more specifically the development of microbubbles for this purpose should focus on a) the development of smaller (100-200 nm) ultrasound responsive drug-filled particles, b) that the mechanisms behind sonoporation should be elucidated more elaborately with advanced microscopy technique and finally c) that a clinically useful microbubble formulation for nucleic acid delivery should be developed.

Algemene Besluiten en Toekomstperspectieven

Kanker is een van de belangrijkste doodsoorzaken in Europa. Hoewel de wetenschappelijke gemeenschap de voorbije kwarteeuw belangrijke vooruitgang heeft geboekt in het basiswetenschappelijk onderzoek naar kanker, is er nog steeds geen doorbraak bereikt in een efficiënte kankertherapie. Kankertherapie (en dan voornamelijk chemotherapie) leidt nog steeds tot zeer nadelige bijwerkingen, bovendien bestaat er geen therapeutisch middel dat doelgericht tumoren aanpakt. Het ideale antikanker geneesmiddel zou dus een selectieve behandeling van de tumor moeten bewerkstelligen zonder ernstige schade aan gezonde weefsels toe te brengen.

In het **eerste hoofdstuk** van deze thesis lichten we de belangrijkste moleculaire mechanismes, die in het voorbije decennium werden opgehelderd, toe die aan de oorzaak liggen van kanker en staan stil bij hun relatie tot kankertherapie. Hier zien we dat de definitie van kanker evolueerde van een groepje “ongecontroleerde” cellen, naar een weefsel dat gekarakteriseerd wordt door cellen die kanker “kenmerken” vertonen en die een gewijzigde communicatie met het naburige weefsel vertonen. In dit hoofdstuk brengen we ook voornamelijk een nieuwe techniek aan die plaats-specifieke geneesmiddelaafgifte kan realiseren in de tumor onder controle van medische beeldvorming, waarbij minder geneesmiddel terechtkomt op plaatsen waar het niet thuishoort. Hiervoor maakt men gebruik van ultrageluid contrastmiddelen (“microbellen”) en ultrageluid (beeldvorming) in tumoren. Deze techniek stelt ons in staat om een therapeutisch middel af te leveren alleen daar waar een ultrageluidsgolf wordt toegepast (dus in de tumor). Deze microbellen kunnen worden beladen met geneesmiddel-beladen nanopartikels die geneesmiddel kunnen bevatten en dat in de omgeving van de tumor kunnen loslaten. Dit kan doordat de microbellen onder invloed van ultrageluid met een hoge intensiteit op een hevige manier gaan

oscilleren, dit leidt uiteindelijk tot de implosie van de microbel. Deze implosie leidt dan tot de verspreiding van het therapeuticum dat op het oppervlak van de bel is geladen in het gewenste weefsel.

Hoewel er voldoende bewijs was dat zo'n nanopartikel-beladen microbellen inderdaad in staat waren om moleculen op een bepaalde plaats af te leveren onder controle van ultrageluid, was er geen materiaal beschikbaar dat kon worden gebruikt voor verdere preklinische en klinische studies. In **hoofdstuk 2** beschrijven we het ontwerp van een veilige, stabiele, en makkelijk te hanteren formulering van liposoom-beladen microbellen die geschikt zou moeten zijn voor verdere klinische ontwikkeling en evaluatie van deze systemen. Deze formulering is gebaseerd op het in elkaar schuiven van de betrokken moleculen door eenvoudigweg een oplossing met de benodigde ingrediënten (fosfolipiden en geneesmiddel (doxorubicine)-beladen liposomen) te schudden aan een hoge snelheid. We hebben het effect op celviabiliteit gemeten van deze formulering en konden constateren dat er een significant effect was indien er ultrageluid werd toegepast op de microbellen beladen met doxorubicine-liposomen. Zelfs wanneer een zeer lage dosis aan geneesmiddel werd gebruikt konden we evengoed een significant effect op het afdoden van kankercellen door dit systeem constateren. Op die manier kunnen we dus besluiten dat deze techniek ons in staat stelt op een zeer efficiënte manier geneesmiddel af te leveren met een materiaal dat geschikt is voor klinisch gebruik.

Vervolgens hebben we besloten om de selectiviteit van ons systeem op te drijven door het meer doelgericht te maken, dit door de liposomen beladen op de microbellen met een antilichaam te bedekken zoals beschreven in **hoofdstuk 3**. Hier tonen we aan dat liposoom-beladen microbellen gericht tegen N-cadherine

(een proteïne dat is upgereguleerd in invasieve tumorcellen) in staat zijn om specifiek te “binden” aan HMB2 cellen die specifiek dit N-cadherine tot expressie brengen in een mengsel met 2 verschillende celtypes. Bovendien tonen we hier ook aan dat we het modelgeneesmiddel propidium jodide specifiek in de doelcellen kunnen afleveren met deze techniek.

In het **vierde hoofdstuk**, wilden we de efficiëntie van het geneesmiddelafgifteproces vergelijken tussen liposoom-beladen microbellen met een verschillend type schaal dat hen omvat (enerzijds lipiden en anderzijds polymeren). We konden duidelijk vaststellen dat ultrageluid geïnduceerde celdood en DOX vrijstelling lager was voor polymeer gestabiliseerde dan voor lipide gestabiliseerde microbellen. Dit kan worden verklaard door het verschil in eigenschappen tussen deze twee verschillende schaaltypes. De eerder elastische lipidschaal zal fragmenteren als gevolg van de implosie die volgt op een hoge intensiteit ultrageluid golf, daar waar de stuggere polymeerschaal eerder zal “scheuren”. Het scheuren van de bellen leidt ertoe dat niet alle liposomen zullen worden aangetast na ultrasound applicatie, daar waar dat wel gebeurt bij fragmentatie van de lipidenbellen. We hebben de microbellen ook opgeladen met temperatuurgevoelige liposomen en zagen een significante toename van het effect op ultrasound geïnduceerde celdood met DOX-beladen liposomen op de microbellen. Dit kan worden verklaard door een toename van de lokale temperatuur als de microbel gaat oscilleren in het ultrageluidsveld, dit leidt tot een destabilisatie van het liposomale membraan waardoor het geneesmiddel vlotter vrijkomt in de omgeving van de cel.

Uiteindelijk moesten we een *in vivo* lakmoesproef uitvoeren op de materialen die werden ontwikkeld. In **hoofdstuk 5** hebben we de efficiëntie van ultrageluid

gestuurde geneesmiddelaafgifte van liposoom-beladen microbellen met verschillende modificaties (gericht naar VEGFR of beladen met thermosensitieve liposomen) getest in tumor dragende muizen en dit werd vergeleken met standaard liposomen. Indocyanine groen (ICG) werd gebruikt als modelgeneesmiddel (beladen in liposomen) omdat deze molecule niet vanuit de bloedbaan in een weefsel (zoals een tumor) kan accumuleren. We observeerden in elke behandelde groep dieren een significante opname van het ICG in de tumor, hoewel de standaard liposomen het efficiëntst bleken te zijn voor dit doel. Inderdaad, deze liposomen zijn in staat gedurende lange tijd in de bloedbaan te circuleren en kunnen dus makkelijk in de tumor accumuleren via het EPR-effect.

In vitro zien we dat ultrageluid in combinatie met geneesmiddel-beladen microbellen zeer efficiënt is in het afleveren van geneesmiddelen in cellen. Een tijdelijke opening van het celmembraan (de zogenaamde sonoporië) zou hiervan aan de basis kunnen liggen. Spijtig genoeg zijn de biofysische mechanismen achter sonoporië nog niet opgehelderd. In **hoofdstuk 6** analyseerden we het intracellulaire lot van adeno geassocieerde virussen (AAV) beladen op het oppervlak van microbellen via avidine-biotine koppeling. AAV is een virale vector die endocytose nodig heeft voor een efficiënte gentransductie. Echter observeren we na ultrageluidsapplicatie op deze bellen dat de AAV partikels zich in het cel cytoplasma bevinden zonder dat dit aanleiding geeft tot een efficiënte transductie. Dit toont aan dat sonoporië de endocytose niet induceert, maar eerder een directe cytoplasmatische afgifte bewerkstelligt.

Wat zijn nu de belangrijkste problemen waarmee we in de toekomst moeten rekening houden bij de verdere ontwikkeling van dit platform? Zoals aangetoond is ultrasound gecontroleerde geneesmiddelaafgifte een zeer efficiënte techniek *in*

vitro hoogstwaarschijnlijk door toedoen van sonoporiatie. Desondanks zien we *in vivo* echter geen toegenomen efficiëntie. Waarschijnlijk speelt de zeer korte circulatietijd van de microbellen hier een uitermate belangrijke rol in. Daarom moeten we verder inzetten op het verkleinen van de microbellen. Hoe kleiner de microbel, hoe langer hun circulatietijd en dus ook hoe meer microbellen kunnen accumuleren in de tumor.

Niet alleen de grootte van de bellen zijn een belangrijk gegeven, het type af te leveren geneesmiddel speelt ook een rol. Bij nucleïnezuren zoals pDNA, siRNA en mRNA moet er theoretisch slechts 1 molecuul in de cel worden afgeleverd om een therapeutisch effect te bekomen. In dit werk hebben we gewerkt met kleine antikankergeneesmiddelen die vooral in relatief hoge concentratie de doelcellen moeten bereiken. Bovendien kan, zoals aangetoond, sonoporiatie worden aangewend om moleculen intracellulair af te leveren en zullen dus vooral geneesmiddelen die in een kleine hoeveelheid efficiënt in het cytoplasma moeten worden afgeleverd het meest kunnen gebruik maken van deze techniek (dus vooral grote moleculen zoals nucleïnezuren). Om te besluiten kunnen we zeggen dat het onderzoek naar deze techniek zich in de toekomst vooral zich moet toespitsen op a) de ontwikkeling van kleinere microbellen (100-200nm), b) de mechanismen achter sonoporiatie moeten worden opgehelderd en c) moet er een manier komen waarmee we ook grotere moleculen (zoals nucleïnezuren) kunnen koppelen aan de microbellen op een manier die ons in staat stelt dit materiaal ook klinisch te testen.

PhD Portfolio

PERSONALIA

Name: Geers

First Name: Bart

Nationality: Belgian

Place and date of birth: Sint-Niklaas, 17th September 1985

Marital status: Partner; Lien Verstraeten

Children: Stan Geers (°12/07/2012)

Private address: Paddeschootdreef 83, 9100 Sint-Niklaas

Professional address: Harelbekestraat 72, 9000 Gent

E-mail: bart.geers@ugent.be

Twitter: @bartgeers

LinkedIn: <http://be.linkedin.com/pub/bart-geers/16/b65/478>

URL: <http://www.biofys.ugent.be>

DEGREES

June 2003: secondary school in latin and mathematics magna cum laude, Sint-Jozef-Klein-Seminare, Sint-Niklaas

June 2008: Pharmacist (Master in Pharmaceutical Sciences) with distinction, Ghent University

PEER REVIEWED PUBLICATIONS (FIRST AUTHOR)

A1 publications

Lentacker I., Geers B., Demeester J., De Smedt S. C., Sanders N.N. Design and evaluation of doxorubicin containing microbubbles for ultrasound triggered doxorubicin delivery: cytotoxicity and mechanisms involved. *Molecular Therapy*, 2010, 18, 101-108 (**JCR 6.8**)

Geers B., Lentacker I., Sanders N.N. Demeester J., Meairs S., De Smedt S.C.: Self-assembled liposome-loaded microbubbles: the missing link for safe and efficient ultrasound guided drug-delivery. *Journal of Controlled Release*, 2011, 10, 249-256 (**JCR 7.2**)

Geers B., Lentacker I., Alonso A., Sanders N.N., Demeester J., Meairs S., De Smedt S.C.: On the mechanisms behind sonoporation. *Molecular Pharmaceutics*, 2011, 8(6), 2244-51 (**JCR 5.4**)

Geers B., Dewitte H., De Smedt S.C., Lentacker I.: Crucial factors and emerging concepts in ultrasound-triggered drug delivery. *Journal of Controlled Release* 2012 (**JCR 7.2**), 2012, 164, 248-255.

Escoffre J.-M., Mannaris C, **Geers B.**, Novell A., Lentacker I, Averkiou M, Bouakaz A.: Doxorubicin liposome-loaded microbubbles for contrast imaging and ultrasound-triggered drug delivery, *IEEE TUFFC*, 2012 (accepted paper) (**JCR 1.6**)

Luan Y., Faez T., Skachkov I, **Geers B.**, Lentacker I, Vandersteen A., Versluis A.M., de Jong N.: Acoustical properties of individual liposome-loaded microbubbles. *Ultrasound in medicine and biology*, 2012; 38; 2174-85 (**JCR 2.2**)

Geers B., De Wever O., Demeester J., Bracke M., De Smedt S.C., Lentacker I.; Targeted liposome-loaded microbubbles for cell specific ultrasound-triggered drug delivery: trying to find a needle in a haystack?; *Small*; accepted (**JCR 8.3**)

Alonso A., Reinz E, Leuchs B., Kleinschmidt J., Fatar M., **Geers B.**, Lentacker I., Hennerici M., De Smedt S.C., Meairs S.: Focal delivery of AAV2/1-transgenes into the rat brain by localized ultrasound-induced BBB opening; *Molecular Therapy/Nucleic acids*; accepted

Dewitte H., **Geers B.**, Demeester J., Himmelreich U., De Smedt S.C., Lentacker I.: Design and Evaluation of Theranostic Perfluorocarbon Particles for Simultaneous Antigen-loading and ¹⁹F-MRI Tracking of Dendritic Cells; *Journal of Controlled Release*; accepted (**JCR 6.5**)

C1 Publications

Geers B., Lentacker I., Alonso A., Meairs S., Demeester J., De Smedt S.C., Sanders N.N.; Virus loaded microbubbles as a tool for targeted gene therapy. *J Control Release*. 2010 Nov 20;148(1):e59.

Geers B. Lentacker I, Alonso A., Meairs S., Demeester J., De Smedt S.C., Sanders N.N.; Virus loaded microbubbles as a tool for targeted gene therapy:. J Control Release. 2010 Nov 20;148(1):e59.

Lentacker I. **Geers B.**, Demeester J, De Smedt SC, Sanders NN.: Tumor cell killing efficiency of doxorubicin-loaded microbubbles after ultrasound exposure J Control Release. 2010 Nov 20;148(1):e113-4

C2 Publications

Patent application: Geers B, Lentacker I., Sanders N.N., De Smedt S.C.: Drug Delivery System: EP 10192068.4-2112.

CONFERENCES OR WORKSHOPS WITH LECTURE (PRESENTING AUTHOR)

Geers B.; Lentacker I.;De Smedt S.C.; Demeester J.; Sanders N.N. AAV-loaded microbubbles a novel tool for targeted gene therapy.14th Forum of pharmaceutical Sciences; 14-15 May 2009, Blankenberge, Belgium

Geers B.; Lentacker I.; De Smedt S.C.: Design and *in vitro* evaluation of AAV2-loaded microbubbles for targeted gene therapy in the brain. 1st ESN Consortium meeting; 25-26 May 2009,Stockholm, Sweden

Geers B., Lentacker I., De Smedt S.C. Sanders N. Virus-loaded microbubbles as a tool for targeted gene delivery: 9th International symposium on therapeutic ultrasound, 23-26 September 2009, Aix-en-Provence, France

Geers B. Lentacker I., De Smedt S.C., Sanders N.N. Sonodrugs partner presentation (May 2009-November2009) Sonodrugs meeting, 10-12 november 2009, Eindhoven, The Netherlands,

Lentacker I. **Geers B.**, Demeester J., De Smedt S.C., Sanders N.N., Tumor cell killing efficiency of doxorubicin-liposome loaded microbubbles after ultrasound exposure: 15th European symposium on ultrasound contrast imaging, Rotterdam, The Netherlands, 20-22 january 2010:

Geers B., Lentacker I., Ghent Research group on nanomedicines partner presentation: Sonodrugs workshop and review meeting, 29-30 june 2010, Eindhoven, The Netherlands:

Geers B. Lentacker I, Alonso A, Meairs S, Sanders N N, De Smedt S C, Targeted stroke therapy: 2nd ESN consortium meeting, 6-7 September 2010, Heidelberg, Germany.

Geers B., Lentacker I., Ghent research group on nanomedicines partner presentation: Sonodrugs workshop, 9-11 november 2010, Paris, France.

Lentacker I. **Geers B.**, De Smedt S.C. Mechanisms of sonoporationm: 16th European symposium on ultrasound contrast imaging, 19-21 january 2011, Rotterdam, The Netherlands.

Geers B., Lentacker I., Sanders N.N., Demeester J., Meairs S., De Smedt S.C. Self-assembled liposome-loaded microbubbles: the missing link for safe and efficient ultrasound-guided drug delivery: 16th European symposium on ultrasound contrast imaging, 19-21 january 2011, Rotterdam, The Netherlands.

Geers B., Lentacker I., Sanders N.N., Demeester J., De Smedt S.C.: Advances in image guided drug delivery, 15th Forum of pharmaceutical sciences, 13-14 may 2011, Spa, Belgium

Geers B., lentacker I., De Smedt S.C. Sonodrugs presentation, Sonodrugs Workshop, 16-18 may 2011, Tours, France

Lentacker I., **Geers B.**, De Smedt S.C., Luan Y, de Jong N., Vulto S., Sio C. Development and characterization of drug loaded microbubbles within the Sonodrugs project. Leeds Microbubble symposium, 4-6 july 2011, Leeds, United Kingdom.

Luan Y., Faez T., Skachkov I., Gelderblom E., **Geers B.**, Lentacker I., van der steen A., Versluis M., de Jong N. Optical Characterization of Individual Liposome Loaded Microbubbles, IEEE ultrasonics symposium, September 2011, Orlando , USA

Escoffre JM. **Geers B.**, Lentacker I, Bouakaz A. : Evaluation of doxorubicin-containing microbubbles for ultrasound-triggered delivery, IEEE ultrasonics symposium, September 2011, Orlando, USA

Geers B., Lentacker I. Sonodrugs partner presentation, Sonodrugs review meeting, 14-16 december 2011, London, UK

Lentacker I.; Geers B, Dewitte H, De Smedt S.C. Nanoparticle loaded microbubbles for ultrasound mediated gene and drug delivery. 12th European symposium on controlled drug delivery

Geers B., De Smedt S., Lentacker I. Injectable drug-loaded bubbles, a magic bullet for image guided cancer therapy?, Knowledge for Growth, 24 May 2012, Ghent, Belgium

CONFERENCES WITH POSTER PRESENTATION (PRESENTING AUTHOR)

Geers B. Lentacker I., Alonso A., Meairs S., Demeester J., De Smedt S.C., Sanders N.N.; Virus loaded microbubbles as a tool for targeted gene therapy:15th European symposium on ultrasound contrast imaging, Rotterdam, The Netherlands.

Geers B. Lentacker I, Alonso A., Meairs S., Demeester J., De Smedt S.C., Sanders N.N.; Virus loaded microbubbles as a tool for targeted gene therapy: 11th European symposium on controlled drug delivery, Egmond-aan-Zee, The Netherlands.

Geers B. Lentacker I, Cool S, Demeester J, De Smedt S.C., Sanders N.N. Ultrasound responsive Doxorubicin-loaded microbubbles; towards an easy applicable drug delivery platform: 11th European symposium on controlled drug delivery, Egmond-aan-Zee, The Netherlands.

Geers B. Lentacker I, Sanders N N, Demeester J, Meairs S, De Smedt S.C. Self-assembled liposome-loaded microbubbles: the missing link for safe and efficient ultrasound guided drug-delivery: 11th international symposium of the International Society of Therapeutic Ultrasound, 11-13 april 2011, New York City, USA.

Geers B, Mühlmeister M, De Wever O, Tiemann K, Bracke M, De Smedt S.C., Lentacker I. Targeted liposome-loaded microbubbles to detect and selectively destroy metastasis cells. 17th European symposium on Ultrasound contrast Imaging, 19-20 January 2012, Rotterdam, The Netherlands

Geers B, Mühlmeister M, De Wever O, Tiemann K, Bracke M, De Smedt S.C., Lentacker I. Targeted liposome-loaded microbubbles to detect and selectively destroy metastasis cells. 12th European symposium on controlled drug delivery, 4-6 April 2012, Egmond aan zee, The Netherlands

Geers B, De Wever O, Bracke M, De Smedt S.C., Lentacker I. Targeted liposome-loaded microbubbles for selective ultrasound assisted circulating tumor cell therapy, World molecular imaging conference, 5-8 September 2012, Dublin, Ireland

AWARDS

Finalist Battle of Talents business/investment game 2012

ATTENDED CONFERENCES

BURST symposium: 28 November 2008, Eindhoven, The Netherlands

14th European symposium on Ultrasound contrast imaging; 22-23 January 2009, Rotterdam, The Netherlands

SHORT RESEARCH VISITS

2-4 february 2009: In vivo experiments with PEGylated AAV loaded microbubbles for targeted gene delivery in the brain. Department of neurology, Universitätsklinikum Mannheim, Heidelberg University, Mannheim, Germany.

12-14 july 2011: in vivo experiments on lipoplex/microbubble coadministration with TIPS ultrasound, Department of cardiology, Westfälische Willems Universität, Münster, Germany

POSTGRADUATE COURSES

22-26 november 2010: Small animal imaging workshop, European institute of molecular imaging, Westfahlishe Willems Universität Münster, Münster, Germany. (ECTS: 8)

Project Management, UGent Doctoral schools (ECTS: 2)

Technology Transfer, UGent Doctoral Schools (ECTS: 2)